INFORMATION TO USERS

This manuscript has been reproduced from the microfilm master. UMI films the text directly from the original or copy submitted. Thus, some thesis and dissertation copies are in typewriter face, while others may be from any type of computer printer.

The quality of this reproduction is dependent upon the quality of the copy submitted. Broken or indistinct print, colored or poor quality illustrations and photographs, print bleedthrough, substandard margins, and improper alignment can adversely affect reproduction.

In the unlikely event that the author did not send UMI a complete manuscript and there are missing pages, these will be noted. Also, if unauthorized copyright material had to be removed, a note will indicate the deletion.

Oversize materials (e.g., maps, drawings, charts) are reproduced by sectioning the original, beginning at the upper left-hand corner and continuing from left to right in equal sections with small overlaps. Each original is also photographed in one exposure and is included in reduced form at the back of the book.

Photographs included in the original manuscript have been reproduced xerographically in this copy. Higher quality 6" x 9" black and white photographic prints are available for any photographs or illustrations appearing in this copy for an additional charge. Contact UMI directly to order.

U·M·I

University Microfilms International
A Bell & Howell Information Company
300 North Zeeb Road, Ann Arbor, MI 48106-1346 USA
313/761-4700 800/521-0600

Order Number 9431858

NMR studies of mating factors from the yeast *Saccharomyces cerevisiae*

Gounarides, John Stephen, Ph.D.

City University of New York, 1994

U·M·I
300 N. Zeeb Rd.
Ann Arbor, MI 48106

NMR STUDIES OF MATING FACTORS FROM THE YEAST *SACCHAROMYCES CEREVISIAE*.

by

JOHN STEPHEN GOUNARIDES

A dissertation submitted to the Graduate Faculty in Chemistry in partial fulfillment of the requirements for the degree of Doctor of Philosophy, The City University of New York.

1994

This manuscript has been read and accepted for the Graduate Faculty in Chemistry in satisfaction of the dissertation requirement for the degree of Doctor of Philosophy.

2/10/94
Date

Fred Naider
Chair of Examining Committee

2/15/94
Date

Robert Rein
Executive Officer

Ruth E. Stark
Dr. Ruth Stark

Max Diem
Dr. Max Diem

Supervisory Committee

THE CITY UNIVERSITY OF NEW YORK

Abstract

NMR Studies of Mating Factors from the Yeast *Saccharomyces cerevisiae*

by

John Stephen Gounarides

Adviser: Professor Fred Naider

Mating in *Saccharomyces cerevisiae* is mediated by the α-factor (WHWLQLKPGQPMY) and the a-factor (YIIKGVFWDPAC[S-farnesyl]OCH_3). The [D-Ala^9]- and [L-Ala^9]α-factors were synthesized and examined in solution and in the presence of lipid vesicles by NMR spectroscopy. NOE and NH dδ/dT data indicated that residues 7-10 of the [D-Ala^9]α-factor adopt a Type II β-turn in DMSO and aqueous solutions. The 10-fold less active [L-Ala^9] analogue did not adopt a regular secondary structure. Transfer NOE data suggested that the Type II β-turn conformation of the [D-Ala^9]α-factor is maintained in the lipid bound state.

Several cyclo^{7,10}[Cys^7,X^9,Cys^{10},Nle^{12}]α-factor analogues (X = D-Ala, L-Ala, D-Val, or Gly) were studied in DMSO/water (80:20) and aqueous solution using NMR spectroscopy. NOE parameters, NH dδ/dT, and $^3J_{\alpha NH}$ coupling constants indicate that residues 7-10 of

cyclo^{7,10}[Cys^{7},D-Ala^{9},Cys^{10},Nle^{12}]- and cyclo^{7,10}[Cys^{7},D-Val^{9},Cys^{10},Nle^{12}]a-factor adopt a Type II β-turn, whereas cyclo^{7,10}[Cys^{7},L-Ala^{9},Cys^{10},Nle^{12}]a-factor adopts a Type I β-turn. In water cyclo^{7,10}[Cys^{7},Cys^{10},Nle^{12}]a-factor adopts at least two distinct conformations, however, in DMSO/water cyclo^{7,10}[Cys^{7},Cys^{10},Nle^{12}]a-factor assumes a Type II β-turn.

Vibrational circular dichroism (VCD) studies suggested that cyclo^{7,10}[Cys^{7},D-Ala^{9},Cys^{10},Nle^{12}]- and cyclo^{7,10}[Cys^{7},L-Ala^{9},Cys^{10},Nle^{12}]a-factors adopt a transient β-sheet and that VCD could be used to distinguish Type I from Type II β-turns.

a-Factor and five a-factor analogues were studied in DMSO-d_6. NH $d\delta/dT$, $^{3}J_{\alpha NH}$ coupling constant, and sequential NOESY data indicated that a-factor is predominantly unstructured in DMSO. Similar results were obtained for the other peptides indicating that S-prenylation of Cys^{12} does not affect the conformation of these peptides.

This thesis is dedicated to my parents,

John and Flavia Gounarides

ACKNOWLEDGEMENTS

I would like to gratefully acknowledge my mentor Dr. Fred Naider. I have observed him to be an excellent chemist and instructor. Over the years he has always been willing to discuss the goals and results of a project. I would especially like to thank him for allowing me the freedom to make many of the decisions for my project.

I would also like to thank the other members of my committee Dr. Ruth Stark and Dr. Max Diem. Dr. Stark has provided me with a great deal of help and advice over the course of my graduate career. Dr. Diem has given me the opportunity to work in his laboratory with Mr. Arthur Barlow and learn about VCD spectroscopy.

I owe Dr. Michelle Broido a special thank you for taking me into her research laboratory group and giving me my introduction to high resolution NMR spectroscopy. A special thank you is also in order for Dr Michael Blumenstein, who has provided me with spectrometer time, hands on aid, and many conversations about spectral interpretation and about science in general.

I would also like to thank all of the members of the Naider group, especially Dr. Chu-Biao Xue, who synthesized most of the peptides that I have studied, Dr. Mike Tallon and Dr. Ariel Ewenson, who helped me when

I attempted the synthesis and purification of the [D-Ala²] and [L-Ala²] analogues, and finally Dr. Eduardo Krainer (although we never got an experiment to work).

In addition I would Like to thank the former members of the Broido Group, Dr. Linda Jelicks, Dr. Sean Cahill, Dr. W. Chen, and Paula Longo. Mr. Steve Bobin and Ms. Elizabeth Zulinska *(moja mała wydra)* of the RCMI sequencing and synthesis facility, located at Hunter college, were extremely helpful in the writing of this thesis.

TABLE OF CONTENTS

List of Tables

List of Figures

List of Abbreviations

Å	Angstrom
Ala	alanine
Asp	aspartic acid
B, B_i	magnetic field, component of magnetic field in i direction
Boc	*tert*butoxycarbonyl
c	velocity of light
C_{18}	octadecyl silica gel, HPLC column
CD	circular dichroism
Cha	β-cyclohexyl-L-alanine
CH_2Cl_2	methylene chloride
COSY	two-dimensional correlated spectroscopy
Cys	cysteine
DCC	dicyclohexylcarbodiimide
DIEA	N,N- diisopropylethylamine
DIPC	N,N'-diisopropyl carbodimide
DMF	dimethylformamide
DMS	dimethylsulfide
DMSO-d_6	dimethyl sulfoxide-d_6
DPPC	dipalmitoylphosphatidylcholine
D_2O	deuterium oxide
DQF-COSY	double-quantum filtered correlated spectroscopy
ECO	extended coupled oscillator model
EDTA	ethylenedinitrilo-tetraacetic acid

FID	free induction decay
FT	Fourier transform
F_1, F_2	frequency dimensions in 2-D NMR experiments
γ	gyromagnetic ratio
Gln	glutamine
Glu	glutamic acid
Gly	glycine
^1H	spin 1/2 isotope of hydrogen
^2H	spin 1 isotope of hydrogen
$\hbar$	Planck's constant ($h = 6.626 \times 10^{-34}$ J Hz^{-1}) divided by 2π
HF	hydrogen fluoride
His	histidine
HOD	water, residual ^1H in D_2O
HPLC	high performance liquid chromatography
Hz	Hertz, cycles per second
I_{kl}	intensity of cross-peak between k and l
Ile	isoleucine
J	spin-spin coupling constant
KHz	kilohertz
Leu	leucine
Lys	lysine
M_{0l}	equilibrium magnetization of spin l
Met	methionine
mg	milligram
MHz	megahertz

ml	milliliter
mM	millimolar
ms	millisecond
NMR	nuclear magnetic resonance
NOE	nuclear Overhauser effect
NOESY	two-dimensional nuclear Overhauser effect spectroscopy
ns	nanosecond
ω_0	Larmor frequency
OMPa	p-methoxyphenylacetic acid
OPa	phenacyl ester
PC	phosphatidylcholine
Phe	phenylalanine
ppm	parts per million
Pro	proline
^{31}P	spin 1/2 isotope of phosphorus
R	rotational strength (VCD)
r_{ij}	internuclear distance between i and j
rf	radiofrequency
ROE	rotating-frame nuclear Overhauser effect
ROESY	two-dimensional rotating-frame nuclear Overhauser effect spectroscopy
s	second
T	absolute temperature
T_1	spin-lattice relaxation time
T_2	spin-spin relaxation time
t_1, t_2	time dimensions in 2-D NMR experiments

TFA	trifluoroacetic acid
TOCSY	total correlated spectroscopy
TRNOE	transferred NOE
TRNOESY	two-dimensional transferred nuclear Overhauser effect spectroscopy
Trp	tryptophan
TSP	3-trimethylsilylpropionate, sodium salt
Tyr	tyrosine
ρ_{ii}	direct relaxation rate (fixed frame)
$\rho_{ii(roe)}$	direct relaxation rate (rotating frame)
σ_{ki}	cross relaxation rate (fixed frame)
$\sigma_{ki(roe)}$	cross relaxation rate (rotating frame)
$\mathbf{r}_{ij}$	distance vector between the coupled dipoles μ_i and μ_j (VCD)
τ_c	correlation time
τ_m	mixing time
V_{ij}	dipole-dipole interaction matrix
VCD	vibrational circular dichroism
1-D, 2-D	one dimensional, two dimensional

CHAPTER I

Introduction:

In many higher organisms cellular communication involves the exchange of intercellular messengers. Many important cellular processes such as growth, differentiation, proliferation, and metabolism are governed by the release and recognition by a receptor of intercellular signal molecules. This opens up the possibility of using therapeutics to regulate cell function and offers an attractive means for attacking a number of pathological processes. Consequently, understanding the mechanisms of intercellular communication on the molecular level has become one of the central goals of current scientific research.

Peptides form an important class of molecules used by cells as intercellular signals. Therefore, there is a considerable amount of interest in studying the interactions of peptide hormones with their receptors. However, direct attempts to do so have frequently been frustrated by the difficulties involved in identifying and isolating receptor molecules. Because of this a great deal of effort has been focused on studying peptide hormones and in the design of agonists and antagonists. An integral part of this research involves determining the conformation of these compounds in solution, through

the use of various spectroscopic techniques. The results obtained are then applied to the design of novel and hopefully more selective agents. Nuclear magnetic resonance (NMR) spectroscopy has proven to be particularly useful in studying peptide conformation in solution. Through the nuclear Overhauser effect, NMR spectroscopy can provide information about interatomic distances and the dynamics of a molecule (1-3). This information can then be used to determine the conformation of a peptide. Unfortunately, it is not always possible to use NMR spectroscopy to study small linear peptides. These molecules are highly flexible and often several conformations will be present in solution (4-10). The resulting NMR parameters, including the NOE, will then be averaged over the various conformers, thus complicating the interpretation of the data in terms of a preferred conformation. Another difficulty is the fact that many small peptides have rotational correlation times which lead to a nulling of the NOE at the fields commonly used in high resolution NMR spectroscopy (1-3, 11,12). This latter difficulty can be overcome by the use of rotating frame Overhauser effect spectroscopy (ROESY) or by the use viscous solvent systems, such as cryogenic mixtures (3,13). Cryogenic solvents have the added advantage of allowing experiments to be performed at low temperatures, which combined with their high

viscosity serves to increase the correlation time of flexible peptides (13). Nonetheless, the interconversion of even a few conformers can make interpretation of NOE data intractable. Over the past few years several authors have put forward computational procedures for dealing with conformational averaging (3,14,15). These methods have been based on averaging the contribution of a limited number of well defined conformers to the observed signal and consequently they may not be applicable to highly flexible molecules. Recently, vibrational circular dichroism has been applied to the study of peptide conformation (16-25). The pico-second time frame of infrared spectroscopy allows separate transitions to be observed for each conformer. In addition, Paterlini *et al.* have suggested that a peptide will exhibit a VCD signal only if it adopts a preferred conformation (24). Therefore, VCD spectroscopy has the potential to become a valuable tool for the study of small highly flexible peptides.

When a peptide hormone binds to its target receptor it probably comes in contact with the lipid environment of the membrane. The conformations of many peptides are significantly altered in the presence of lipid (26-35) and it has been suggested that the cell membrane plays a critical role in ligand-receptor interactions (36,37). Significantly, for analogues of enkephalin (26) and

luteinizing hormone releasing hormone (27) biological activity has been correlated with the membrane-bound conformation rather than with the conformations observed in solution. Because of this, many researchers have turned their attention towards studying lipid-peptide interactions.

The yeast *Saccharomyces cerevisiae* makes an attractive model for the study of peptide hormone-receptor interactions. The yeast has the advantages of being genetically well characterized and readily grown in the laboratory (38). In *S. cerevisiae* sexual conjugation between α- and a-haploid cells is mediated by two diffusible peptide pheromones; the α-factor (WHWLQLKPGQPMY), and the a-factor (YIIKGVFWDPAC[farnesyl]OCH_3) (38-41). These peptides exhibit many of the characteristics of mammalian hormones (41-43). Models for the receptors of these pheromones suggest that they have structural motifs common to mammalian receptors (44-47). Moreover, it is thought that signal transduction in yeast is mediated by a G-protein complex system similar to that found for a number of mammalian systems (46,47).

This thesis focuses on NMR spectroscopic studies of a number of linear and cyclic analogues of the α-mating factor in solution and in the presence of phospholipid vesicles. In addition, the potential of VCD spectroscopy for studying peptide conformation, as applied to this

system, was explored. Finally, the conformation of the α-factor and several a-factor analogues in DMSO was examined by NMR spectroscopy. The biology and biochemistry of the α- and a-mating factors is discussed below. Pertinent details of the spectroscopic experiments used are given in chapter II. Materials and Methods are contained in chapter III. The results of studies on α-factor and a-factor peptides are presented in chapters IV and V, respectively. The discussion and implications of these results comprise chapter VI.

Background:

The life cycle of the yeast *S. cerevisiae* is shown in Figure 1. *S. cerevisiae* can exist either as a diploid cell or as one of two types of haploid cell, which are given the designation a and α (38). Both diploid and haploid cells are able to asexually reproduce by budding (38). Diploid cells have the ability to respond to conditions of nutrient deprivation by undergoing meiosis and sporulation (38). Upon germination each spore releases two α haploid and two a haploid cells. Haploid cells are not capable of sporulation. However, in the presence of each other, the two haploid cell-types can undergo sexual conjugation which results in the formation of a diploid cell (38).

Sexual conjugation between α- and a-haploid cells is

Figure 1: Life cycle of the yeast *Saccharomyces cerevisiae* (*reference* 38).

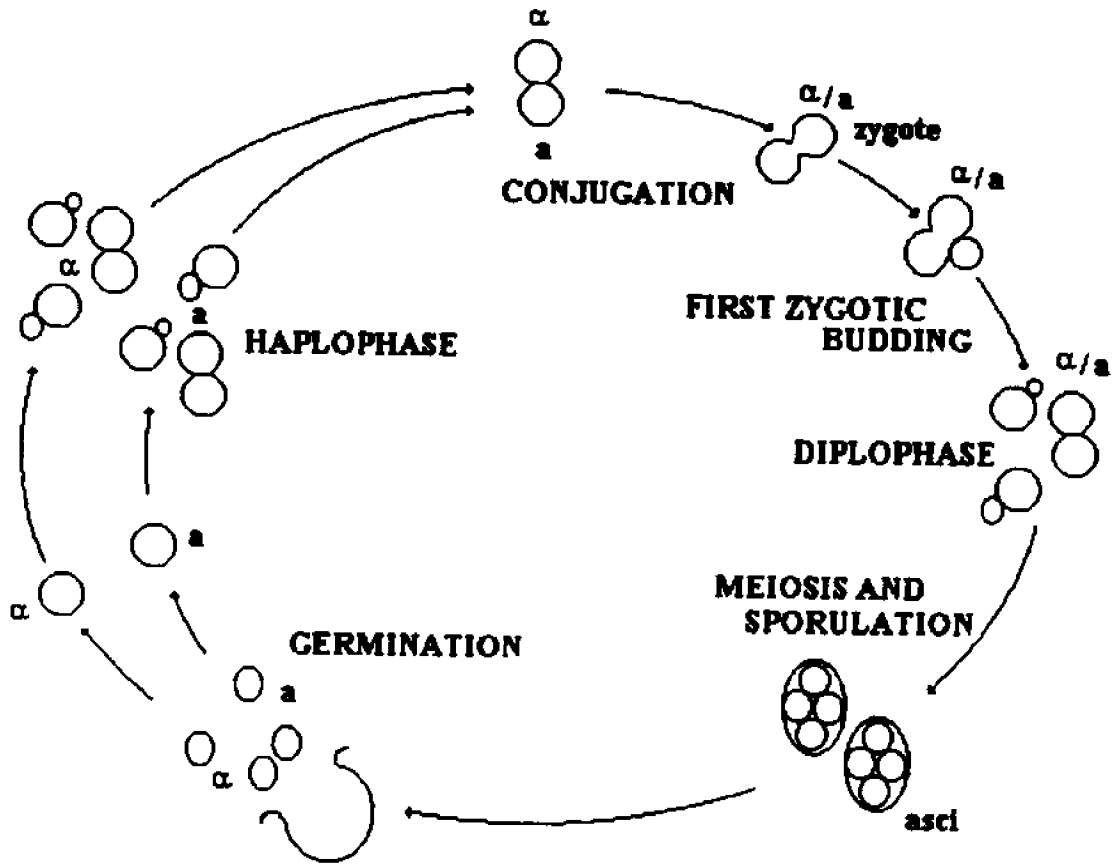
α
a
CONJUGATION
α/a
zygote
α/a
FIRST ZYGOTIC
BUDDING
α/a
DIPLOPHASE
MEIOSIS AND
SPORULATION
asci
GERMINATION
a
α
HAPLOPHASE
α
a
α
a

initiated by two diffusible peptide pheromones (38-41). These peptide pheromones are known as the α-factor (WHWLQLKPGQPMY) and a-factor (YIIKGVFWDPAC[farnesyl]OCH_3) and are secreted by α- and a-haploid cells, respectively. Both pheromones elicit similar responses in their respective target cells, that prepare these cells for fusion with their mating partners (38,41-43). Responses include an increase in cell surface agglutinability towards the cell of the opposite mating type, which enhances cell-cell contact; the arrest of the cell cycle in the G-1 phase of the growth cycle, which synchronizes the cell division cycles of both mating cells; the biosynthesis of a new cell wall and membrane which are suitable for cell fusion; and marked morphological changes (shmooing) which aid cells in finding mating partners (38,41,48-54).

The α- and a-factor receptors are coded by the STE-2 and STE-3 genes, respectively (44-46,55). Based on hydropathy profiles structural models have been proposed for both of these receptor proteins. The proposed models for both receptors contain seven trans membrane helices connected by hydrophilic loops (44-46,55). This structural motif is similar to those derived for mammalian receptors such as the β_2-adrenergic receptor and rhodopsin (56,57). In addition, there is evidence based on studies done on mutant yeast strains which

indicates that G-proteins play an integral role in the signal transduction from the mating-factor receptors in *S. cerevisiae* (46,58-63). G-proteins have been found to mediate signal transduction in mammalian receptor systems, including the β_2-adrenergic receptor, muscarinic acetylcholine receptor, and rhodopsin (56,64). Furthermore, the primary structures for these yeast G-proteins appear to be highly homologous to mammalian G-proteins (60,63). Interestingly, mutant yeast cells which expressed both the β_2-adrenergic receptor protein and the α-subunit of the G-protein complex, responded to both adrenergic agonists and antagonists (65). The latter result indicates that yeast cells have an effector system which is compatible with this receptor.

The α-factor has been the subject of numerous structure-activity studies (38,39,66-74). The results of these studies indicate that the residues at the C- and N-termini play an integral role in the activity of the pheromone. For example, the substitution of His^2 by D-histidine, leucine, lysine, or phenylalanine resulted in a virtually inactive pheromone (66). Likewise, the removal of Tyr^{13} decreases activity 1000 fold (39). In addition, modification of this residue either by ammonolysis (formation of an amide) or by esterification of the C-terminal carboxyl group leads to a 10^3-10^4 fold decrease in activity (38,39).

The importance of the peptide termini is further highlighted by a recent study involving two truncated analogues of α-factor (71). One analogue lacked the first two N-terminal residues, the des-Trp^{1},des-His^{2} [Nle^{12}]α-factor, while the other analogue, the des-Met^{12}, des-Tyr^{13}-α-factor, had the last two C-terminal residues removed. Both of these analogues are inactive, however, the des-Trp^{1},des-His^{2}[Nle^{12}]α-factor was found to be an antagonist and interestingly, the des-Met^{12},des-Tyr^{13}-α-factor was found to increase the activity of the native pheromone. This result represents the first reported example of a peptide fragment that acts as a synergist for its parent pheromone.

In contrast to the above results the α-factor receptor appears to tolerate the extension of the α-factor peptide sequence on the N-terminus by up to four residues (68). In addition, the des-Trp^{1}-α-factor exhibits high activity (39). In fact, both the tridecapeptide α-factor and the des-Trp^{1} dodecapeptide analogue have been isolated from the culture medium of the α-haploid cells (38,39). The des-Trp^{1} dodecapeptide may be an artifact of the process used for the isolation of the α-factor. Masui *et al.* (39) reported that both peptides have same activity. However, the results of Shenbagamurthi *et al.* (72) indicated that the activity of the dodecapeptide is 6% that of the tridecapeptide.

Shenbagamurthi *et al.* observed that dodecapeptide α-factor analogues which contained D-alanine, or D-leucine in position 9 were observed to have consistently higher activity than corresponding analogues which incorporated L-alanine or L-leucine in this position (74). Furthermore, the CD spectra obtained for the des-Trp^1[Cha^3,L-Ala^9] and des-Trp^1[Cha^3,L-Leu^9] analogues in solution were significantly different (indicating different conformational preferences) from the spectra of the native tridecapeptide or the des-Trp^1[Cha^3]α-factor analogues which contained either D-alanine or D-leucine in position nine (74). These results suggested that the activity of the pheromone was correlated with a conformational feature, specifically a Type II β-turn centered about Pro^8-Gly^9. This conformational feature (illustrated in Figure 2 along with Type I β-turn) has been found in several peptides which contained a Pro-Gly sequence. Moreover, based on both theoretical and experimental precedent the substitution of a D-residue for glycine in α-factor would be expected to favor a Type II β-turn conformation, whereas substitution with a L-residue is expected to destabilize this conformation (75,76).

The conformation of α-factor in solution and in the presence of lipid has been the subject of a number of NMR studies (77-82). Higashijima *et al.* proposed a structure

Figure 2: Type I and Type II β-turns.
From reference 83.

Type I β-turn

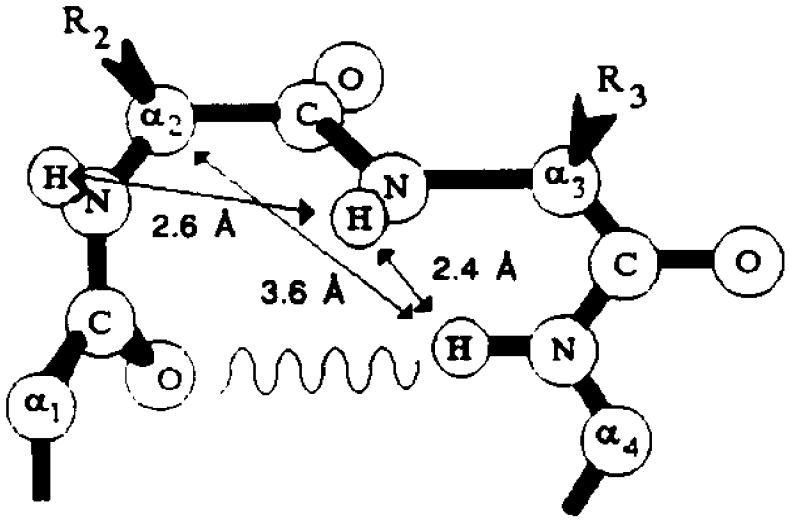

$\phi_2 = -60°$, $\psi_2 = -30°$, $\phi_3 = -90°$, $\psi_3 = 0°$

Type II β-turn

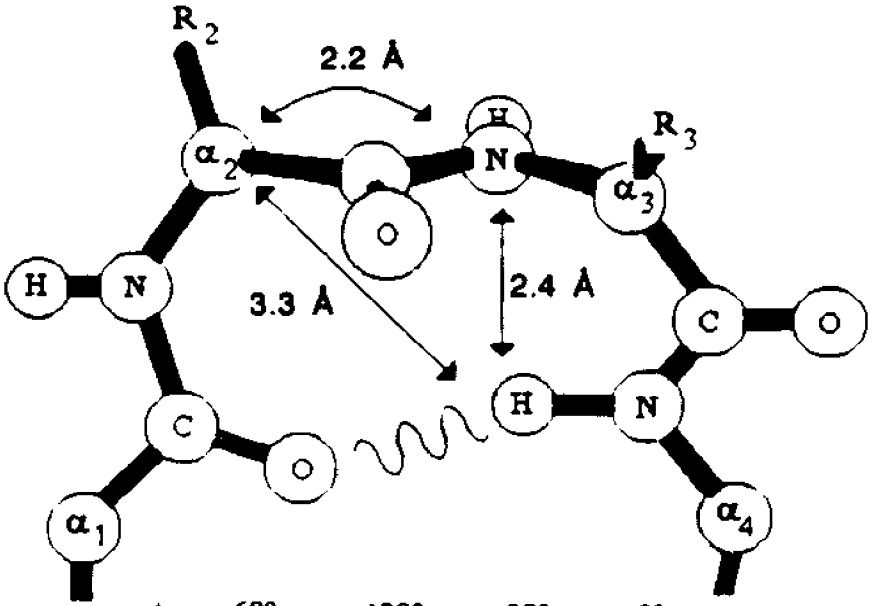

$\phi_2 = -60°$, $\psi_2 = 120°$, $\phi_3 = 90°$, $\psi_3 = 0°$

for α-factor in solution which included a helical N-terminus spanning residues 1-6 and β-turns spanning residues 7-10 and 10-13 (79). This structure was based on the pH dependencies of the amide chemical shifts, $^3J_{\alpha NH}$ coupling constants, amide temperature coefficients, and Gd(III) induced relaxation effects. However, it should be noted that none of these parameters gives direct internuclear distance information. In a later study this same group concluded based on the results of one-dimensional transfer NOE experiments that in the presence of lipid residues 1-6 of the α-factor adopted a helical conformation while the remainder of peptide adopted an extended conformation (80,81). However, these transfer NOE experiments were performed in D_2O and therefore no NOEs involving exchangeable protons, specifically those involving the back-bone amide protons, could be observed. These latter NOE connectivities are often critical for structure determination (3,83). The results of the Masui group can be contrasted with those of Jelicks *et al.* using two-dimensional NMR techniques (77,78). Jelicks *et al.* found that the α-factor is a highly flexible molecule in both DMSO and aqueous solution (78). Nevertheless, the results obtained in their study were consistent with the pheromone adopting a transient Type II β-turn centered about Pro^8 and Gly^9. No evidence for any other conformational feature in solution other than

the Type II β-turn was observed in this study. These authors reported similar results for the des-Trp^1[Cha^3,D-Ala^9] and des-Trp^1[Cha^3,D-Leu^9] analogues in DMSO (78). In contrast, the less active des-Trp^1[Cha^3,L-Ala^9] and des-Trp^1[Cha^3,L-Leu^9] analogues appeared to adopt random conformations (78). It was also reported by Jelicks *et al.* that in the presence of lipid vesicles the N-terminus of α-factor assumed a compact structure and the peptide maintained the Type II β-turn conformation observed in solution (77).

Our research group is interested in the relationship between conformation and activity in the α-factor. I have, therefore, synthesized the [D-Ala^9] and [L-Ala^9] analogues of α-factor and subjected these peptides to a detailed conformational analysis using NMR spectroscopy. The primary aim of my analysis was 1) to determine if the [D-Ala^9]- and [L-Ala^9]α-factors have significantly different biological activities, and 2) to study the conformations of these two peptides in DMSO, water, and in the presence of lipid. Such a study would extend the findings of Jelicks *et al.* (77,78) who examined the des-Trp^1[Cha^3,X^9]α-factor analogues only in DMSO. Since tridecapeptide α-factor is considerably more hydrophobic than the homologous dodecapeptide (Naider, unpublished results) it was anticipated that the tridecapeptides would interact more strongly with lipid vesicles. We

were, therefore, especially interested in examining the conformation of analogues which incorporated D-alanine or L-alanine in position 9 in the presence of lipid. Unilamellar DPPC vesicles were used as a model for the lipid membrane environment of the α-factor receptor.

Recently, Garcia-Echeverria *et al.* have reported that a cyclo^{1,4}[Cys,Pro,D-Val,Cys] tetrapeptide adopted a Type II β-turn in water (84,85). Previous studies on the cyclo^{1,4}[Cys,Pro,L-Ala,Cys] and cyclo^{1,4}[Cys,Pro,D-Ala,Cys] tetrapeptides in DMSO and CCl_3 indicated that these peptides adopted Type I and Type II β-turns, respectively (86). In order to further investigate the biological significance of the Type II β-turn conformation, Xue *et al.* have synthesized a number of cyclic α-factor analogues, in which residues 7-10 of the native pheromone are replaced by cyclo^{7,10}[Cys,Pro,X,Cys] units (Figure 3). These peptides were designed to adopt β-turn conformations centered on residues 8 and 9 and are constrained by a disulfide bond. Significantly, these cyclic peptides have a higher activity than do their corresponding linear homologues. This result may support the importance of a β-turn for biological activity in α-factor. Moreover, the reduced flexibility of these peptides (due to the formation of the disulfide bridge) makes these molecules preferred models for a detailed

Figure 3: Structures of the linear and cyclic α-factor analogues examined in this thesis.

Trp^{1}-*His*^{2}-*Trp*^{3}-*Leu*^{4}-*Gln*^{5}-*Leu*^{6}-*Lys*^{7}-*Pro*^{8}-D-*Ala*^{9}-*Gln*^{10}-*Pro*^{11}-*Met*^{12}-*Tyr*^{13}

Trp^{1}-*His*^{2}-*Trp*^{3}-*Leu*^{4}-*Gln*^{5}-*Leu*^{6}-*Lys*^{7}-*Pro*^{8}-L-*Ala*^{9}-*Gln*^{10}-*Pro*^{11}-*Met*^{12}-*Tyr*^{13}

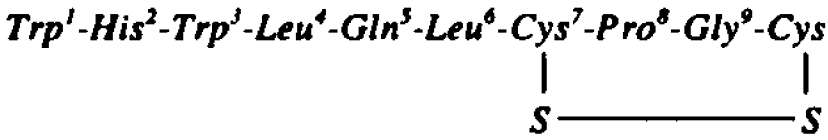

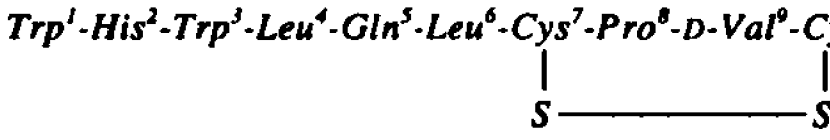

investigation by NMR. We were interested in determining if the cyclo^{7,10}[Cys^{7},X^{9},Cys^{10},Nle^{12}]a-factor analogues would adopt β-turn conformations as expected, or if the incorporation of the cyclo^{1,4}[Cys,Pro,X,Cys] unit into a-factor would cause an alteration of the conformation of this segment relative to the tetrapeptide. In addition, the constrained nature of these peptide presented an opportunity to investigate possible interactions between the C- and N-terminal residues of these peptides. In this thesis results of a detailed conformational analysis of the cyclo^{7,10}[Cys^{7},Pro^{8},X^{9},Cys^{10},Nle^{12}]a-factor analogues, where X = Gly, L-Ala, D-Ala, or D-Val (Figure 3), in aqueous and DMSO/water solution using one- and two dimensional NMR and vibrational circular dichroism is presented.

a-Factor is coded by two genes, **MFa1** and **MFa2**, as 36 and 38 residue peptides, respectively (87). These precursor peptides contain only one copy of the pheromone each and both a-factor precursor peptides contain the C-terminus sequence CVIA (87). This sequence is representative of the Cys-AAX (where A is any aliphatic amino acid and X is any amino acid) motif which is also found in the precursors of *RAS* and nuclear lamin proteins, as well as a number of other mammalian proteins (88-101). Interestingly, the maturation of a-factor is

similar to that of *RAS* proteins (100,102-106). This process involves the S-farnesylation of Cys, proteolytic cleavage of the three residues distal to Cys, and carboxyl methyl esterification.

Because it is an example of a newly identified class of prenylated peptides the a-factor is currently the subject of intense study. The purpose of prenylation in these peptides is not yet fully understood. However, it is believed that prenyl groups play a significant role in membrane trafficking. For example, there is evidence that the prenylation of *RAS* proteins is essential for their proper membrane association (103,104,106). *RAS* proteins have been associated with intestinal carcinomas. Consequently, a-factor and other prenylated peptides such as the M-factor of *Schizosaccharomyces pombe* (107) may provide insight into the function of peptide prenylation and, therefore, to novel therapeutic treatments.

In order to ascertain the influence of S-alkylation on the conformation of a-factor, this pheromone and several analogues were studied in solution by ^{1}H NMR spectroscopy. Due to the extremely poor solubility of a-factor in aqueous media, DMSO was chosen as the solvent. The a-factor peptides examined in this study are presented in Figure 4. Recent studies from our group show that the farnesyl group can be replaced by other hydrophobic groups with only a moderate reduction in

Figure 4: Structures of a-factor peptides used in this study.

a-Factor and a-Factor Analogues

a-Factor:

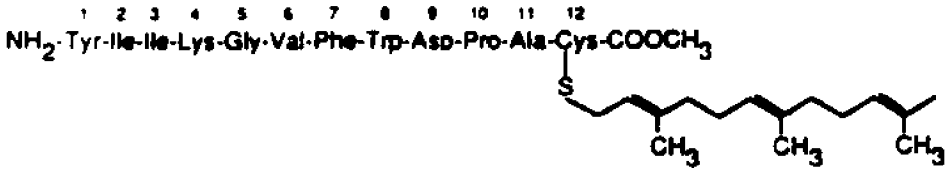

Nonmethylated a-Factor:

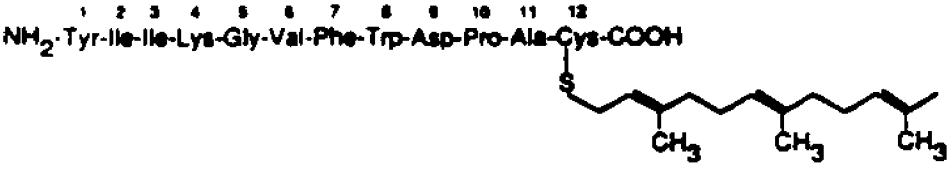

a-Factor Peptide:

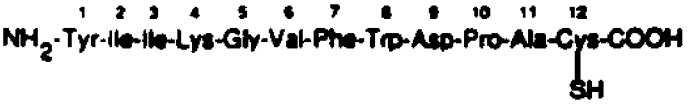

S-Methyl a-Factor:

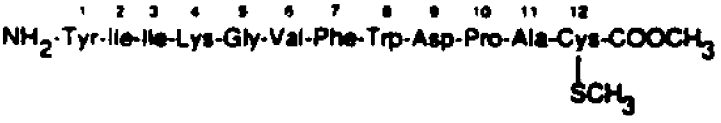

S-Hexadecanyl a-Factor:

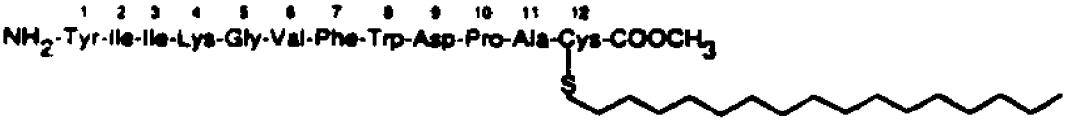

S-Geranyl a-Factor:

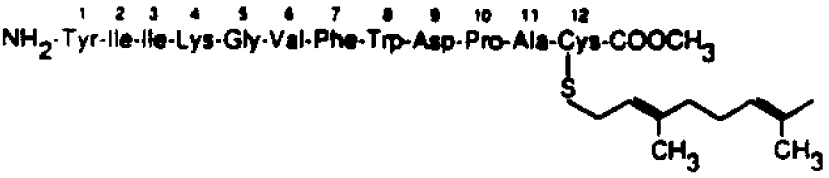

activity (108,109). Removal of both the S-farnesyl and methyl ester groups, however, results in a greater than 10^4 reduction in activity. The S-hexadecyl, S-methyl, and S-geranyl analogues were chosen so that the effects of S-alkyl size and degree of saturation on peptide conformation could be examined. The nonesterified a-factor analogue and a peptide corresponding to the unmodified a-factor sequence were examined as additional controls.

CHAPTER II

NMR BACKGROUND:

CORRELATED SPECTROSCOPY:

The COSY (correlated spectroscopy) experiment is used primarily for the resonance assignment of complex molecules (2,83,110-114). In COSY spectra cross-peaks appear between resonances which are spin-coupled, thus allowing the spin-spin coupling networks to be traced out and identified (2,83,110,111). Auto-correlation peaks in COSY spectra appear along the diagonal and are representative of the one-dimensional spectrum (110,114). In its simplest form the pulse sequence for the COSY experiment consists of two pulses (Figure 5a).

The first pulse rotates the magnetization from the Z-axis into the transverse plane (110,111,114). The spins are then allowed to evolve with respect to chemical shift and *J*-coupling for an incremented time period, t_1 (110,111,114). Following this, new coherences are generated by the application of a second pulse (110,111,114). The desired coherence order is selected by the proper phase-cycling of the pulses and receiver (111,114). The resulting COSY cross-peaks are anti-phase with respect to the active *J*-coupling (the coupling

FIGURE 5: Pulse sequences for two-dimensional experiments used. All pulses are π/2 except for the spin-lock pulse (ROESY sequence).

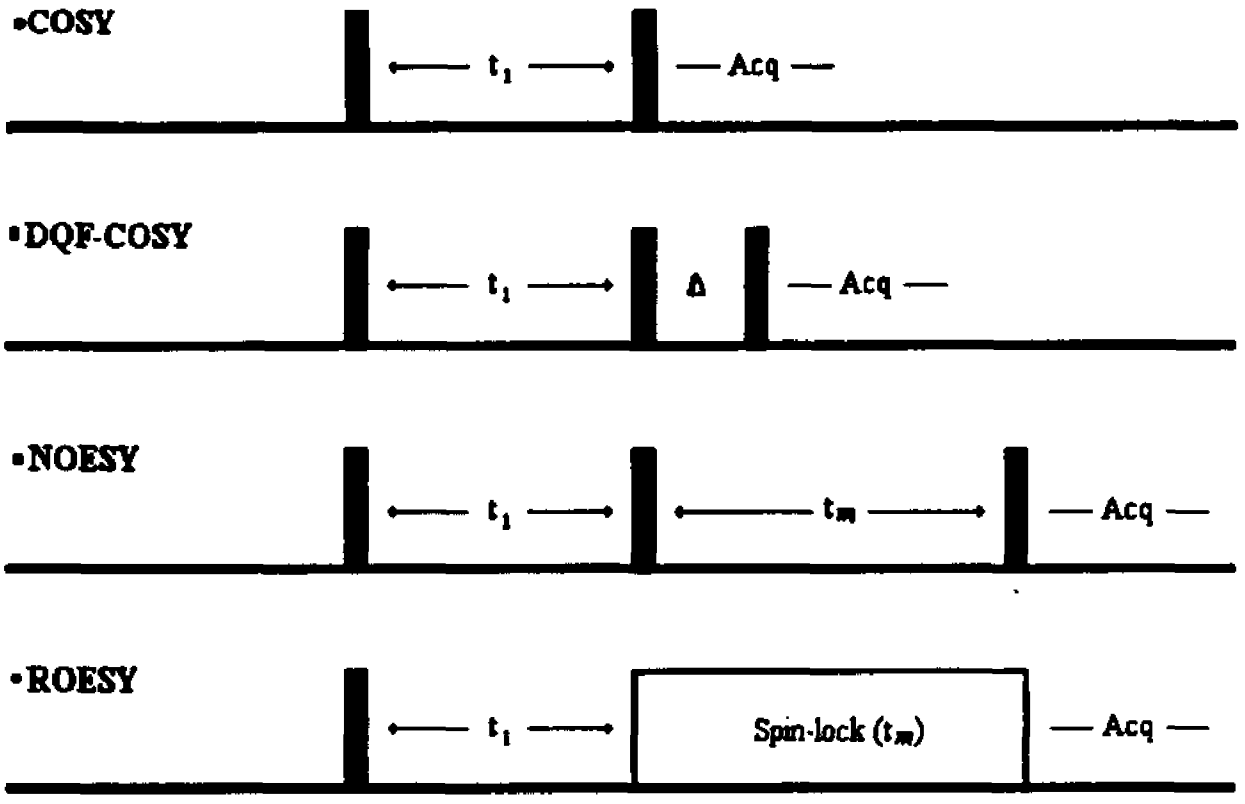
•COSY
t1
Acq
•DQF-COSY
t1
Δ
Acq
•NOESY
t1
tm
Acq
•ROESY
t1
Spin-lock (tm)
Acq

involved in the coherence transfer) and are in-phase with respect to all other (passive) couplings (83,114). The anti-phase splitting of the COSY cross-peaks can be used to obtain *J*-coupling constants for compounds which show a significant amount of spectral overlap in the 1-D spectrum. This method is generally valid provided that the COSY spectrum is collected in the pure absorption mode and with sufficient resolution (83,112). However, caution must be used when applying the method to larger molecules where the resonance line width approaches the value of the *J*-coupling, as anti-phase cancellation will cause the *J*-coupling to appear larger than its true value (83,110).

The diagonal peaks in COSY spectra are in-phase dispersive signals in both frequency dimensions (111,113,114). Because of the dispersive nature of the diagonal signals nearby cross-peaks are often severely distorted and in certain instances not observed at all. The problem is alleviated in the double-quantum filtered (DQF-) COSY experiment (111,113,114). In the DQF-COSY pulse sequence (Figure 5b) a third pulse is applied after a short delay of approximately 10 μs. This third pulse along with the proper phase-cycling removes the single spin coherence which leads to dispersive signals (111,113,114). The diagonal peaks thus become anti-phase and absorptive. An additional benefit is the removal of

strong singlets which may obscure cross-peaks that are near to the diagonal. A serious disadvantage to the DQF-COSY experiment is that it is a factor of two less sensitive than the COSY experiment (111,114).

NUCLEAR OVERHAUSER EFFECT SPECTROSCOPY:

The two dimensional nuclear Overhauser effect spectroscopy (NOESY) experiment provides information about the secondary structure and dynamics of a molecule, and is also often used to supplement resonance assignment information from COSY experiments (3,83). The NOESY pulse sequence is shown in Figure 5c. Non-equilibrium magnetization is created by the first two pulses and NOE enhancements are allowed to evolve during the mixing time, τ_m (3,114,115). The resulting NOEs appear as cross-peaks in the NOESY spectrum (3,114,115). The initial build-up of the NOESY cross-peak intensity (I_{kl}) is a function of the cross-relaxation rate, σ_{kl}, and the mixing time (τ_m) according to equation 1 (3,116).

(1) $$I_{kl} = \sigma_{kl}\tau_m$$

Therefore, extending the mixing time leads to stronger NOESY cross-peaks and allows observation of NOEs between protons that are further apart in space. However, at longer mixing times spin-diffusion may become prominent (3,83). The intensity of diagonal peaks (I_{ll}) in the

NOESY spectrum decreases as a function of the selective spin-lattice relaxation rate (ρ_{11}) as described by equation 2 (3,83,115,116).

(2) $$I_{11} = (1-\rho_{11}\tau_m)M_{01}$$

where M_{01} represents the equilibrium magnetization of spin 1. The NOESY cross-peak is also affected by spin-lattice relaxation and after sufficiently long mixing times the NOEs will have decayed to zero (3,83, 115). Provided that the initial rate approximation (i.e. equation 1) is valid and the internuclear distance r_{kl} is known, an unknown internuclear distance r_{ij} can be estimated from NOE intensities according to equation 3 (3,83,116).

(3) $$r_{ij} = r_{kl}(I_{kl}/I_{ij})^{-6}$$

Both the cross-relaxation rate (σ_{kl}) and spin lattice relaxation rate (ρ_{11}) are functions of the correlation time (τ_c) and internuclear distances, r_{kl}, and are described by equations 4 and 5, respectively (1,3).

(4) $$\sigma_{kl} = (1/10)\hbar^2\gamma^4 r_{kl}^{-6}[6\tau_c/(1-4\omega_0^2\tau_c^2) - \tau_c]$$

(5) $$\rho_{11} = (1/10)\hbar^2\gamma^4\textstyle\sum r_{kl}^{-6}[6\tau_c/(1-4\omega_0^2\tau_c^2) + 3\tau_c/(1-\omega_0^2\tau_c^2) + \tau_c],$$

where $\hbar$ is Planck's constant divided by 2π, γ is the gyromagnetic ratio specific to the nuclear species, ω_0 is the Larmor frequency, and τ_c is the correlation time. The validity of equation 3 is contingent on using interactions which have similar correlation times. In addition, the correlation time (τ_c) can be obtained from the ratio of the sum of cross-relaxation rates ($\sum\sigma_{kl}$) for a given resonance (l) to its selective spin-lattice relaxation rate (ρ_{ll}). In the extreme narrowing region ($\omega_0\tau_c < 1$) NOESY cross-peaks are negative relative to the diagonal, while, when $\omega_0\tau_c > 1$ NOESY cross-peaks are positive relative to the diagonal. At intermediate correlation times ($\omega_0\tau_c \approx 1$) the NOE approaches zero.

The NOESY pulse sequence also generates coherent magnetization transfer between *J*-coupled spins (3,117, 118). The presence of cross-peaks arising from *J*-couplings is not desirable as they can cause distortions to the shape and intensity of the NOE cross-peak. Most coherence pathways generated by this experiment are suppressed by phase-cycling (3,114). However, the phase-cycling employed in the NOESY experiment does not remove signals which arise from *zero*-quantum coherence (3,114, 117,118). Many NOESY pulse programs incorporate either a 180° or a small random time variation to the mixing time as a means of suppressing *zero*-quantum coherence (3,117,118).

In situations where a ligand molecule undergoes exchange between being bound to a larger molecule or molecular complex and unbound in solution, the transferred NOE (TRNOE) experiment can be used to obtain information about the conformation and dynamics of the ligand in the bound state (3,119-126). This experiment exploits the fact that NOE enhancements that evolve when the ligand is bound can be observed on the resonances of the unbound ligand. A schematic for the transferred NOE phenomenon is shown in Figure 6. When free in solution a ligand will be characterized by a short correlation time relative to the macromolecule. When the ligand binds to the macromolecule it is characterized by the longer correlation time of the macromolecule and therefore the cross-relaxation rate, for the resonances of the ligand will increase. If the dissociation rate for the ligand-macromolecule complex is fast relative to the spin-lattice relaxation rate the NOE enhancements that evolve for the bound ligand will be "transferred" to the resonances of the free ligand. This is an advantage as the resonances of the unbound ligand are usually much narrower than for the bound ligand.

Since the relaxation parameters from both the bound and unbound ligand contribute to the observed TRNOE enhancement it is desirable to perform the TRNOE experiment under conditions where the contribution from

FIGURE 6: Schematic for transfer NOE phenomenon.

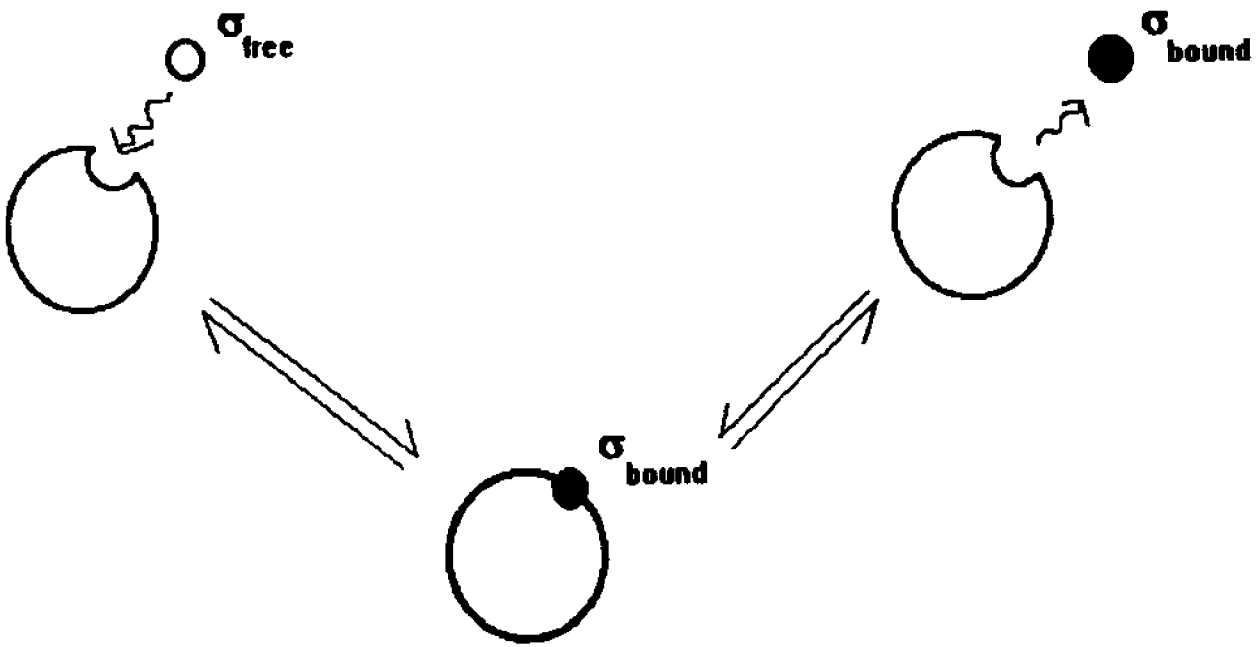
σ free
σ bound
σ bound

the unbound ligand to the observed enhancement is negligible. This may be accomplished by increasing the sample temperature (thereby making $\omega_0\tau_c \leq 1$) or by using a shorter mixing time. It is often advantageous to use shorter mixing times for the TRNOE experiment relative to the NOE experiment as spin-diffusion can be prevalent for the bound ligand (120,121). Furthermore, as a resonance becomes more constrained in the bound state the accompanying increase in the spin-lattice relaxation rate can lead to a decrease in the observed TRNOE intensity as the mixing time is extended (120). The transfer NOE is also sensitive to the fraction of bound ligand. The observed cross-relaxation increasing proportionally with the fraction of bound ligand. However the observed spin-lattice relaxation rate will also increase with the fraction of bound ligand. As a result of this the TRNOE intensity for a given mixing time may decrease as the fraction of bound ligand increases (120).

ROTATING FRAME OVERHAUSER EFFECT SPECTROSCOPY:

The pulse sequence for the rotating frame Overhauser effect spectroscopy (ROESY) experiment is shown in Figure 5d. As in the NOESY experiment, cross-peaks in the ROESY spectrum arise between dipolar coupled spins (3,11,12, 127-129). However, unlike the NOESY experiment the

diagonal-peaks are always 180° out of phase with the cross-peaks (3,127,128). In the ROESY experiment a B_1-field of suitable power is applied for the duration of the mixing time. The B_1-field, also known as a spin-locking field, locks components of the transverse magnetization generated by a 90° pulse along the field. Magnetization which is not spin-locked is rapidly dephased due to the inhomogeneity of the B_1-field. Therefore, in contrast to the NOESY experiment where enhancements evolve between elements of longitudinal magnetization, enhancements in the rotating frame (ROEs) evolve between elements of transverse magnetization.

The ROESY experiment has several advantages over the more conventional NOESY experiment. In the rotating-frame cross-relaxation ($\sigma_{kl(roe)}$) and spin-lattice relaxation ($\rho_{ll(roe)}$) are described by equations 6 and 7, respectively (3,127,130,131).

$$(6) \qquad \sigma_{kl(roe)} = (1/20)\hbar^2\gamma^4 r_{kl}^{-6}[4\tau_c + 6\tau_c/(1+\omega_0^2\tau_c^2)]$$

$$(7) \qquad \rho_{ll(roe)} = (1/20)\hbar^2\gamma^4\textstyle\sum r_{kl}^{-6}[5\tau_c + 9\tau_c/(1+\omega_0^2\tau_c^2) + 6\tau_c/(1+4\omega_0^2\tau_c^2)].$$

As there are no subtractive terms for the rotating frame cross-relaxation rate (equation 6) the ROE is always positive (180° out of phase with the diagonal in the

ROESY experiment) and increases with τ_c. Therefore, the ROESY experiment can be utilized for situations were NOEs are not observed due to an unfavorable correlation time.

Another advantage of the ROESY experiment is that in the rotating frame spin-lattice relaxation is always greater than the cross-relaxation rate (3,128). Because of this, spin-diffusion is less of a problem in this experiment relative to the NOESY experiment. In addition, spin-diffusion usually can be readily detected as the sign of the enhancement alternates upon each consecutive magnetization transfer (3,128). Direct magnetization transfers give rise to a positive enhancement, secondary magnetization transfers (and all even ordered transfers) result in negative enhancement, and tertiary (and all odd magnetization transfers) will again result in positive enhancements. Finally, cross-peaks between spins undergoing chemical exchange are negative relative to the ROE cross-peak (3,11,127) thereby, facilitating identification of this phenomenon.

Under spin-lock conditions magnetization can be transferred not only through cross-relaxation, but also through scalar spin-spin couplings (3,132-134). Both the COSY-type (anti-phase) transfer, and the Hartmann-Hahn transfer can occur in ROESY spectra (3,133). Total correlated spectroscopy (TOCSY) and Homonuclear Hartmann-Hahn (HOHAHA) experiments exploit the latter phenomenon

in order to map out spin-spin coupling networks (114, 132). Hartmann-Hahn transfer cross-peaks have the same sign as the diagonal peaks (the coherence transfer being in phase), and therefore should be readily distinguishable from direct ROE enhancements (3,132-134). Since ROE cross-peaks and Hartmann-Hahn cross-peaks have opposite signs their coincidence will result in a decrease in the observed ROE intensity.

Magnetization transfer through the Hartmann-Hahn transfer can also lead to false enhancements (3). A schematic for the mechanism of this process is presented in Figure 7. If we consider the situation of three spins labeled A, B, and C, where only spins A and B are *J*-coupled and only spins B and C are close in space. Magnetization from spin A can be sent through the A-B coupling via the Hartmann-Hahn transfer and the cross-relaxation between spins B and C to spin C. The result of this would be the observation of an enhancement between spin A and spin C although no direct enhancement exists between these two spins.

Because of the above phenomena it is desirable to suppress Hartmann-Hahn magnetization transfer in the ROESY experiment. To this end Kessler *et al* (135) have proposed using a fast sequence of small flip-angle pulses to generate the spin-lock field. Since the efficiency of the Hartmann-Hahn transfer decreases as the differences

FIGURE 7: Schematic for false cross-peaks in ROESY experiments.

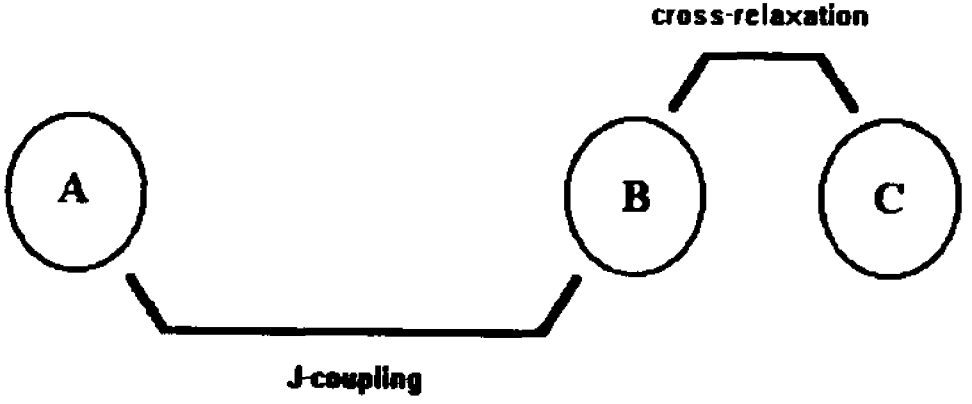
cross-relaxation
A
B
C
J-coupling

in the resonance offset of the spins increases a more common approach is the use of weak rf-fields combined with the judicious placement of the carrier frequency. This procedure takes advantage of the fact that cross-relaxation is much less sensitive to resonance offset than the Hartmann-Hahn transfer. However, the ROE cross-peak is measurably affected by offset and any attempts to determine internuclear distances from ROE data must take this offset dependence into account (129,131,133).

SATURATION TRANSFER:

The occurrence of chemical exchange can, under certain circumstances, be detected by the saturation transfer experiment (3). In this experiment a proton resonance is irradiated, leading to equal populations in its two energy levels. As the proton undergoes chemical exchange the equalized energy levels are carried along to the new site, resulting in a decreased resonance intensity for the proton in the new site. It is this phenomenon which leads to chemical exchange cross-peaks in NOESY and ROESY spectra.

In order for the transfer of saturation to be observed, the chemical exchange rate must be slow on the chemical shift time scale, so that distinct resonances are observed for the proton in each site. However, the

exchange rate must be fast relative to the spin-lattice relaxation rate, so the spins do not relax back to equilibrium prior to the exchange (3).

The experimental procedure for the saturation transfer is the same as that used for the one-dimensional NOE experiment. Therefore, it is necessary to be able to distinguish between the two effects. In the extreme narrowing regime the saturation transfer effect can be differentiated from the NOE as the latter will give rise to positive enhancements (3). When $\omega_o\tau_c>1$ the situation is more difficult, since all enhancements will be negative. However, increasing the exchange rate, for example by raising the temperature, will increase the saturation transfer effect. The intensity of NOE enhancement will usually decrease as the temperature is increased, due to shortening of τ_c (3).

Vibrational Circular Dichroism:

Vibrational circular dichroism (VCD) is the measurement of the differential absorption of left- and right-circularly polarized light by the vibrational transitions of chiral molecules (22). The VCD signal arises from the dipolar coupling of vibrational transitions. Therefore, VCD has the stereochemical specificity found for electronic CD with the added

advantage of narrower spectral features. The VCD spectrum can be semi-qualitatively interpreted in terms of molecular conformation using the extended coupled oscillator model (ECO). The ECO model is an extension of the equations derived by Tinoco (136), for the interpretation of electronic CD spectra and is based on the exciton formalism. In the exciton formalism the excitation is delocalized over an array of identical oscillators. In the ECO model the rotational strength R, upon which the intensity of the VCD signal depends, for *n* interacting dipoles is given by equation (8).

$$(8) \qquad R_k = -(\pi \nu_0 / c) \sum_{i=1}^{n} \sum_{j>1}^{n} c_{ik} c_{jk} [\mathbf{T}_{ij} \bullet \mu_i \times \mu_j]$$

where $\mathbf{T}_{ij}$ is the distance vector between the coupled dipoles μ_i and μ_j, c is the velocity of light, and ν_0 is the frequency expected for the non-coupled transition (23,137). The terms c_{ik} and c_{jk} are the eigenvector components of the dipole-dipole interaction matrix $\mathbf{V}_{ij}$ (equation 9)

$$(9) \qquad \mathbf{V}_{ij} = (\mu_i \bullet \mu_j) / |\mathbf{T}_{ij}|^3 - 3 (\mu_i \bullet \mathbf{T}_{ij}) (\mu_j \bullet \mathbf{T}_{ij}) / |\mathbf{T}_{ij}|^5 .$$

However, the above equations are not necessary for the qualitative identification of peptide secondary structure

FIGURE 8: VCD (top) and absorption (bottom) spectra for polylysine in a) α-helical, d) β-sheet, c) "random", and b) unstructured states (*from reference* 24).

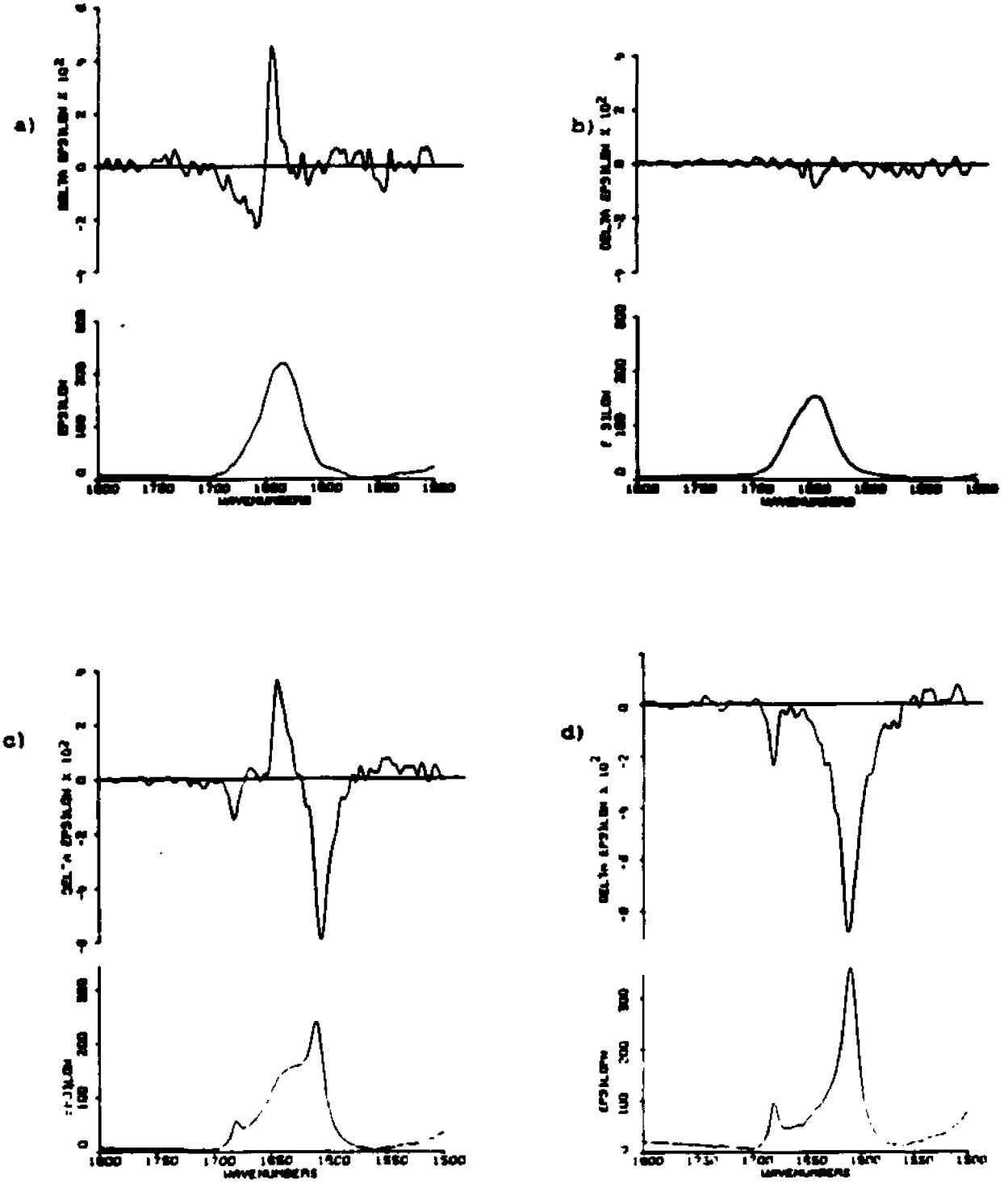
a)
b)
c)
d)

Figure 9: VCD spectrum of cyclo(Gly-Pro-Gly-D-Ala -Pro). *From reference* 16.

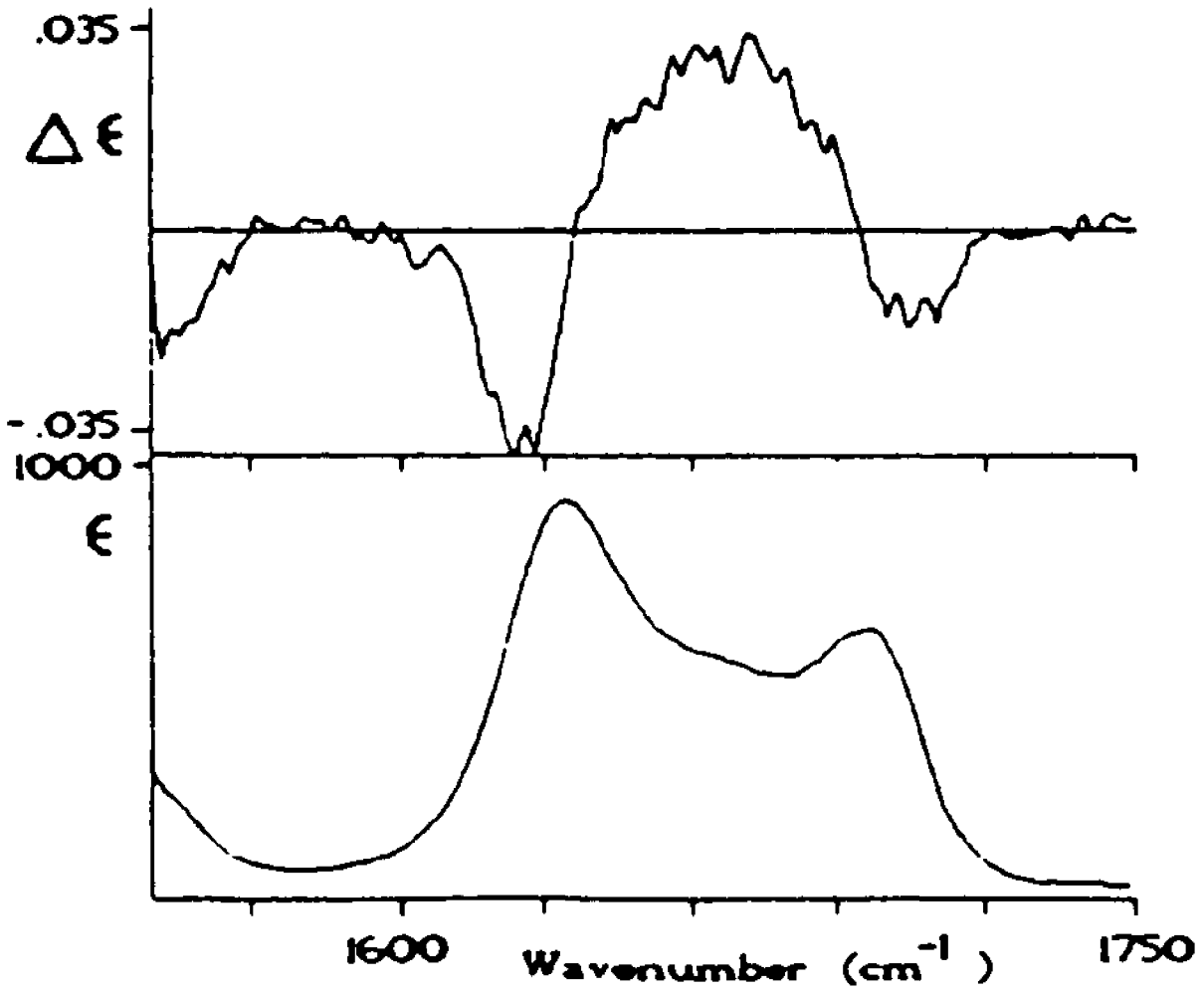
.035
Δ ε
-.035
1000
ε
1600
Wavenumber (cm-1)
1750

(see Figures 8 & 9). A near conservative positive negative (from low to high wavenumber) couplet is observed for peptides with α-helical conformations (Figure 8a; 24). For peptides which adopt an extended helix (a left-handed helix with 2.2-2.5 residues per turn) the sign of the couplet is reversed (Figure 8c; 24). In the VCD β-pleated sheet conformations exhibit strong negative monosignate signals (Figure 8b; 24). It should be noted that the ECO model is not applicable for β-sheet conformations and it is thought that the signal observed for the β-sheet is due to enhanced magnetic moments m generated by a circulatory oscillation of charge density (24). A negative-positive-negative pattern has been observed by Wyssbrod and Diem for a cyclic pentapeptide (Gly-Pro-Gly-D-Ala-Pro) which was known to adopt a Type II β-turn and a γ-turn (Figure 9; 16). Interestingly, the results of Paterlini *et al.* (24) observed no VCD signal for poly(L-Lysine) under conditions in which this peptide was expected to be unstructured (Figure 8d). This result suggested to these authors that truly unstructured peptides do not give rise to VCD signals.

CHAPTER III

Materials and Methods:

Sample Preparation

The peptides discussed in this thesis are shown in Figures 3 and 4. All NMR samples were contained in Wilmad 528-pp (5 mm) NMR tubes. a-Factor samples in DMSO-d_6 (100%, Cambridge Isotope Laboratories) had an approximate concentration of 2.5 mg/0.5 mL. The chemical shifts and line widths of a-factor did not change upon dilution from 3.1 mM to 0.1 mM indicating that aggregation was not occurring at the concentrations used. a-Factor samples were dried overnight with an Abderhalden drying pistol at 65°C to remove loosely bound water carried over from lyophilization.

Linear [D-Ala^9]- and [L-Ala^9]a-factor analogues in aqueous solution (90% H_2O/10% D_2O [CIL]) were approximately 4.0 mg/0.5 mL. The pH of the above aqueous samples was adjusted to 4.6 (uncorrected) using dilute (100 mM) stock solutions of NaOH or HCl. For the cyclo^{7,10}[Cys^7,X^9,Cys^{10},Nle^{12}]a-factor analogues in aqueous solution peptide concentrations were approximately 2.0 mg/mL and the pH was 2.9 (uncorrected). Samples of the cyclo^{7,10}[Cys^7,X^9,Cys^{10},Nle^{12}]a-factor analogues in DMSO/mixed solvent used for NMR spectroscopy were approximately 3.0 mg/0.5 mL 80% DMSO-d_6/20% H_2O (v/v).

Samples of the cyclo^{7,10}[Cys^{7},X^{9},Cys^{10},Nle^{12}]α-factor analogues in DMSO/water solution used for VCD spectroscopy were approximately 8.0 mg/0.5 mL 80% DMSO/20% D_2O (v/v).

Chain perdeuterated L-α-dipamitoylphosphatidylcholine (DPPC-d_{62}) was purchased from Cambridge Isotope Laboratories (CIL) and was used without further purification. Lipid vesicles were prepared as 16 mM DPPC solutions using a 5 mM sodium acetate buffer (pH 4.6, 10% D_2O, 50 μM EDTA) (see below). The EDTA was added to remove paramagnetic impurities which may be present in the lipid vesicle solution. This lipid vesicle solution was then used to produce either a 8 mM DPPC:4 mM peptide sample or 8 mM DPPC:2 mM peptide sample which was then used for NMR studies.

Peptide Synthesis

Synthesis of the linear [D-Ala^{9}]- and [L-Ala^{9}]α-factor analogues was begun using the tetrapeptide, Boc-Gln-Pro-Met-(2BrZ)Tyr, attached to a PAM resin. For all amino acids the N-α-position was Boc protected. The side chains of Trp, His, Lys, and Tyr were protected using formyl, tosyl, 2-chlorobenzyloxycarbonyl, and 2-bromobenzyloxycarbonyl groups, respectively. Deprotection was achieved by acidolysis with 40% trifluoroacetic acid (TFA, Aldrich) in methylene

chloride (CH_2Cl_2, Fisher). Dimethyl sulfide (1%, DMS, Aldrich) was added as a scavenger. The two glutamine residues were deprotected by treatment with 4 M HCL/1% DMS in dioxane. After deprotection the resin was washed with CH_2Cl_2 and neutralized with 10% N,N-diisopropylethylamine (DIEA, Aldrich) in CH_2Cl_2. The next Boc protected amino acid was coupled to the peptide with N,N'-diisopropyl carbodimide (DIPC) in CH_2Cl_2. 1-Hydroxybenzotriazole (HOBT)/dicyclohexylcarbodiimide (DCC) in dimethylformamide (DMF, J. T. Baker Chemical Company) replaced the DIPC as the coupling reagents for the two glutamine residues. All residues were coupled at least twice regardless of results of the Kaiser test (138). Additional couplings were performed when necessary. After each coupling step the resin was washed with CH_2Cl_2.

Once assembly of the peptide chain was completed the N-α-terminal Boc group was deprotected and the peptide was cleaved from the resin by treatment with anhydrous hydrogen fluoride (HF, Matheson) for 1 hr at -5°C. Prior to cleavage anisole (10 %) was added to the reaction flask as a scavenger. The crude peptide was washed with diethyl ether to remove the anisole. Peptide was then extracted from the resin with 10% acetic acid in H_2O. The resulting solution was evaporated to low volume and was lyophilized. Deformylation of Trp was achieved by

treatment with 1 M piperidine in 60% aqueous DMF for 24 hours at 0°C. After evaporation and lyophilization the peptide was purified to over 97% homogeneity by reversed-phase HPLC using an acetonitrile:water:trifluoroacetic acid gradient. Both the [D-Ala^9]- and [L-Ala^9]α-factor analogues gave the expected amino acid ratios.

The cyclic α-factor analogues were synthesized by Dr. Chu-Biao Xue using the solid state methodology described by Xue *et al.* (70). Boc-Tyr(2-BrZ)-OCH_2-PAM-resin was used to begin synthesis. All N-α-positions were BOC protected and the Trp, His, and Cys side chains were protected using formyl (For), tosyl (Tos), and acetaminomethyl (Acm) groups, respectively. Upon completion of the peptide chain and deprotection of the Boc group the resin was treated with 3 equivalents of $Tl(TFA)_3$ in TFA -anisole (20:1, 30 ml/g of resin) at 0°C for 1 hour to form intramolecular disulfide bonds. The resin was then washed three times with TFA, CH_2Cl_2, DMF, and methanol, dried, and subjected to HF cleavage. The peptide was extracted with DMF and treated with piperidine to remove the formyl protecting groups. The solution was then concentrated at high vacuum and the residue was taken up in water/DMF, acidified to pH 3 with acetic acid and treated with HOBt to remove the incompletely deprotected tosyl group. The crude peptide was purified using reversed-phase HPLC to over 98%

homogeneity. The cyclo^{7,10}[Cys^{7},X^{9},Cys^{10},Nle^{12}]a-factor analogues gave the expected amino acid ratios and molecular ions.

The a-factor and a-factor analogues were synthesized by Dr. Chu-Biao Xue. The a-factor, nonmethylated a-factor, S-hexadecyl a-factor, S-methyl a-factor, and S-geranyl a-factor peptides were synthesized using either total solution-phase peptide synthesis or a combination of solid-phase and solution-phase methods as described by Xue et. al. (109,139,140). The nonfarnesylated, nonmethylated a-factor analogue was prepared entirely by solid-phase peptide synthesis. All a-factor peptides were purified to over 98% homogeneity using reversed phase HPLC and were characterized by amino acid analysis and FAB mass spectrometry.

Lipid Vesicle Preparation

An appropriate amount of chain perdeuterated L-a-dipamitoylphosphatidylcholine, DPPC-d_{62}, (CIL) was weighed and dissolved in approximately 5 mL of $CDCl_3$. The solvent was then evaporated under a stream of dry nitrogen gas. During this procedure the vial was constantly rotated so that the DPPC residue would form a film. The sample was then placed under high vacuum overnight to remove the final traces of chloroform. A 5 mM sodium acetate buffer (pH 4.6, 10% D_2O, 50 µM EDTA)

was added to the sample to result in a 16 mM solution. In addition five small glass beads were added to the vial. The sample was then vortexed until the lipid film was completely dispersed. The glass beads were used to aid in the dispersal of the lipid film. The resulting solution was then transferred to a polycarbonate vial and vesicles were prepared by low power sonication according to the procedure described by Barrow and Lentz (141). A Heat Systems W-380 Sonicator equipped with a cup horn was used for the sonication of all lipid samples. During sonication the sample temperature was maintained at approximately 55°C. The sonication procedure was continued until the samples were optically clear. Most samples required less than one hour to reach optical clarity (translucent). The samples were centrifuged for 10-20 minutes at 13,000 rpm in a micro centaur microcentifuge to remove multilamellar aggregates. The lipid vesicle solution (16 mM) was then either combined with an equal volume of an 8 mM peptide solution to result in a 8 mM DPPC:4 mM peptide solution or with an equal volume of buffer solution and two volumes of an 8 mM DPPC:4 mM peptide solution to result in a 8 mM DPPC:2 mM peptide solution. All NMR experiments were performed immediately after formation of the lipid vesicle solution and completed within 72 hrs. During this time samples remained optically clear and ^{1}H NMR spectra were

unchanged.

NMR Spectroscopy:

All NMR spectroscopy was performed on the 400 MHz (^{1}H) JEOL GX-400 spectrometer of the CUNY NMR facility located at Hunter College. Data processing was performed off-line on the μ-Vax of the RCMI Computer Graphics Facility, using the FTNMR-51 package (Hare Research). All spectra were accumulated at 25°C unless otherwise noted. Chemical shifts are reported relative to the residual proton resonance of DMSO at 2.49 ppm (DMSO and DMSO/water samples) or to the H_2O signal at 4.78 ppm at 25°C (aqueous samples). Selective saturation was used for the suppression of the H_2O signal in all experiments.

Typically, one-dimensional ^{1}H spectra were acquired with 16 K points over a spectral width of 5500.6 Hz. Usually an exponential multiplication with 0.5 Hz line broadening was applied prior to Fourier transformation. One-dimensional saturation transfer experiments were used to verify the occurrence of *cis-trans* isomerism about the Pro^{10} amide bond in the a-factor peptide. In these experiments selective irradiation was applied at low power to either the *cis* or *trans* NH resonance of Asp^9 or Ala^{11} at all times except during the acquisition period. ^{31}P NMR spectra were acquired with 1024 acquisitions and

16K complex points over a spectral width of 5500.6 Hz. ^{31}P chemical shifts are reported relative to external 1% H_3PO_4 (in D_2O) at 0.0 ppm.

Phase sensitive DQF-COSY (111,113), NOESY (115), and ROESY (127) spectra were recorded using the method of States *et al.* (142). Two-dimensional spectra were collected with 2048 complex points in t_2, 128-384 t_1 increments, and post acquisition delays of 1.5-2.0 s. The spectral width in each dimension was 5500.6 Hz. DQF-COSY spectra of samples in all solvents and NOESY spectra of samples in DMSO and DMSO/water were collected with 32 acquisitions per t_1 increment. NOESY and ROESY spectra run on the ♯-factor analogues in aqueous solution were collected with 64-128 acquisitions per t_1 increment. TRNOESY experiments were performed using the standard NOESY pulse sequence, which was not equipped to remove signals arising from *zero*-quantum coherence. TRNOESY spectra were collected with 256 t_1 increments and 32 acquisitions per t_1 increment. Absolute value COSY spectra were collected with 256 t_1 increments and were used for the measurement of amide temperature coefficients. In all cases the t_1 dimension was zero-filled in order to obtain a 1K by 1K spectrum of real data. For spectra of aqueous samples the center of the spectrum was set to the frequency of the water resonance in order to remove images from imperfect quadrature

detection. Setting the carrier frequency to that of the water resonance also reduced the possibility of coherent magnetization transfer (Hartmann-Hahn transfer) between the amide and α-protons in ROESY spectra (3). The Hartmann-Hahn match was also minimized by the use of a weak spin-locking field (3.1 KHz) for ROESY experiments.

Mixing times of 100, 200, and 400 ms were used for NOESY experiments performed on samples in DMSO. For aqueous samples a 400 ms mixing time and a 250 ms spin-lock time were used for NOESY and ROESY experiments, respectively. For the TRNOESY experiments a 75 ms mixing time was used. NOESY spectra of the cyclic α-factor analogues in DMSO/water were acquired at two mixing times. The first mixing time was either 100 or 200 ms, and the second mixing time was 400 ms.

Apodiziation of COSY and DQF-COSY data was accomplished by the application of either a squared-sine bell multiplication or a π/2 shifted squared-sine bell multiplication in the t_2 time dimension and the application of a π/2 shifted squared-sine bell multiplication in the t_1 time dimension. NOESY spectra were processed using a π/2 shifted squared-sine bell multiplication in both time dimensions. For ROESY spectra a skewed π/2 shifted squared-sine bell multiplication was applied in both time dimensions. A cubic spline baseline correction was applied to the F_2

dimension of all NOESY and ROESY spectra and in addition a 4th order polynomial baseline correction was applied to the F_1 dimension of TRNOESY spectra. For all NOESY and ROESY spectra t_1-ridges were reduced by multiplying the first t_1 increment by 0.5 prior to the second Fourier transformation (143).

Internuclear distances for the cyclic analogues were estimated (± 0.1 Å) from the NOESY cross-peak intensities using equation 3 ($r_{ij} = r_{kl}[I_{kl}/I_{ij}]^{-6}$). Only the internuclear distances obtained from the 100 and 200 ms NOESY spectra were used for further analysis and it was assumed that the initial rate approximation was valid (i.e $I_{kl} = -\sigma_{kl}\tau_m M_{0l}$ is valid) at these short mixing times. Cross-peak volumes were measured with the algorithm provided for that purpose in the FT-51 software package. For the cyclo^{7,10}[Cys^7,L-Ala^9,Cys^{10},Nle^{12}]- and cyclo^{7,10}[Cys^7,L-Ala^9,Cys^{10},Nle^{12}]α-factor analogues in DMSO/water the NOESY cross-peak between the Pro^8 and Pro^{11} geminal β-protons was used in equation 3 to calibrate the relationship between NOE intensity and internuclear separation. For the cyclo^{7,10}[Cys^7,D-Val^9,Cys^{10},Nle^{12}]α-factor the Cys^{10}αCH-Cys^{10}NH cross-peak was used in equation 3 to determine the internuclear distances of the other NOE interactions. For this peptide the Cys^{10}αCH-Cys^{10}NH internuclear distance was assumed to be 2.8 ± 0.2 Å. The use of αCH_i-NH_i connectivities in this manner has

been suggested by Saltis & Liepins (116).

Vibrational Spectroscopy

Peptide samples were contained between CaF_2 windows separated by 50 μm path length teflon spacers. Infrared VCD and absorption spectra were collected in the amide I' region (1600-1750 cm^{-1}) using a dispersive VCD instrument optimized in the 6 μm spectral region. Sample cells were maintained at 25°C during data acquisition by a circulating water bath. Each spectrum consists of 30 coadded scans and possesses a spectral resolution of 5 cm^{-1}. Back ground subtraction (subtraction of the spectra of the solvent without peptide) was performed for all spectra.

Molecular Modeling

Molecular models of the cyclo^{1,4}[Cys^1,Pro^2,X^3,Cys^4] tetrapeptides (X = Gly, D-Ala, L-Ala, D-Val) were generated using the MacroModel software package on the Evens and Sutherland system of the RCMI Computer Graphics Facility. The completed peptide structures were minimized using the AMBER force fields provided with the software package. The resulting structures were used solely to aid in the stereospecific assignment of the β-protons of Cys^7 and Cys^{10} of the cyclo^{7,10}[Cys^7,X^9,Cys^{10}, Nle^{12}]α-factor analogues. In order to understand the

unusual internuclear distances obtained for the cyclo^{7,10}[Cys^{7},D-Val^{9},Cys^{10},Nle^{12}]α-factor an energy minimized structure for the cyclo^{1,4}[Cys^{1},Pro^{2},D-Val^{3},Cys^{4}] tetrapeptide fragment was generated using the SYBYL software package (Tripos) run on an Iris work station (Silicon graphics) of the Sandoz research institute (East Hanover). An idealized Type II β-turn was used as a starting conformation. Experimental distance constraints were introduced by adding an extra potential energy term proportional to the square of the difference between the actual and target distances. Energy minimizations were performed with a combination of steepest descents and conjugate gradient methods until the energy difference between successive iterations differed by less than 0.001 kcal/mol.

CHAPTER IV

α-FACTOR RESULTS:

Activity of Linear α-Factor Analogues:

The activity of the [D-Ala^9] and the [L-Ala^9] analogues was determined in the laboratory of Dr. Jeffery Becker using the shmoo assay (38). The [D-Ala^9]α-factor was found to have an activity comparable to that of the native pheromone. The [L-Ala^9]α-factor analogue was found to be 10 fold less active than the native pheromone.

Resonance Assignment of the Linear and Cyclic α-Factor Analogues:

A prerequisite to any analysis by NMR spectroscopy is the assignment of the observed resonances. The cyclic and linear α-factor analogues were assigned in the manner described by Wüthrich (83). Individual amino acids were identified from their characteristic spin-spin coupling patterns in the DQF-COSY spectrum. In Figure 10 the spin-coupling pathway for Lys^7 of the [L-Ala^9]α-factor in DMSO is traced out. Duplicated amino acids were sequentially assigned using αCH_i-NH_{i+1} NOESY cross-peaks. For example, in the [D-Ala^9] and [L-Ala^9] analogues one of the leucines (Leu^4) is expected to exhibit αCH_i-NH_{i+1} NOESY connectivities to Trp^3 and Gln^5, while the other leucine

FIGURE 10: DQF-COSY spectrum of the [D-Ala^9]α-factor in DMSO at 25°C. The spin system of Lys^7 is shown (solid line)

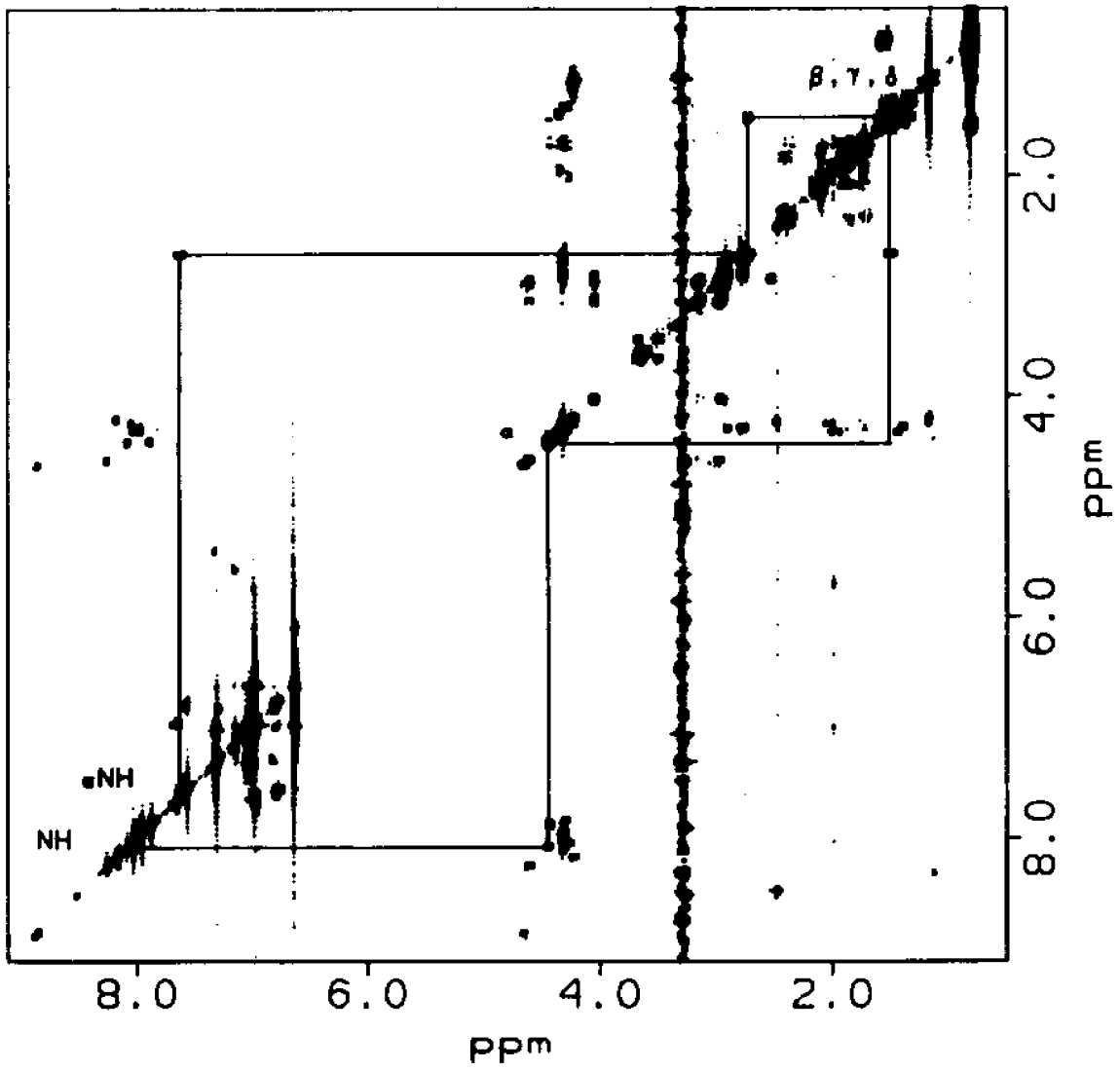
β, γ, δ
αNH
NH
8.0
6.0
4.0
2.0
ppm
2.0
4.0
6.0
8.0
ppm

(Leu^6) is expected to show connectivities to Gln^5 and Lys^7. These connectivities, which allow sequential assignment to be made, can be observed in Figures 11, 13, 14, and 15. The Aromatic resonances of Trp^1, His^2, Trp^3, and Tyr^{13} were identified from their spin-spin connectivity pattern in the DQF-COSY spectrum. Intraresidue connectivities between the βCH and aromatic resonances were used to sequentially assign two Trp aromatic ring systems. Side-chain resonances, such as the His^2 C_2H & C_4H, Gln^5 γNH_2, Gln^{10} γNH_2, and Met^{12} SCH_3, which did not give rise to cross-peaks in the DQF-COSY spectrum were assigned either from analysis of intraresidue NOESY connectivities or from their chemical shift in one-dimensional spectrum. The complete resonance assignments for the linear [D-Ala^9]- and [L-Ala^9]α-factor analogues and for the cyclo^{7,10}[Cys^7,X^9,Cys^{10}, Nle^{12}]α-factor analogues are given in Tables 1-6. The assignments presented in this thesis support those made on the native pheromone by Jelicks *et al.* (78) with the exception of the backbone and β-proton resonances of His^2 and Trp^3, which should be interchanged. This reversal is also supported by the assignments made on the [^{2}H-Trp^3]α-factor by M. Tallon (personal communication).

TABLE 1

^{1}H Assignments for [D-Ala^9]α-factor in DMSO (D) and in water (W).

Residue		NH	αCH	βCH	γCH	δCH	εCH	Other
Trp^1	D	----	4.05	3.15 2.97				ring protons 7.58,6.807 .01,7.32 7.15 indole NH 10.92
	W	----	4.21	3.21 3.14				ring protons 7.49,7.217 .05,7.48 7.06 indole NH 10.03
His^2	D	8.86	4.65	3.02				C_2H 8.99 C_4H 7.31
	W	____	4.56	3.08 2.97				C_2H 8.42 C_4H 7.10
Trp^3	D	8.27	4.61	3.17 2.98				ring protons 7.66,6.97 7.05,7.32 7.16 indole NH 10.82
	W	8.05	4.54	3.26 3.16				ring protons 7.63,7.16 7.20,7.43 7.24 indole NH 10.12
Leu^4	D	8.49	4.35	1.46	1.59	0.85		
	W	8.17	4.25	1.52	1.52	[a] 0.88 0.81		
Gln^5	D	8.05	4.27	1.76	2.11			γNH_2 [a] 7.32,6.81 7.30,6.84

	W	8.17	4.25	2.00 1.90	2.29			γNH_2 7.52,6.86
Leu[6]	D	7.84	4.30	1.38	1.57	0.79		
	W	8.24	4.34	1.64 1.56	1.52	[a] 0.88 0.81		
Lys[7]	D	8.08	4.44	1.50	1.34	1.50	2.75	ϵNH_3 7.63
	W	8.22	4.60	1.78 1.64	1.42	1.67	2.96	ϵNH_3 ----
Pro[8]	D	----	4.27	2.05	1.86	3.69 3.50		
	W	----	4.32	2.27	2.07 1.99	[a] 3.81 3.80 3.65 3.61		
D-Ala[9]	D	8.19	4.23	1.19				
	W	8.60	4.32	1.39				
Gln[10]	D	7.88	4.42	1.88 1.73	2.10			γNH_2[a] 7.32,6.81 7.30,6.84
	W	7.96	4.60	2.10 1.98	2.36			γNH_2 7.52,6.86
Pro[11]	D	----	4.34	2.00	1.90	3.62		
	W	----	4.37	2.19 1.78	2.06 1.99	[a] 3.81 3.80 3.65 3.61		
Met[12]	D	8.03	4.31	1.86 1.73	2.42 2.39			S-CH_3 2.00
	W	8.26	4.32	1.91 1.84	2.47 2.38			S-CH_3 2.03
Tyr[13]	D	7.97	4.32	2.93 2.77				$C_{2,6}H$ 6.99 $C_{3,5}H$ 6.64
	W	7.53	4.40	3.08 2.87				$C_{2,6}H$ 7.08 $C_{3,5}H$ 6.79

[a]These resonances could not be assigned to individual residues of duplicated amino acids.

TABLE 2

^{1}H Assignments for [L-Ala^3]α-factor in DMSO (D) and in water (W).

Residue		NH	αCH	βCH	γCH	δCH	εCH	Other
Trp^1	D	----	4.03	3.13 2.95				ring protons 7.57,6.78 6.99,7.31 7.14 indole NH 10.91
	W	----	4.21	3.21 3.14				ring protons 7.50,7.22 7.07,7.48 7.07 indole NH 10.04
His^2	D	8.86	4.67	3.03				C_2H 8.96 C_4H 7.32
	W	____	4.56	3.09 2.99				C_2H 8.41 C_4H 7.11
Trp^3	D	8.27	4.62	3.16 2.96				ring protons 7.67,6.97 7.04,7.31 7.16 indole NH 10.81
	W	8.05	4.52	3.26 3.16				ring protons 7.63,7.18 7.22,7.43 7.25 indole NH 10.14
Leu^4	D	8.41	4.35	1.43	1.60	0.83		
	W	8.14	4.24	1.51	1.44	0.88 0.81		
Gln^5	D	8.06	4.27	1.84	2.09			γNH_2 [a] 7.29,6.79 7.24,6.74

	W	8.18	4.21	2.01 1.93	2.27			γNH_2 [a] 7.55,6.88 7.52,6.86
Leu^6	D	7.92	4.28	1.39	1.54	0.80		
	W	8.23	4.32	1.62	1.58	0.91 0.85		
Lys^7	D	7.97	4.42	1.61 1.48	1.31	1.50	2.73	ϵNH_3 7.63
	W	8.26	4.57	1.78	1.42	1.67	2.98	ϵNH_3 ----
Pro^8	D	----	4.31	1.95 1.72	1.87 1.79	3.64 3.46		
	W	----	4.36	2.29 1.91	2.02 1.99	[a] 3.77 3.59 3.67		
Ala^9	D	7.98	4.17	1.15				
	W	8.38	4.26	1.37				
Gln^{10}	D	7.90	4.45	1.85 1.64	2.09			γNH_2 [a] 7.29,6.79 7.24,6.74
	W	8.19	4.60	2.09 1.92	2.36			γNH_2 [a] 7.55,6.88 7.52,6.86
Pro^{11}	D	----	4.29	2.00	1.85 1.79	3.64		
	W	----	4.34	2.20 1.78	2.02 1.97	[a] 3.77 3.67 3.59		
Met^{12}	D	7.99	4.30	1.85 1.74	2.42 2.38			S-CH_3 2.01
	W	8.30	4.37	1.98 1.88	2.48 2.36			S-CH_3 2.08
Tyr^{13}	D	7.99	4.30	2.91 2.76				$C_{2,6}H$ 6.98 $C_{3,5}H$ 6.63
	W	7.64	4.41	3.13 2.88				$C_{2,6}H$ 7.11 $C_{3,5}H$ 6.83

[a]These resonances could not be assigned to individual residues of duplicated amino acids.

TABLE 3

^{1}H Assignments for cyclo^{7,10}[Cys^7,D-Val^9,Cys^{10},Nle^{12}]α-factor in DMSO\water (80:20).

Residue	NH	αCH	βCH	γCH	δCH	εCH	Other
Trp^1	----	----	----				ring protons 7.39,6.62 6.92,7.29 7.08 indole NH 10.72
His^2	8.71	4.57	3.04 2.98				C_2H 8.60 C_4H 7.18
Trp^3	8.22	4.56	3.17 2.95				ring protons 7.64,6.97 7.05,7.34 7.15 indole NH 10.70
Leu^4	8.43	4.29	1.63 1.43	1.52 1.40	0.80 0.74		
Gln^5	8.04	4.26	1.87 1.73	2.11			γNH_2 7.45,6.78
Leu^6	8.15	4.19	1.49 1.42	1.53	0.80 0.74		
Cys^7	8.23	4.63	3.43 2.50				
Pro^8	----	4.50	2.01 1.79	2.05 1.77	3.45		
D-Val^9	8.29	3.84	2.17	0.84			
Cys^{10}	7.44	4.30	3.16 2.96				
Pro^{11}	----	4.28	2.00 1.71	1.86	3.66 3.48		
Nle^{12}	7.98	4.14	1.50 1.41	1.53	1.14	0.75	
Tyr^{13}	7.87	4.35	2.90 2.77				$C_{2,6}H$ 6.96 $C_{3,5}H$ 6.61

TABLE 4

^{1}H Assignments for cyclo^{7,10}[Cys^7,D-Ala^9,Cys^{10},Nle^{12}]α-factor in Water (W) and in DMSO\water (80:20) (C).

Residue		NH	αCH	βCH	γCH	δCH	εCH	Other
Trp^1	W	----	4.18	3.22 3.13				ring protons 7.61,7.15 7.18,7.44 7.02 indole NH 10.00
	C	----	----	3.09 2.99				ring protons 7.39,6.63 6.92,7.29 7.08 indole NH 10.72
His^2	W	8.31	4.50	3.06 2.96				C_2H 8.45 C_4H 7.10
	C	8.71	4.57	3.04 2.98				C_2H 8.57 C_4H 7.17
Trp^3	W	8.04	4.48	3.21 3.13				ring protons 7.46,7.02 7.19,7.41 7.21 indole NH 10.11
	C	8.22	4.56	3.15 2.96				ring protons 7.63,6.97 7.06,7.34 7.15 indole NH 10.70
Leu^4	W	8.21	4.24	1.48	1.44	0.85 0.79		
	C	8.43	4.29	1.43 1.40	1.53	0.80 0.75		
Gln^5	W	8.14	4.27	2.05 1.89	2.26			γNH_2 7.58,6.88
	C	8.03	4.27	1.86 1.72	2.10			γNH_2 7.47,6.83

Leu[6]	W	8.51	4.32	1.63 1.56	1.59	0.88 0.82		
	C	8.19	4.19	1.50 1.40	1.53	0.80 0.75		
Cys[7]	W	8.06	4.47	3.34 2.96				
	C	8.22	4.62	3.43 2.51				
Pro[8]	W	----	4.35	2.24 1.96	2.01 1.94	* 3.80 3.79 3.61 3.59		
	C	----	4.28	2.02 1.80	2.05 1.76	3.44		
D-Ala[9]	W	8.82	4.19	1.41				
	C	8.76	3.92	1.22				
Cys[10]	W	7.90	4.46	3.28 2.97				
	C	7.49	4.25	3.18 3.13				
Pro[11]	W	----	4.33	2.19 1.79	2.01 1.94	* 3.80 3.79 3.61 3.59		
	C	----	4.30	2.00 1.70	1.86	3.65 3.48		
Nle[12]	W	8.14	4.16	1.58 1.47	1.50	1.15	0.74	
	C	8.00	4.16	1.49 1.40	1.52 1.41	1.15 1.12	0.75	
Tyr[13]	W	7.77	4.47	3.06 2.87				$C_{2,6}H$ 7.07 $C_{3,5}H$ 6.78
	C	7.89	4.35	2.89 2.77				$C_{2,6}H$ 6.96 $C_{3,5}H$ 6.61

*These resonances could not be assigned to individual residues of duplicated amino acids.

TABLE 5

^{1}H Assignments for cyclo^{7,10}[Cys^7,L-Ala^9,Cys^{10},Nle^{12}]α-factor in Water (W) and in DMSO\water (80:20) (C).

Residue		NH	αCH	βCH	γCH	δCH	εCH	Other
Trp^1	W	----	4.21	3.23 3.13				ring protons 7.62,7.17 7.21,7.47 7.04 indole NH 10.02
	C	----	----	3.07 2.97				ring protons 7.38,6.61 6.92,7.28 7.08 indole NH 10.70
His^2	W	8.32	4.54	3.10 2.99				C_2H 8.47 C_4H 7.14
	C	8.72	4.58	3.05 2.96				C_2H 8.63 C_4H 7.18
Trp^3	W	8.04	4.52	3.25 3.16				ring protons 7.49,7.06 7.21,7.44 7.25 indole NH 10.12
	C	8.22	4.56	3.17 2.98				ring protons 7.63,6.98 7.05,7.34 7.15 indole NH 10.68
Leu^4	W	8.24	4.28	1.46	1.45	0.89 0.82		
	C	8.44	4.26	1.46 1.42	1.53 1.40	[a] 0.80 0.74		
Gln^5	W	8.17	4.30	2.06 1.90	2.29			γNH_2 7.57,6.80

	C	8.02	4.24	1.86 1.75	2.09			γNH_2 7.40,6.74
Leu[6]	W	8.64	4.29	1.70	1.63	0.92 0.87		
	C	8.11	4.14	1.50 1.41	1.53 1.40	[a] 0.80 0.74		
Cys[7]	W	8.15	5.01	3.35 3.27				
	C	8.34	4.67	3.16 3.04				
Pro[8]	W	----	4.29	2.36 1.96	2.13 2.07	3.73 3.66		
	C	----	4.13	2.13 1.73	1.88 1.76	3.64 3.31		
Ala[9]	W	8.15	4.47	1.41				
	C	8.02	4.24	1.23				
Cys[10]	W	7.85	----	3.46 3.13				
	C	7.50	4.48	3.38 2.90				
Pro[11]	W	----	4.37	2.24 1.81	2.03	3.84 3.64		
	C	----	4.26	2.01 1.68	1.83	3.67 3.50		
Nle[12]	W	8.19	4.23	1.59 1.48	1.20 1.10	1.13	0.74	
	C	7.96	4.11	1.46 1.40	1.51 1.41	1.15 1.13	0.75	
Tyr[13]	W	7.97	4.54	3.08 2.93				$C_{2,6}H$ 7.11 $C_{3,5}H$ 6.79
	C	7.86	4.34	2.89 2.78				$C_{2,6}H$ 6.95 $C_{3,5}H$ 6.60

[a]These resonances could not be assigned to individual residues of duplicated amino acids.

TABLE 6

^{1}H Assignments for cyclo^{7,10}[Cys^7,Cys^{10},Nle^{12}]α-factor in Water (W) and in DMSO\water (80:20) (C).

Residue		NH	αCH	βCH	γCH	δCH	εCH	Other
Trp^1	W	----	4.23	3.21 3.14				ring protons 7.63,7.19 7.21,7.47 7.07 indole NH 10.01
	C	----	----	3.10 2.96				ring protons 7.39,6.63 6.92,7.29 7.08 indole NH 10.72
His^2	W	8.32	4.61	3.10 3.01				C_2H 8.49 C_4H 7.12
	C	8.71	4.56	3.02 2.94				C_2H 8.58 C_4H 7.14
Trp^3	W	8.06	4.58	3.25 3.15				ring protons 7.48,7.05 7.22,7.43 7.24 indole NH 10.12
	C	8.23	4.54	3.17 2.96				ring protons 7.62,6.97 7.05,7.33 7.13 indole NH 10.69
Leu^4	W	8.22	4.30	1.48	1.48	0.81 0.75		
	C	8.47	4.26	1.42	1.52	[a] 0.80 0.72		
Gln^5	W	8.17	4.34	2.06 1.93	2.31			γNH_2 7.63,6.88

	C	8.01	4.24	1.88 1.76	2.10			γNH_2 7.47,6.82
Leu[6]	W	8.60	4.36	1.68 1.58	1.63	0.88 0.82		
	C	8.14	4.15	1.52 1.44	1.53	* 0.80 0.72		
Cys[7]	W	8.11	4.91	3.36 3.13				
	C	8.25	4.62	3.27 2.78				
Pro[8]	W	----	4.40	2.31 2.18	1.98	3.68		
	C	----	4.20	2.07 1.74	1.96 1.77	3.52 3.38		
Gly[9]	W	8.73	3.95					
	C	8.59	3.71 3.57					
Cys[10]	W	7.89	----	3.38 3.26				
	C	7.48	4.39	3.29 3.01				
Pro[11]	W	----	4.41	2.24 2.04	2.02 1.85	3.86 3.64		
	C	----	4.27	2.01 1.70	1.84	3.67 3.50		
Nle[12]	W	8.18	4.24	1.60 1.53	1.22 1.10	1.15	0.74	
	C	8.00	4.14	1.43 1.38	1.52 1.40	1.15 1.13	0.74	
Tyr[13]	W	7.92	4.62	3.10 2.95				$C_{2,6}H$ 7.12 $C_{3,5}H$ 6.80
	C	7.88	4.34	2.88 2.76				$C_{2,6}H$ 6.96 $C_{3,5}H$ 6.61

*These resonances could not be assigned to individual residues of duplicated amino acids.

Conformational Analysis of the Linear α-Factor Analogues in Solution:

In the NOESY and ROESY spectra of the [L-Ala^9] and [D-Ala^9] analogues of α-factor in both aqueous and DMSO solution strong Lys$^7{}_{\alpha CH}$-Pro$^8{}_{\beta CH}$ and Gln$^{10}{}_{\alpha CH}$-Pro$^{11}{}_{\beta CH}$ NOESY connectivities were observed. These connectivities indicate that the Lys^7-Pro^8 and Gln^{10}-Pro^{11} amide bonds are predominantly *trans* (83). A *cis* amide bond is indicated by the presence of additional resonances in the spectrum, a sequential αCH-αCH NOE connectivity, or by exchange cross-peaks in the NOESY spectrum. No evidence for a *cis* proline bond, as indicated by the above criteria was observed for the [D-Ala^9] and [L-Ala^9] analogues in either aqueous or DMSO solutions. This result is consistent with the findings of Jelicks *et al.* on the α-factor (78).

All of the expected αCH_i-NH_{i+1} NOE connectivities were observed in the NOESY and ROESY spectra of the [D-Ala^9] analogue in aqueous solution. A prominent feature of the NOESY and ROESY spectra of the [D-Ala^9]α-factor in water is the very strong cross-peak between the Pro^8 αCH and the Ala^9 NH (Figure 11). This cross-peak is the strongest feature in the αCH-NH region of the ROESY and NOESY spectra of the α-factor. Another significant feature is the Ala$^9{}_{\alpha CH}$-Gln$^{10}{}_{NH}$ NOE cross-peak, which has a very weak intensity. There are only two other sequential

αCH_i-NH_{i+1} NOE connectivities in the NOESY spectrum (Figure 11a), the $His^{2}{}_{\alpha CH}$-$Trp^{3}{}_{NH}$ and $Met^{12}{}_{\alpha CH}$-$Tyr^{13}{}_{NH}$ cross-peaks, which have intensities as weak as that of the $Ala^{9}{}_{\alpha CH}$-$Gln^{10}{}_{NH}$ NOESY connectivity. Both the His^{2}-Trp^{3} and Met^{12}-Tyr^{13} residue pairs are located at the termini of the peptide. Residues located at the termini of a peptides may have significantly shorter correlation times (τ_c) relative to centrally located residues and therefore, may exhibit relatively weaker NOE intensities (144).

In the rotating-frame, cross-relaxation is less sensitive to short correlation times than it is in the laboratory frame (127,130). Consequently, it is expected that cross-peaks that are weak in the NOESY spectrum due to short correlation time effects will have significantly stronger intensities in the ROESY spectrum. This was found to be the case for the $His^{2}{}_{\alpha CH}$-$Trp^{3}{}_{NH}$ and the $Met^{12}{}_{\alpha CH}$-$Tyr^{13}{}_{NH}$ connectivities, which both show a significant increase in the ROESY spectrum (Figure 11b). In contrast the intensity of the $Ala^{9}{}_{\alpha CH}$-$Gln^{10}{}_{NH}$ cross-peak remains weak in the ROESY spectrum. This result indicates that the weak intensity of the $Ala^{9}{}_{\alpha CH}$-$Gln^{10}{}_{NH}$ NOESY cross-peak is not the result of an unfavorable correlation time.

The strong intensity of the $Pro^{8}{}_{\alpha CH}$-$Ala^{9}{}_{NH}$ cross-peak and the weak intensity of the $Ala^{9}{}_{\alpha CH}$-$Gln^{10}{}_{NH}$ NOE connectivity are consistent with a type II β-turn

FIGURE 11: The αCH-NH region of the a) 400 ms NOESY spectrum; b)250 ms ROESY spectrum; of the [D-Ala^9]α-factor in water (25°C; pH 4.6).

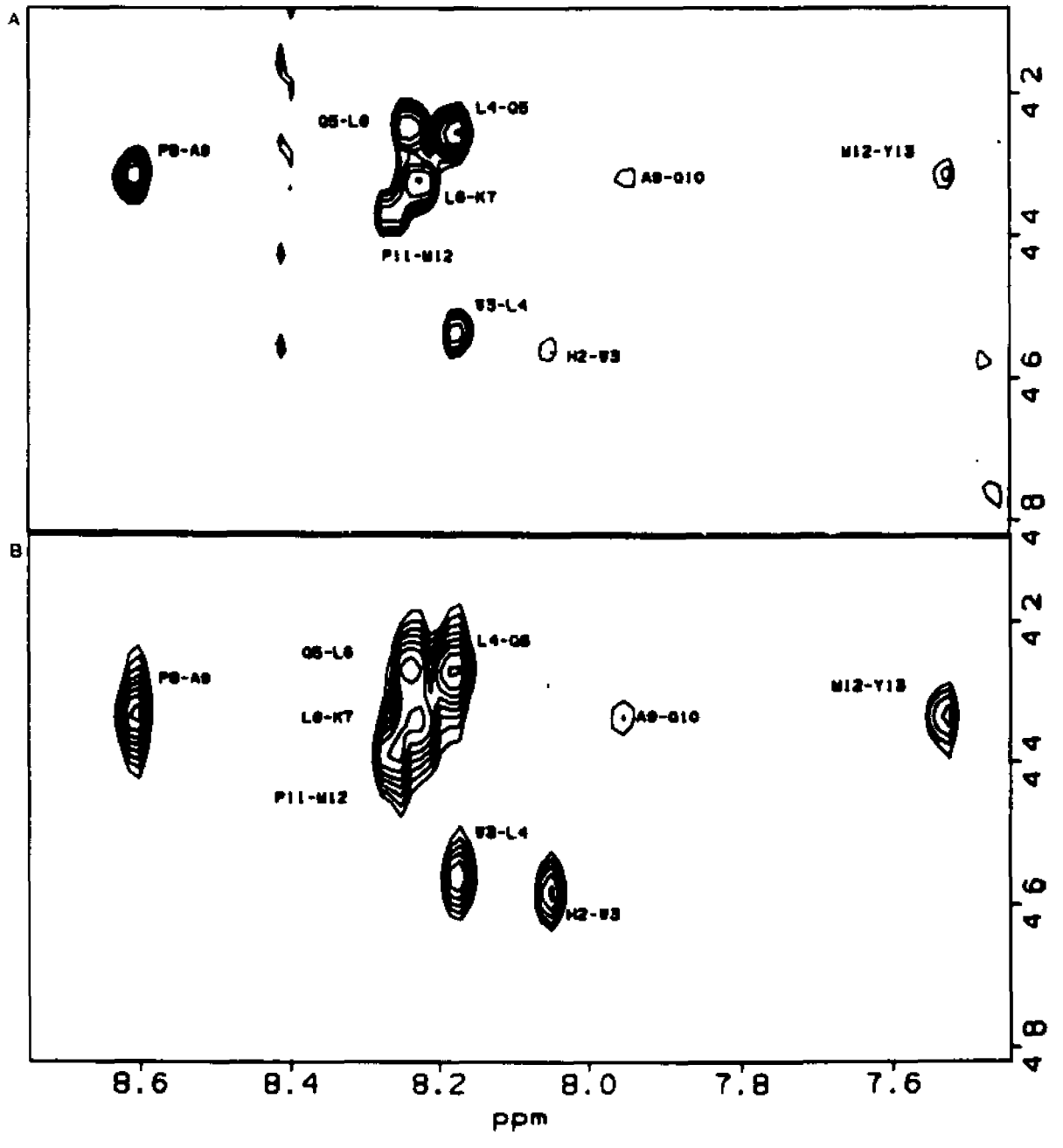
A
B
P8-A9
Q5-L6
L4-Q5
L6-K7
P11-M12
A9-Q10
M12-Y13
V3-L4
H2-V3
8.6
8.4
8.2
8.0
7.8
7.6
ppm
4.2
4.4
4.6
4.8

centered about the Pro[8] and D-Ala[9] residues (3,83,145). A non-sequential αCH_{i+1}-NH_{i+3} NOE connectivity between Pro[8] and Gln[10] would be expected for this β-turn conformation (3,83,145). However, this cross-peak was not observed. If present, the $Pro^{8}_{\alpha CH}$-Gln^{10}_{NH} cross-peak would be obscured due to spectral overlap with the $Ala^{9}_{\alpha CH}$-Gln^{10}_{NH} connectivity. No attempt was made to observe the $Pro^{8}_{\alpha CH}$-Gln^{10}_{NH} cross-peak by α-deuteration of the Ala[9] residue as it was anticipated that the $Pro^{8}_{\alpha CH}$-Gln^{10}_{NH} interaction, which has an internuclear distance of approximately 3.3 Å in a β-turn (see Table 7), would be below the detection limit at the peptide concentrations available to us. In addition to the above αCH_{i}-NH_{i+1} connectivities it is expected that a strong sequential NH-NH connectivity would be observed between the i^{th}+2 and i^{th}+3 residues of a β-turn. The Ala[9]-Gln[10] NH-NH connectivity is the only NH-NH connectivity observed in either the ROESY or NOESY spectrum of the [D-Ala[9]]α-factor in aqueous solution (Figure 12a). The observation of this NH_{i}-NH_{i+1} cross-peak provides further support for the presence of the β-turn suggested by the $Pro^{8}_{\alpha CH}$-Ala^{9}_{NH} and $Ala^{9}_{\alpha CH}$-Gln^{10}_{NH} cross-peaks.

In contrast, no NH-NH cross-peaks are observed in either the NOESY or ROESY spectrum of the [L-Ala[9]]α-factor analogue in aqueous solution (Figure 12b). The αCH-NH region of the NOESY and ROESY spectra of the

TABLE 7

Short (≤5.0 Å) Interproton Distances, in Angstroms, Found in Polypeptide Secondary Structures. Values given are from *Reference 3*.

Distance	α-helix	3_{10}helix	β-Anti-parallel sheet	β-parallel sheet	Type I β-turn[a]	Type II β-turn[a]
$d_{\alpha N}(i,i)$	2.7	2.7	2.8	2.8	2.7/2.8	2.7/2.2
$d_{\beta N}(i,i)$[b]	2.0-3.4	2.0-3.4	2.4-3.7	2.6-3.8	2.0-3.5	2.0-3.4 /3.2-4.0
$d_{\alpha N}(i,i+1)$	3.5	3.4	2.2	2.2	3.4/3.2	2.2/3.2
$d_{NN}(i,i+1)$	2.8	2.6	4.3	4.2	2.6/2.4	4.5/2.4
$d_{\beta N}(i,i+1)$[b]	2.5-3.8	2.9-4.0	3.2-4.2	3.7-4.4	2.9-4.1 /3.6-4.4	3.6-4.4
$d_{\alpha N}(i,i+2)$	4.4	3.8			3.6	3.3
$d_{NN}(i,i+2)$	4.2	4.1			3.8	4.3
$d_{\alpha N}(i,i+3)$	3.4	3.3			3.1-4.2	3.8-4.7
$d_{\beta N}(i,i+3)$[b]	2.5-4.4	3.1-5.1				
$d_{\alpha N}(i,j)$			3.2	3.0		
$d_{NN}(i,j)$			3.3	4.0		
$d_{\alpha\alpha}(i,j)$			2.3	4.8		

[a]For turns treat residue i as residue 2/residue 3, except for $d_{\alpha N}(i,i+3)$, where i is residue 1. [b]Distances involving β-protons are the lower and upper limits to the range of distances possible. A CH_2 fragment is assumed and the nearest proton of the pair is considered.

FIGURE 12: The NH-NH region of the 400 ms NOESY spectrum of the a) [D-Ala^9]α-factor; b) [L-Ala^9]α-factor; in water (25°C; pH 4.6). Arrow indicates expected position of Ala^{9}_{NH}-Gln^{10}_{NH} cross-peak.

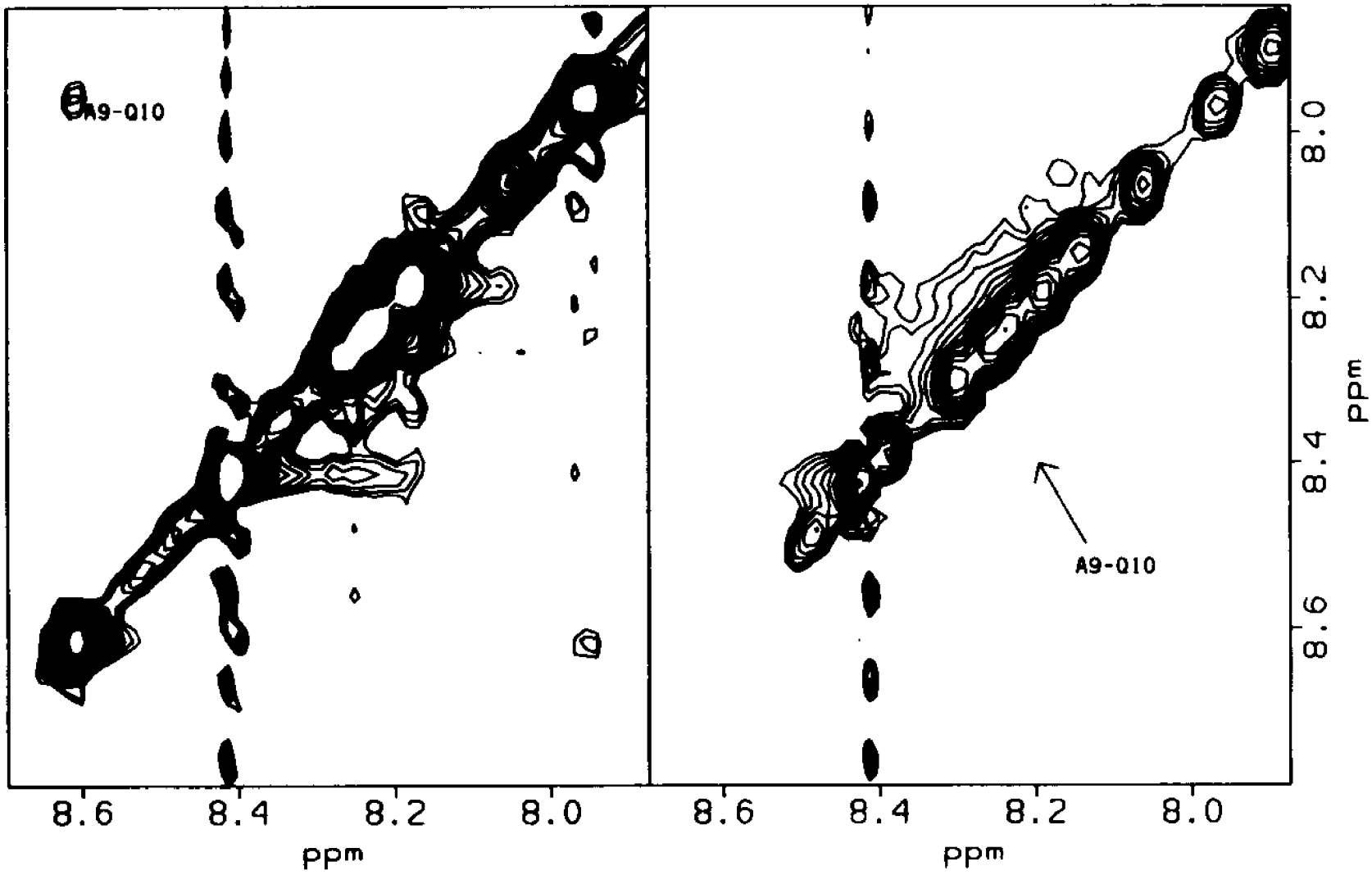
A9-Q10
8.6
8.4
8.2
8.0
ppm
8.6
8.4
8.2
8.0
ppm
A9-Q10

FIGURE 13: The αCH-NH region of the a) 250 ms ROESY spectrum; b) 400 ms NOESY spectrum; of the [L-Ala^{9}]α-factor in water (25°C; pH 4.6).

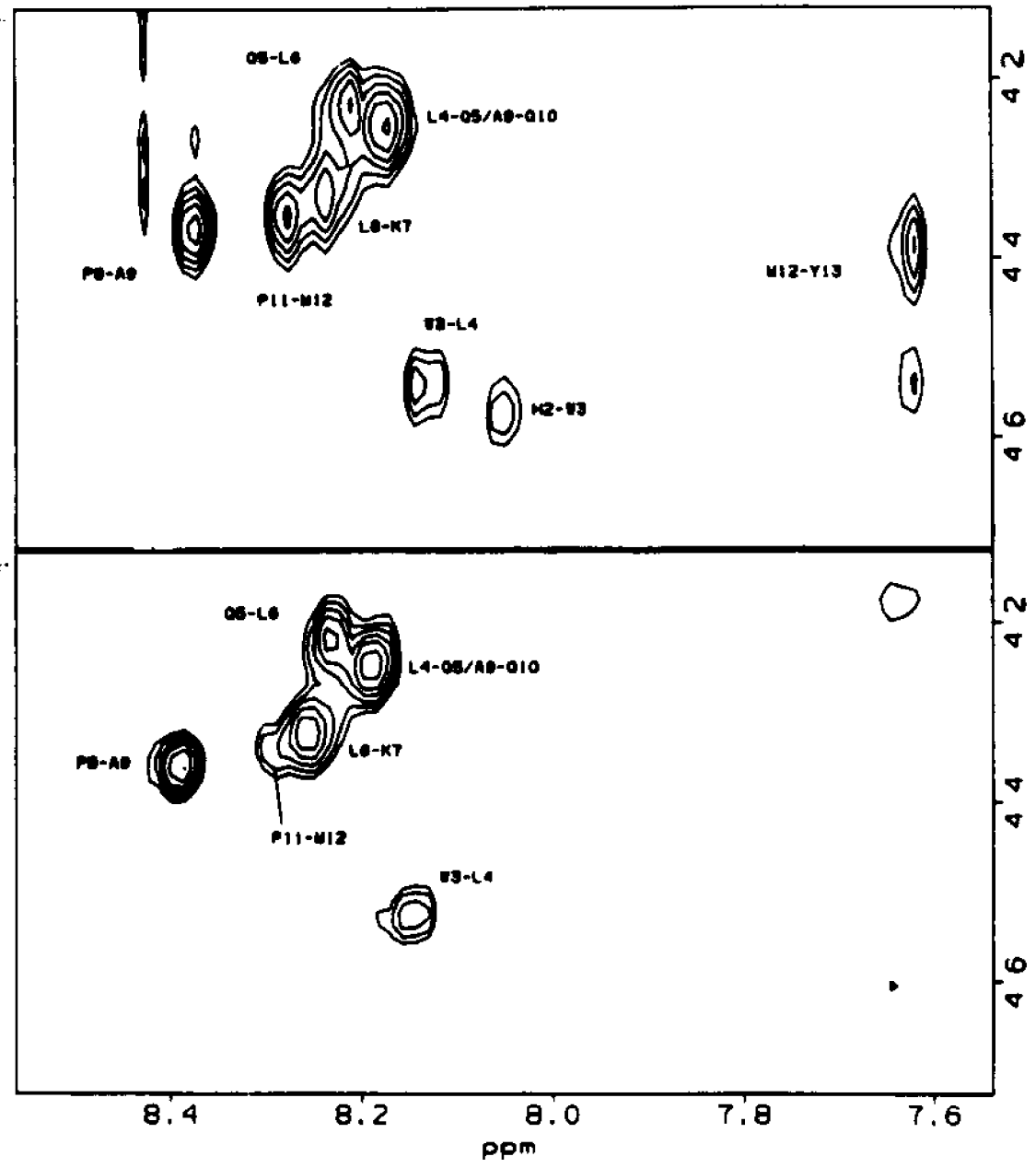
G5-L6
L4-G5/A9-G10
L6-K7
P8-A9
P11-M12
V3-L4
K2-V3
M12-Y13
G5-L6
L4-G5/A9-G10
L6-K7
P8-A9
P11-M12
V3-L4
4.2
4.4
4.6
8.4
8.2
8.0
7.8
7.6
ppm

[L-Ala^9]α-factor does not suggest the presence of a predominant secondary structure (Figure 13). In the NOESY and ROESY spectra of the [L-Ala^9]α-factor analogue in aqueous solution the Pro$^8{}_{\alpha CH}$-Ala$^9{}_{NH}$ cross-peak is of similar intensity to that of the Gln$^5{}_{\alpha CH}$-Leu$^6{}_{NH}$ and Pro$^{11}{}_{\alpha CH}$-Met$^{12}{}_{NH}$ connectivities. The spectral overlap of the Leu$^4{}_{\alpha CH}$-Gln$^5{}_{NH}$ and Ala$^9{}_{\alpha CH}$-Gln$^{10}{}_{NH}$ cross-peaks precludes an estimation of the intensity of the latter peak. The absence of NH-NH cross-peaks (Figure 12b), suggests the absence of a highly populated compact conformation in the [L-Ala^9]α-factor.

The Met$^{12}{}_{\alpha CH}$-Tyr$^{13}{}_{NH}$ cross-peak is absent in the 400 ms NOESY spectrum of [L-Ala^9]α-factor (Figure 13b). The His$^2{}_{\alpha CH}$-Trp$^3{}_{NH}$ connectivity is not shown in Figure 13b due to its extremely weak intensity. The absence of the Met$^{12}{}_{\alpha CH}$-Tyr$^{13}{}_{NH}$ cross-peak and the extremely weak intensity of the His$^2{}_{\alpha CH}$-Trp$^3{}_{NH}$ cross-peak indicates that these connectivities experience shorter effective correlation times relative to all other αCH_i-NH_{i+1} moieties in either the [D-Ala^9]- or [L-Ala^9]α-factor (3). Shorter correlation times have been reported for peptides in a "random coil" state relative to when these peptides adopt stable conformations (144,146). Therefore, the shorter correlation times experienced by the terminal residues of the [L-Ala^9] analogue relative to those of the [D-Ala^9]α-factor is consistent with the [L-Ala^9] analogue being

less structured than the [D-Ala^9]α-factor.

In DMSO all of the αCH_i-NH_{i+1} NOE connectivities are observed in the NOESY spectrum of the [D-Ala^9]α-factor (Figure 14). As was found in aqueous solution the Pro$^8{}_{\alpha CH}$-Ala$^9{}_{NH}$ cross-peak is observed to have a very strong intensity while the Ala$^9{}_{\alpha CH}$-Gln$^{10}{}_{NH}$ connectivity is relativity weak. This result suggests that in DMSO residues 7-10 of the [D-Ala^9]α-factor adopt a Type II β-turn.

For the [L-Ala^9]α-factor in DMSO the spectral overlap in the NOESY spectrum is severe and the Leu^6-Lys^7, Pro^8-Ala^9, Pro^{11}-Met^{12}, and Met^{12}-Tyr^{13} αCH_i-NH_{i+1} NOE connectivities form a single, coalesced cross-peak (Figure 15). Although no information about the intensity of the Pro$^8{}_{\alpha CH}$-Ala$^9{}_{NH}$ can be ascertained the Ala$^9{}_{\alpha CH}$-Gln$^{10}{}_{NH}$ cross-peak is very strong (Figure 15). The relative intensity of the Ala$^9{}_{\alpha CH}$-Gln$^{10}{}_{NH}$ cross-peak is significantly stronger than would be expected if the Pro^8 and Ala^9 residues were involved in a β-turn (3,83,145). The presence of the His$^2{}_{\alpha CH}$-Trp$^3{}_{NH}$ and Met$^{12}{}_{\alpha CH}$-Tyr$^{13}{}_{NH}$ cross-peaks in the NOESY spectra of the [L-Ala^9]α-factor in DMSO is presumably due the greater viscosity of DMSO relative to water, which would lead these interactions to have longer effective correlation times.

All possible sequential NH-NH cross-peaks, except

FIGURE 14: The αCH-NH region of the 400 ms NOESY spectrum of the [D-Ala^9]α-factor in DMSO (25°C).

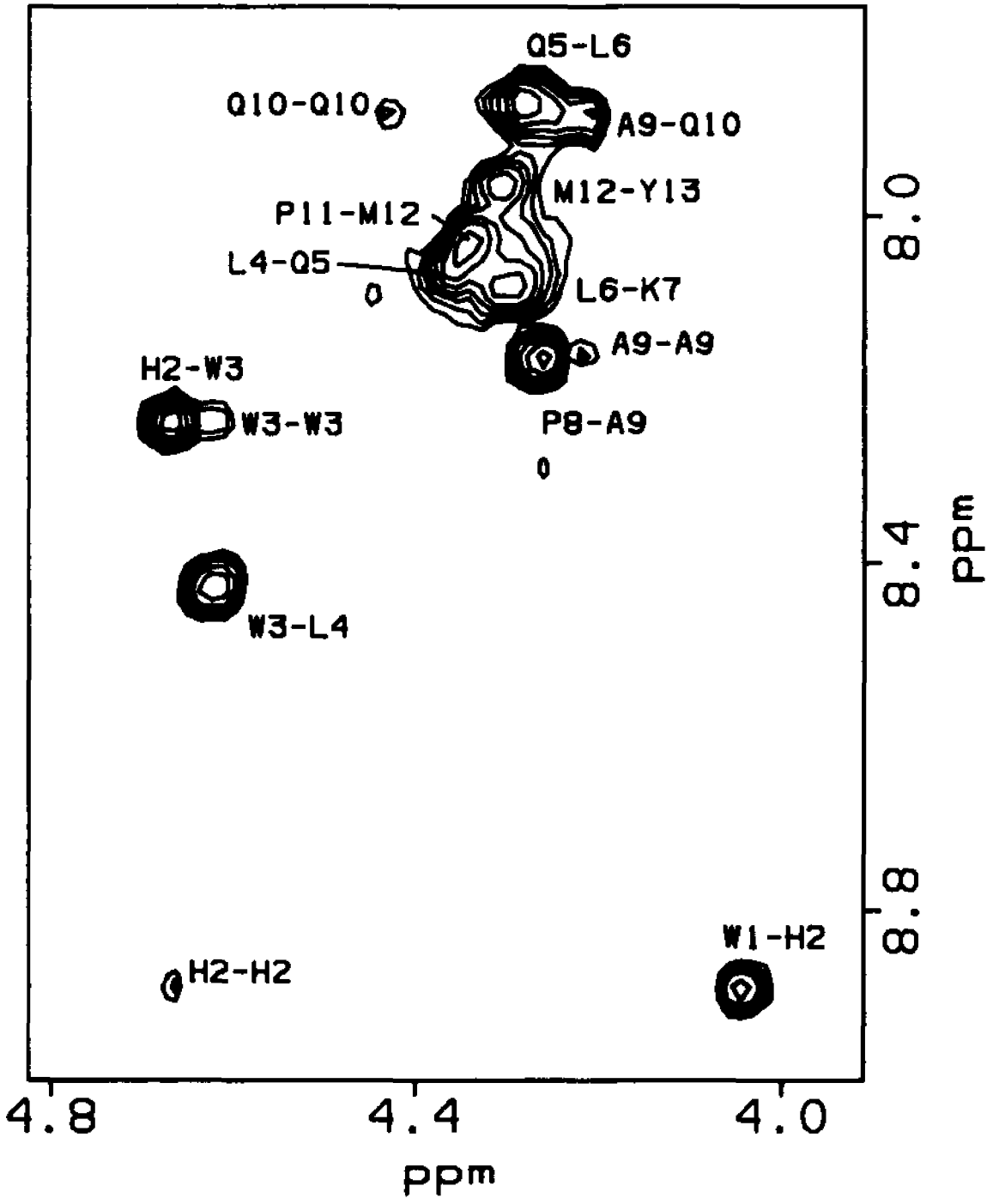
Q5-L6
Q10-Q10
A9-Q10
M12-Y13
P11-M12
L4-Q5
L6-K7
A9-A9
H2-W3
W3-W3
P8-A9
W3-L4
W1-H2
H2-H2
8.0
8.4
8.8
ppm
4.8
4.4
4.0
ppm

FIGURE 15: The αCH-NH region of the 400 ms NOESY spectrum of the [L-Ala^{9}]α-factor in DMSO (25°C).

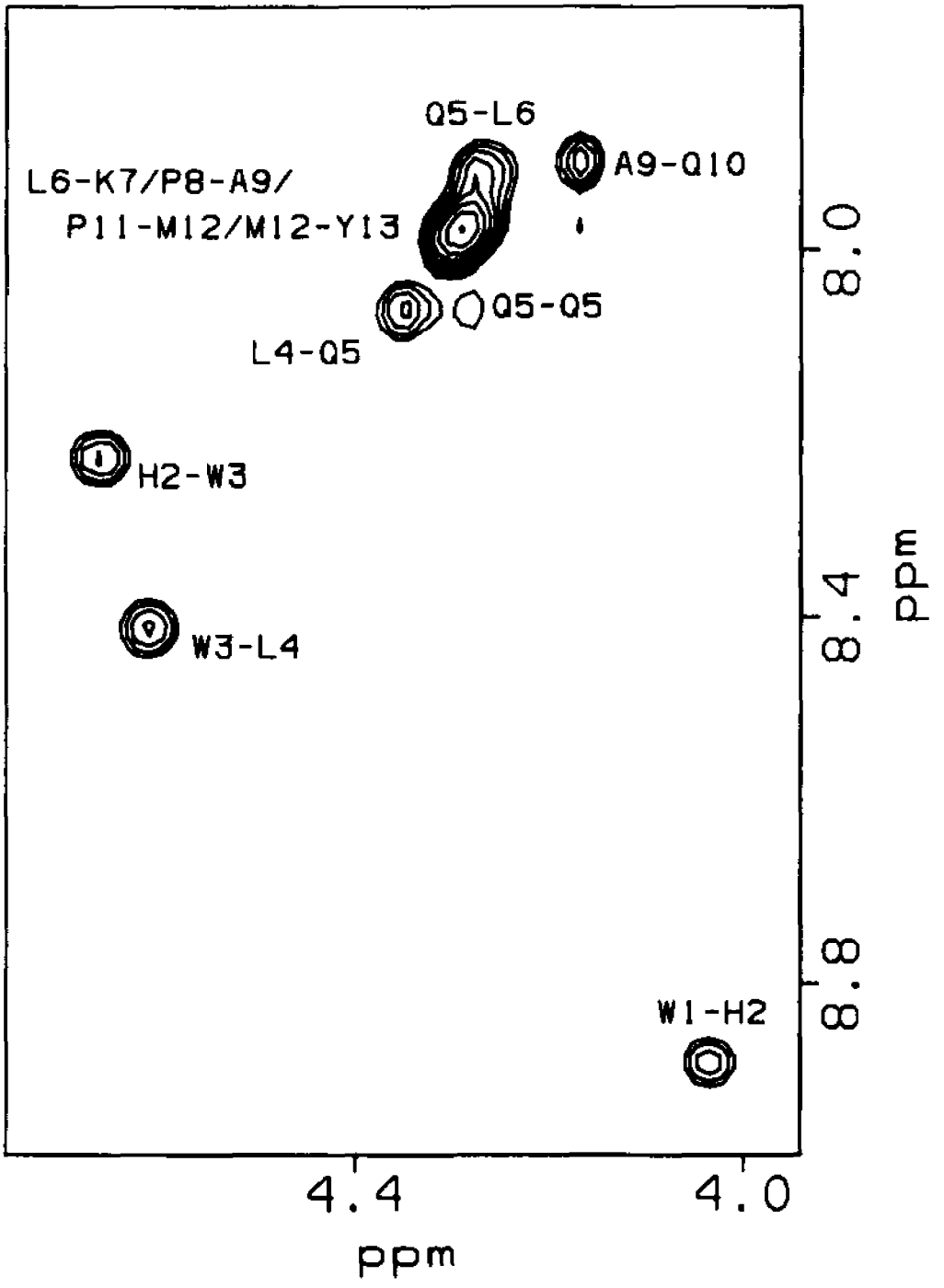
Q5-L6
A9-Q10
L6-K7/P8-A9/
P11-M12/M12-Y13
Q5-Q5
L4-Q5
H2-W3
W3-L4
W1-H2
8.0
8.4
8.8
ppm
4.4
4.0
ppm

FIGURE 16: The NH-NH region of the 400 ms NOESY spectrum of the a) [D-Ala^9]α-factor; b) [L-Ala^9]α-factor; in DMSO (25°C).

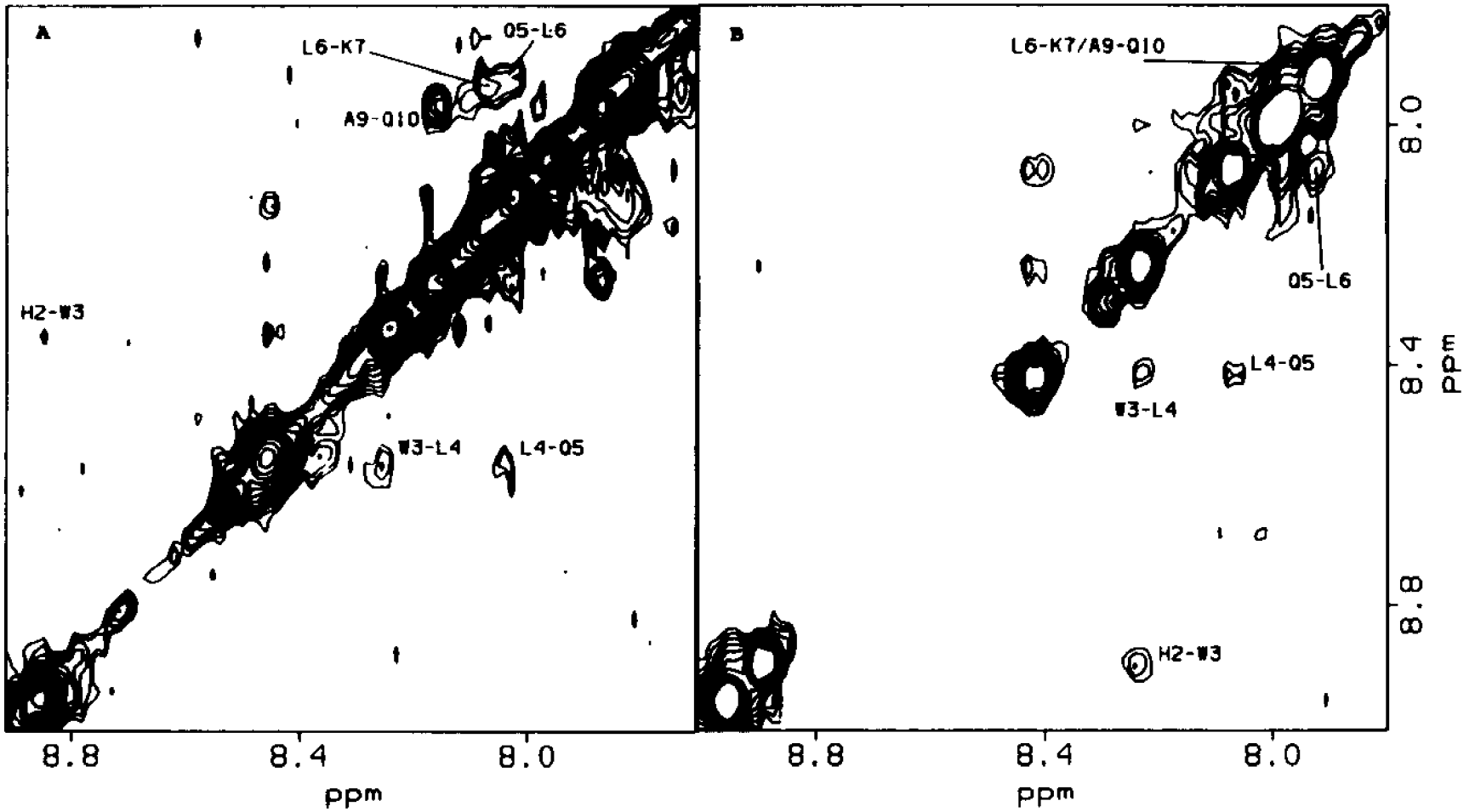
A
L6-K7
O5-L6
A9-Q10
H2-W3
W3-L4
L4-O5
8.8
8.4
8.0
ppm
B
L6-K7/A9-Q10
O5-L6
L4-O5
W3-L4
H2-W3
8.0
8.4
8.8
ppm

for the Met[12]-Tyr[13] NH-NH cross-peak are observed in the NOESY spectra of both the [D-Ala[9]] and [L-Ala[9]] analogues in DMSO (Figure 16). The Met[12]-Tyr[13] NH-NH connectivity in both analogues would be hidden by the diagonal, if present. The absence of long range αCH_i-NH_{i+3}, αCH_i-βCH_{i+3}, αCH_i-NH_{i+4}, or αCH_i-NH_{i+2} NOE connectivities suggests that the observed NH-NH cross-peaks are associated with predominately unstructured peptide segments (147). However, the intensity of the Ala[9]-Gln[10] NH-NH connectivity in the spectra of the [D-Ala[9]]α-factor (Figure 16a) is significantly stronger than those of all other NH-NH cross-peaks and supports the presence in this peptide of a Type II β-turn conformation centered about residues 8 and 9 (3,83,145).

The temperature dependencies of the amide proton chemical shifts (NH $d\delta/dT$) were determined over the range 19-49°C in DMSO and 10-38°C in water (Table 8). The Gln[10] in the [D-Ala[9]] analogue in water has a NH $d\delta/dT$ of -3.6 ppb/K. This is significantly lower than the NH $d\delta/dT$ exhibited by other residues in the [D-Ala[9]] peptide and is less than half the magnitude of the $d\delta/dT$ for the corresponding resonance in the [L-Ala[9]] peptide (-8.2 ppb/K). The relatively low Gln[10] NH $d\delta/dT$ clearly indicates that this proton is solvent shielded to a large

TABLE 8

Amide proton temperature coefficients for the linear α-factor peptides in DMSO and in water. The values reported in ppb/K.

	[D-Ala^9]		[L-Ala^9]	
NH	DMSO	water	DMSO	water
His^2	-4.3	---	-4.5	---
Trp^3	-3.5	-7.3	-4.0	-7.5
Leu^4	-6.1	-5.9[a]	-6.6	-5.4
Gln^5	-4.0	-5.9[a]	-4.7	-5.5
Leu^6	-4.6	-8.6	-4.3	-8.2
Lys^7	-5.2	-7.0	-4.7	-7.7
Ala^9	-5.4	-8.0	-3.7	-8.2
Gln^{10}	-3.3	-3.6	-5.0	-8.2
Met^{12}	-4.2	-7.9	-6.2	-8.0
Tyr^{13}	-5.4	-4.3	-6.2	-5.7

[a]resonances were overlapping

TABLE 9

$^3J_{\alpha NH}$ coupling constants values for the linear α-factor analogue peptides at 25°C in DMSO and in water.

	[L-Ala^9]		[D-Ala^9]	
NH	DMSO	water	DMSO	water
His^2	8.1[a]	---	7.3	---
Trp^3	6.9	6.3	6.6	6.2
Leu^4	7.4	6.6	7.7	7
Gln^5	7.7	7	7	7
Leu^6	8.2	6.6	6.9	6
Lys^7	8[b]	6.8	7.1	7
Ala^9	7	5.9	7.6	6.1
Gln^{10}	7.5	7	7.4	6.6
Met^{12}	9[a]	7.0	7	6
Tyr^{13}	9[a]	7.1	7.6	7.0

[a] $^3J_{\alpha NH}$ values measured from high resolution 1-dimensional spectra are reported to the nearest 0.1 Hz.

[b] $^3J_{\alpha NH}$ values measured from DQF-COSY spectra are reported to the nearest Hz.

degree, presumably through intramolecular hydrogen bonding. As in water, the lowest NH $d\delta/dT$ of either peptide in DMSO is found for Gln^{10} of the [D-Ala^9]α-factor. However, the $d\delta/dT$ for the Gln^{10} NH resonance of the [D-Ala^9]α-factor analogue in DMSO (-3.3 ppb/K) is above the range which has been associated with strong hydrogen bonding in this solvent (148,149) and the difference between the NH temperature coefficients of the two peptides is smaller than that found in water.

Where $^3J_{\alpha NH}$ coupling constants could not be measured from high resolution one-dimensional spectra, due to spectral overlap, they were estimated from DQF-COSY spectra zero-filled to a digital resolution of 1.38 Hz/pt in the *F2* dimension. The $^3J_{\alpha NH}$ coupling constants of the [D-Ala^9] and [L-Ala^9] α-factors in DMSO and in water (Table 9) are in the range of 6.6-8.8 and 5.9-7.1, respectively. The $^3J_{\alpha NH}$ coupling constants indicate that both peptides are undergoing rapid conformational averaging (148,149).

<u>Conformational Analysis and Interaction of the Linear α-Factor Analogues with Lipid Vesicles</u>:

The ^{31}P spectrum of a 8 mM lipid solution at 40°C, prepared as unilamellar vesicles (see Materials and Methods), showed a single, apparently isotropic peak. In

the presence of 0.5 mM $PrCl_3$ (shift reagent) the ^{31}P spectrum consisted of two peaks (data not shown). The ratio of the two peaks was approximately 2:1. This is approximately the ratio expected for lipid in the outer leaflet relative to the inner leaflet. The larger peak is shifted downfield relative to the chemical shift of the peak observed prior to the addition of $PrCl_3$, while the chemical shift of the smaller peak is the not shifted by the addition of $PrCl_3$. These results indicate that the larger peak corresponds to the lipid in the outer leaflet and that the lipid solution consists of predominately lipid vesicles. Addition of either the [D-Ala^9]- or [L-Ala^9]α-factor analogues (approximately 2.0 mM peptide) to the lipid solution ($PrCl_3$ present) resulted in an instantaneous intensity increase in the downfield resonance and a corresponding intensity decrease in the non-shifted resonance (data not shown). This result indicates that the [D-Ala^9]- or [L-Ala^9]α-factor analogues interact with unilamellar lipid vesicles in a manner that causes them to become leaky. Naider *et al.* (150) reported that addition of α-factor lead to a broadening of the resonance corresponding to the outer leaflet. This suggests that the [D-Ala^9] and [L-Ala^9] analogues have stronger interaction with lipid than the native pheromone. Based on the residual of the non-shifted resonance it would appear that not all of the lipid

vesicles have been induced to leak. In addition, none of the lipid:peptide samples exhibited visual evidence of aggregation for a minimum of 72 hours. Similar results were observed for the interaction of the synthetic peptide GALA (WEAALAEALAEALAEHLAEALAEALEALAA) with egg PC (151). Parente *et al.* (151) explain these observations using a model in which 8-12 individual GALA molecules form a transmembrane pore. Once associated in a transmembrane pore the individual GALA peptides are not readily redistributed to other lipid vesicles (151). Therefore, not all of the lipid vesicles are induced to leak. Although it is possible that the [D-Ala^9] and [L-Ala^9]α-factor peptides interact with DPPC vesicles in this manner the results of TRNOE experiments (*vide infra*) indicate that the majority of the α-factor analogues are in fast exchange between the lipid-bound and free states.

The ^{1}H resonances for both the [D-Ala^9] and [L-Ala^9] analogues broadened upon addition of lipid vesicles. However, the chemical shifts did not significantly change relative to those of the peptides in the absence of lipid vesicles. Similar results were obtained for enkephalin analogues (26) and the α-factor (27,77) in the presence of lipid. Only one peak was observed for each peptide resonance and the resonances sharpened with increasing temperature. One interpretation of these results is that the exchange rate was fast on the chemical shift time

scale. This conclusion was confirmed by the results of two-dimensional transfer NOE (TRNOESY) experiments, the success of which depends on a fast exchange rate (see Chapter II).

TRNOESY experiments were performed on samples of 8 mM DPPC:4 mM peptide and 8 mM DPPC:2 mM peptide. Unilamellar vesicles are expected to have an average rotational correlation time (τ_c) of approximately 10^{-6} Rad s^{-1} (152). Therefore, the spin-lattice relaxation and cross-relaxation rates of the peptide resonances will be strongly affected by interaction with lipid vesicles. In order to minimize contributions from the unbound peptide TRNOESY spectra were acquired with mixing times of 75 ms. At this mixing time the spectra of the unbound peptides were almost devoid of cross-peaks and the few cross-peaks that were present were extremely weak (see Figure 17). In contrast, strong cross-peaks were observed in the 75 ms NOESY spectra of the [D-Ala^9]- and [L-Ala^9]α-factor analogues in the presence of DPPC vesicles (Figures 18 & 19). This can also be seen in Figure 20, which shows slices through the NH resonances of Trp^3 and Met^{12} in 75 ms NOESY spectra of the [L-Ala^9]α-factor in the absence (Figure 20a) and presence of lipid vesicles (Figure 20b,c). In the absence of lipid the cross-peaks are extremely weak relative to the diagonal signal (Figure 20a). Upon addition of DPPC vesicles a drastic increase

FIGURE 17: The αCH-NH region of the 75 ms NOESY spectrum of the [D-Ala^9]α-factor in water (25°C; pH 4.6). Note the absence of cross-peaks.

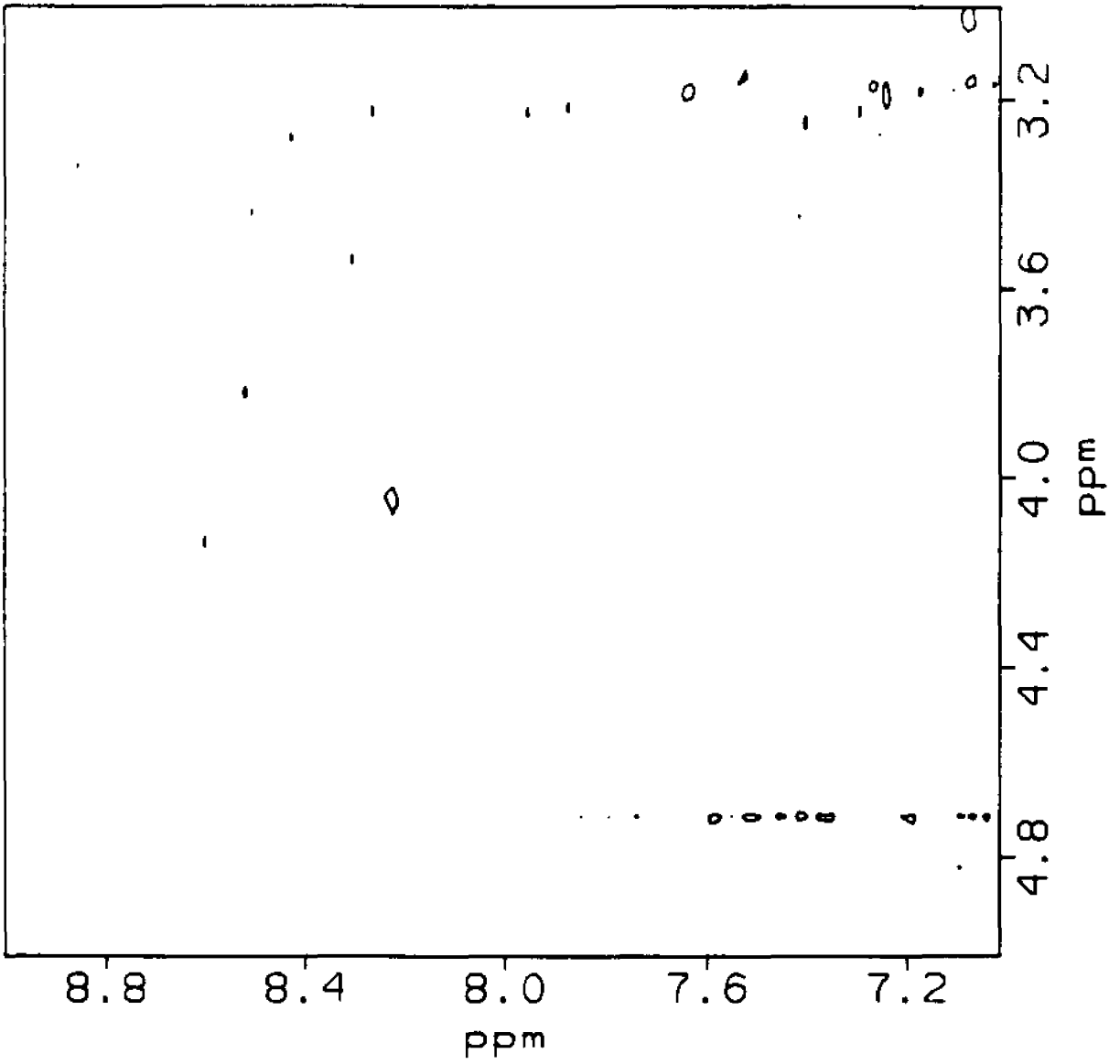
8.8
8.4
8.0
7.6
7.2
ppm
3.2
3.6
4.0
4.4
4.8
ppm

FIGURE 18: The αCH-NH region of the 75 ms TRNOESY spectrum of the [D-Ala^9]α-factor in the presence of lipid 8 mM DPPC:4 mM peptide (25°C; pH 4.6).

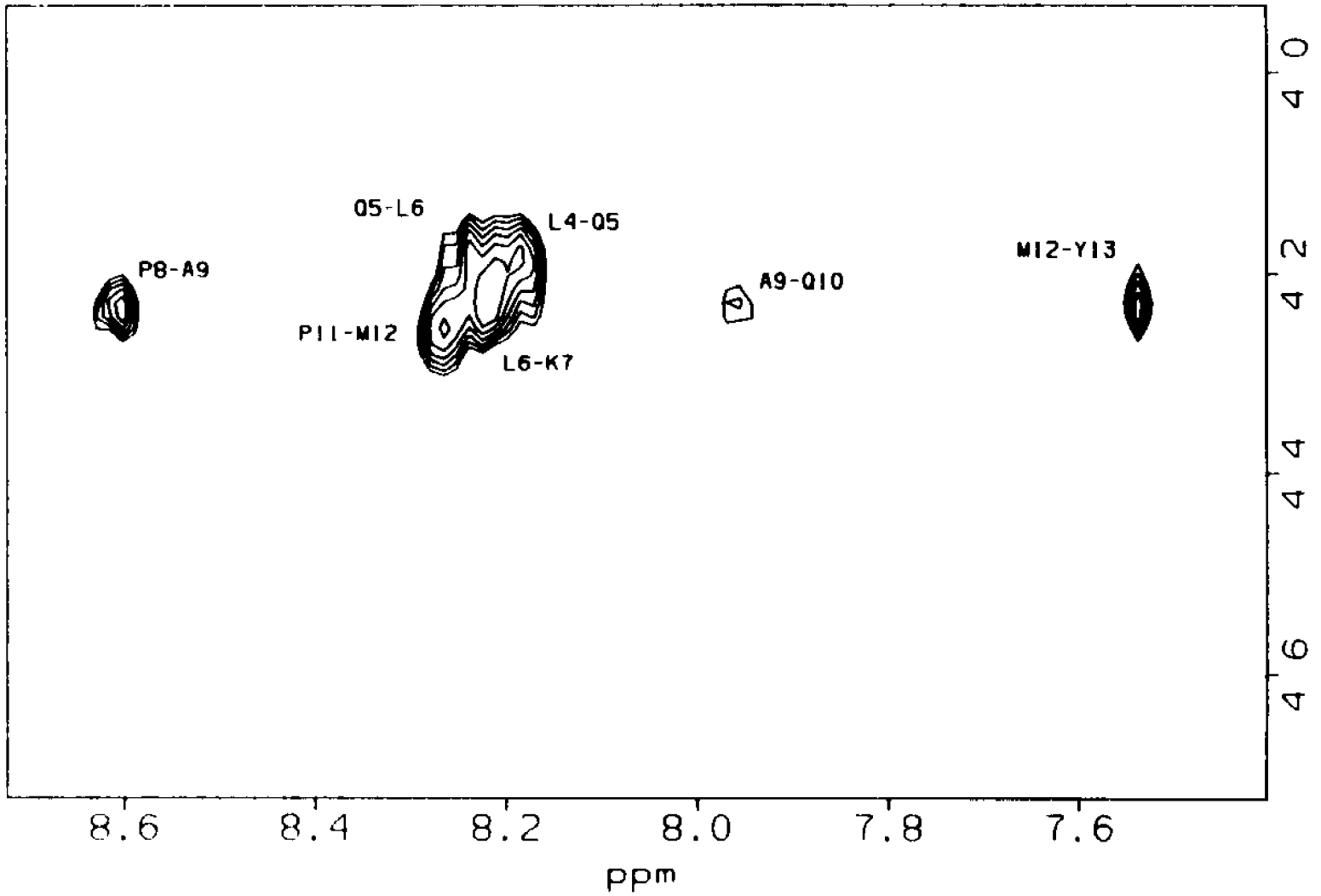
Q5-L6
L4-Q5
P8-A9
A9-Q10
M12-Y13
P11-M12
L6-K7
4.0
4.2
4.4
4.6
8.6
8.4
8.2
8.0
7.8
7.6
ppm

FIGURE 19: The αCH-NH region of the 75 ms TRNOESY spectrum of the [L-Ala^9]α-factor (Top) 8 mM DPPC:4 mM peptide; (bottom) 8 mM DPPC:2 mM peptide (25°C; pH 4.6).

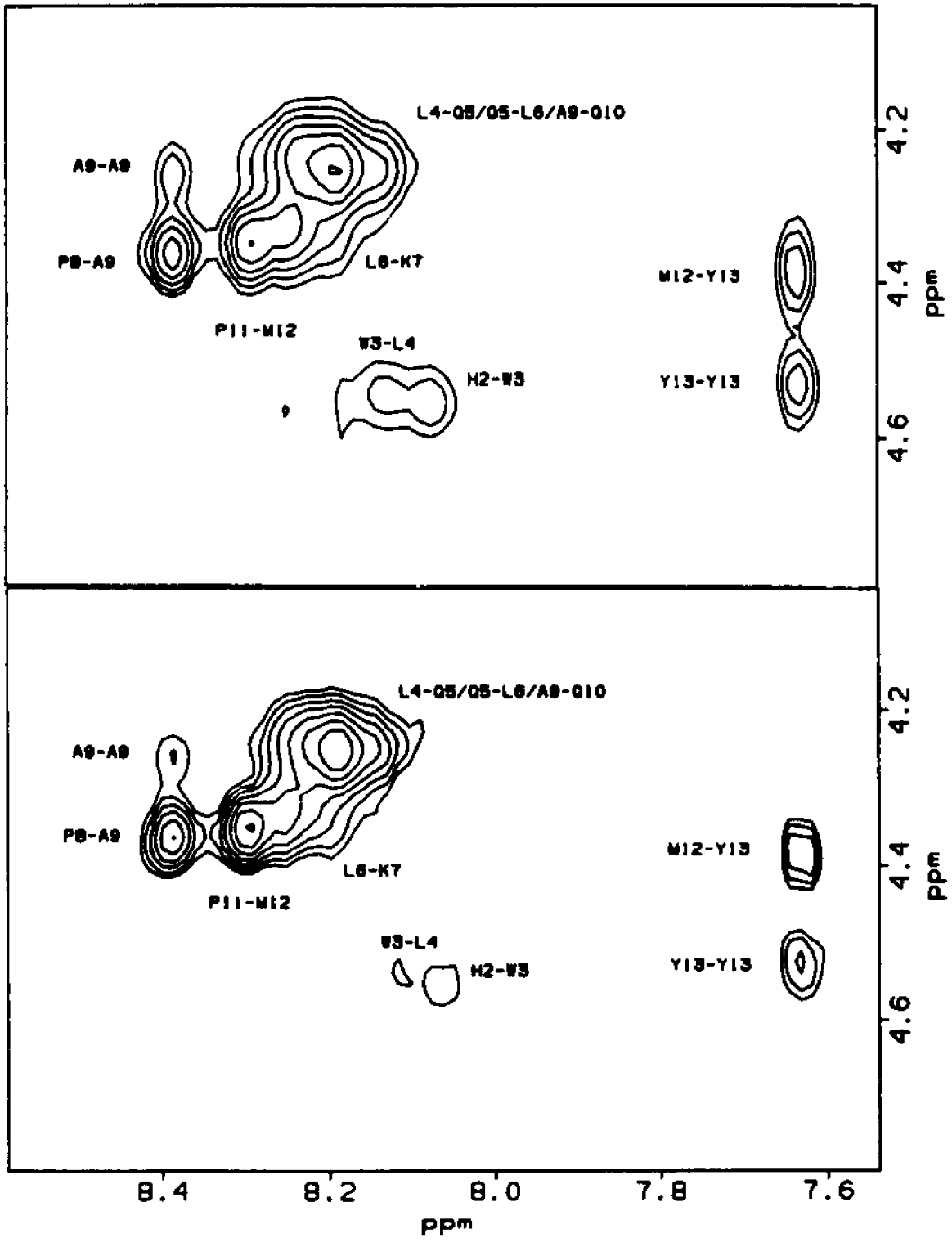
L4-O5/O5-L6/A9-O10
A9-A9
P8-A9
L6-K7
P11-M12
W3-L4
H2-W3
M12-Y13
Y13-Y13
4.2
4.4
4.6
ppm
L4-O5/O5-L6/A9-O10
A9-A9
P8-A9
L6-K7
P11-M12
W3-L4
H2-W3
M12-Y13
Y13-Y13
4.2
4.4
4.6
ppm
8.4
8.2
8.0
7.8
7.6
ppm

FIGURE 20: 1-D slices through the Trp^{3} and Met^{12} NH resonances of the 75 ms TRNOESY spectra of the [L-Ala^{9}]α-factor. a) Peptide in aqueous solution; no lipid present; b) 8 mM DPPC:4 mM peptide; c) 8 mM DPPC:2 mM peptide (25°C; pH 4.6).

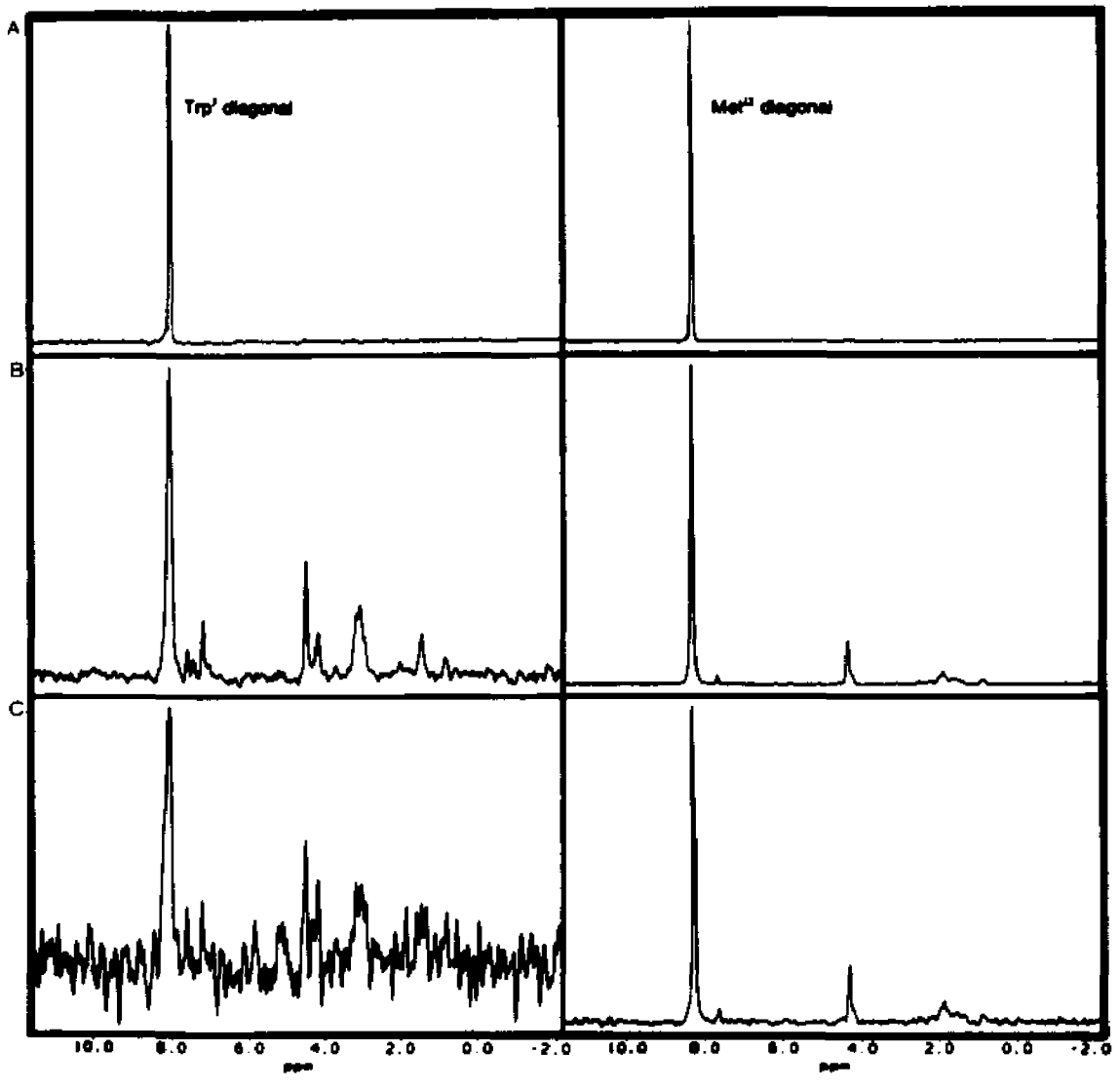
A
B
C
Trp' diagonal
Met[2] diagonal
10.0
8.0
6.0
4.0
2.0
0.0
-2.0
ppm

in the cross-peak intensity relative to the diagonal peak intensity is observed (Figure 20b,c). This result indicates that the cross-relaxation rate (NOE build up rate) for peptide resonances increases in the presence of lipid (153,154). The absence of connectivities in water together with the increase in NOE intensity (increased cross-relaxation rate) in the presence of lipid, indicates that the peptides interact with the lipid and that we are observing a TRNOE phenomenon (120,124). This conclusion is supported by the relative changes observed for the relaxation parameters of residues at the N- and C-terminus of the α-factor analogues (*vide infra*) as the [lipid]/[peptide] was increased.

In the TRNOESY spectrum of the [D-Ala^9] peptide in 8 mM DPPC the Pro$^8{}_{\alpha CH}$-Ala$^9{}_{NH}$ TRNOESY cross-peak is very strong and the Ala$^9{}_{\alpha CH}$-Gln$^{10}{}_{NH}$ TRNOESY cross-peak is weak (Figure 18). These results are consistent with the [D-Ala^9]α-factor maintaining the Type II β-turn upon interaction with the lipid. No evidence for any other predominant conformational feature was observed in the TRNOESY spectra of this peptide. In the 75 ms NOESY spectrum of the [L-Ala^9]α-factor in the presence of lipid the Pro$^8{}_{\alpha CH}$-Ala$^9{}_{NH}$ connectivity is also strong (Figure 19). However, little can be discerned concerning the lipid bound conformation of the [L-Ala^9]α-factor analogue as many of the αCH_i-NH_{i+1} cross-peaks are broadened and form

a single coalesced peak (see Figure 19). For both peptides only the Ala^{9}-Gln^{10} and Met^{12}-Tyr^{13} NH-NH cross-peaks were visible in the NH-NH region of the TRNOESY spectra.

As judged by the signal to noise ratio, the Trp^{3} NH diagonal signal shows a greater decay rate with increased [lipid]/[peptide] ratio, relative to that of the Met^{12} NH diagonal in the [L-Ala^{9}] analogue (Figure 20). Diagonal signals in NOESY spectra decay with a rate equal to the selective spin-lattice relaxation rate, $1/T_1^S$ (3,155, 156). This parameter increases with $\tau_{c\ eff}$ and has been used for monitoring ligand binding (157,158). Due to its dependence on both the cross-relaxation rate and the selective spin-lattice relaxation rate the TRNOE can be used in an analogous manner. As can be seen in Figure 19 the $His^{2}_{\beta CH}$-Trp^{3}_{NH} and $Trp^{3}_{\beta CH}$-Leu^{4}_{NH} TRNOE cross-peaks of the [L-Ala^{9}] analogue exhibited a marked decrease in intensity relative to the $Tyr^{13}_{\beta CH}$-Tyr^{13}_{NH} and $Met^{12}_{\beta CH}$-Tyr^{13}_{NH} TRNOE cross-peaks as the [lipid]/peptide] ratio was increased. The above observations indicate that Trp^{3} and Leu^{4} have a greater spin-lattice relaxation rate than do Met^{12} and Tyr^{13} and is consistent with the N-terminus of the [L-Ala^{9}]α-factor interacting more strongly with the lipid than does the C-terminus of this peptide. This conclusion is in agreement with the findings of Wakamatsu *et al.* on α-factor (80,81).

FIGURE 21: The αCH-NH region of the 75 ms TRNOESY spectrum of the [D-Ala^{9}]α-factor 8 mM DPPC:2 mM peptide (25°C; pH 4.6). Note the absence of the $M^{12}{}_{\alpha CH}$-$Y^{13}{}_{NH}$ cross-peak.

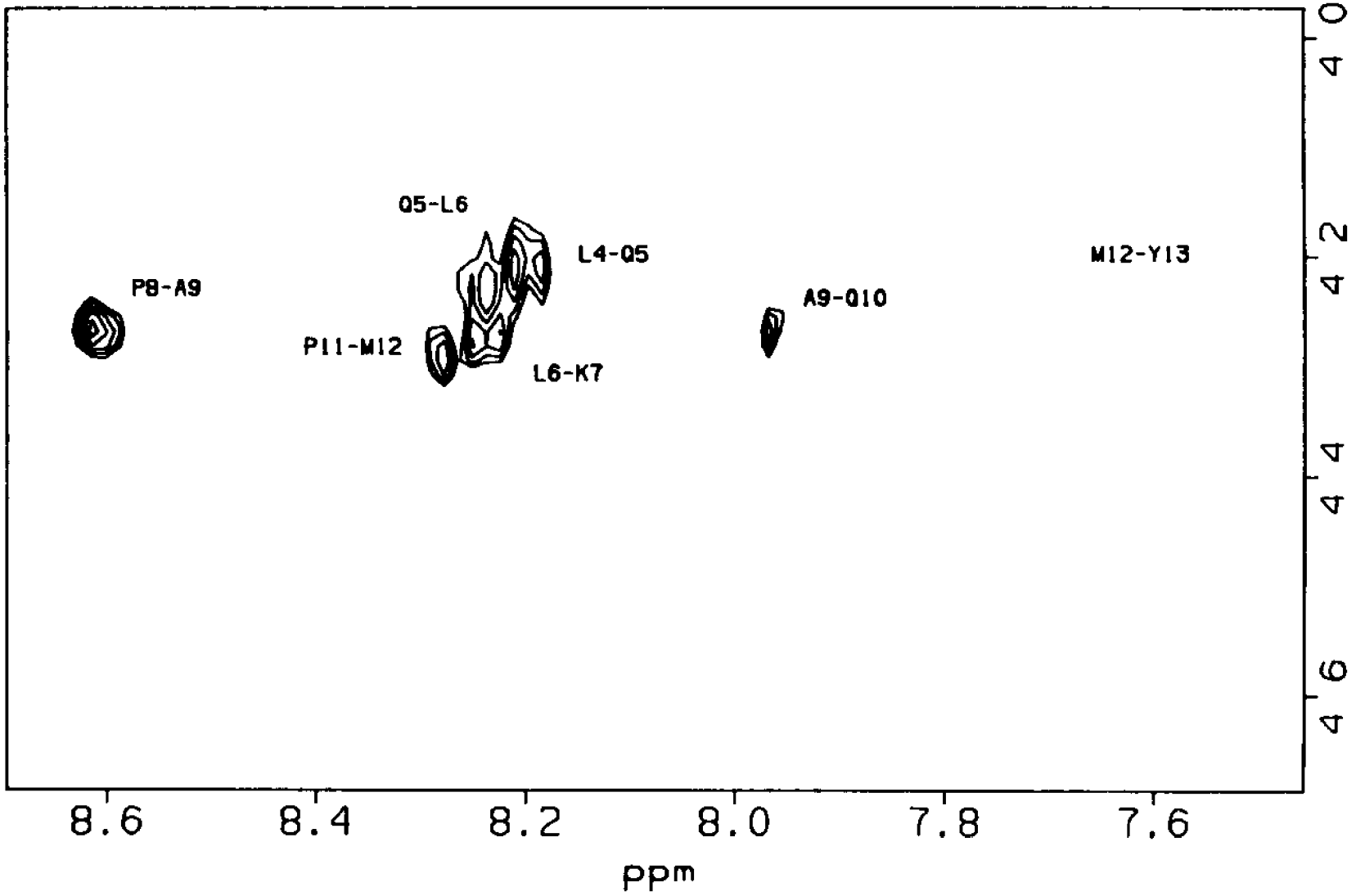
Q5-L6
L4-Q5
M12-Y13
P8-A9
A9-Q10
P11-M12
L6-K7
4.0
4.2
4.4
4.6
8.6
8.4
8.2
8.0
7.8
7.6
ppm

111

FIGURE 22: Aromatic region of a) [D-Ala^{9}]α-factor; b) [L-Ala^{9}]α-factor. Samples are 8 mM DPPC:2 mM peptide. Distortions to the Tyr^{13} $CH_{2,6}$-$CH_{3,5}$ NOESY cross-peak shape are due to the superposition of *zero*-quantum *J*-cross-peaks (25°C; pH 4.6).

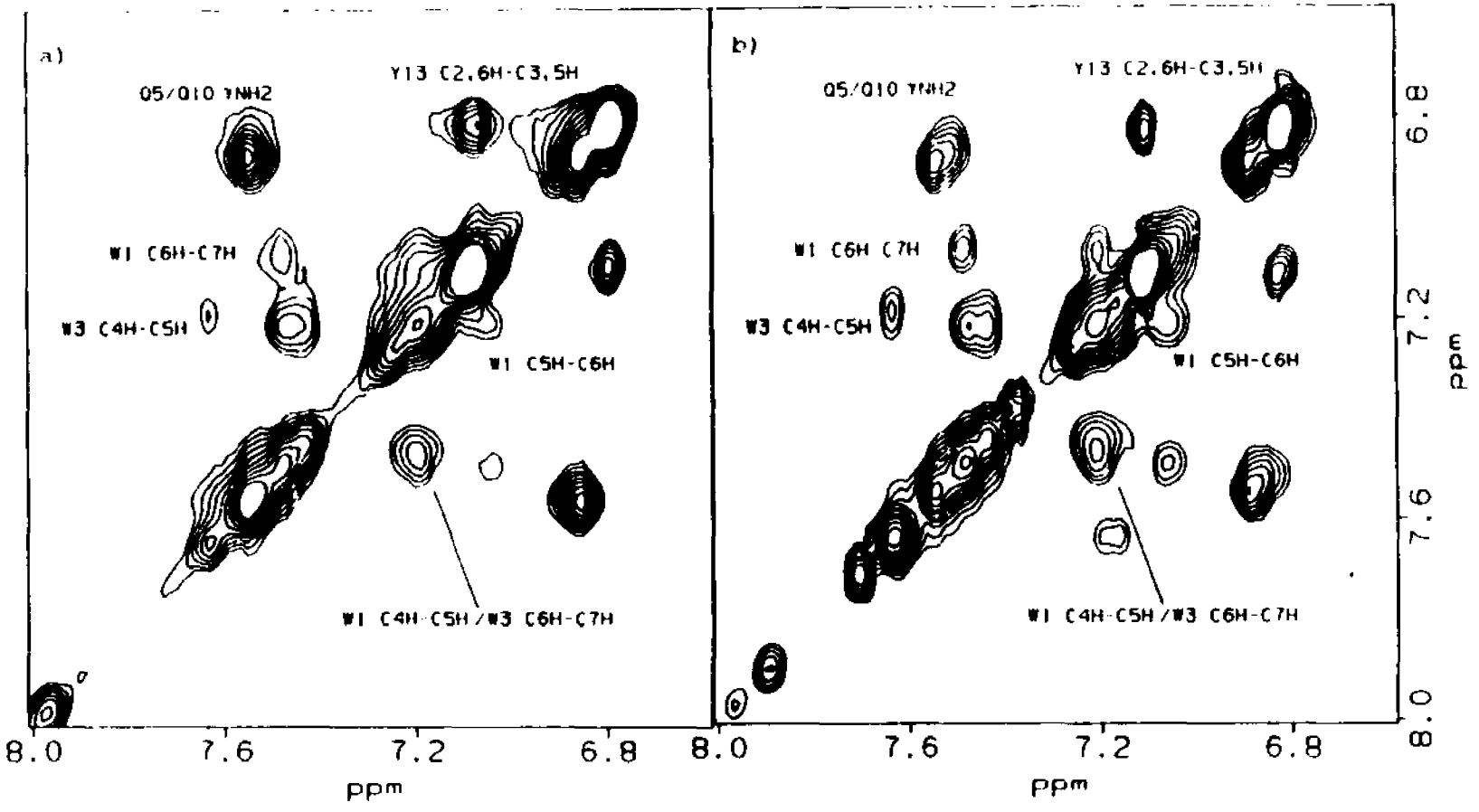
a)
Q5/Q10 γNH2
Y13 C2,6H-C3,5H
W1 C6H-C7H
W3 C4H-C5H
W1 C5H-C6H
W1 C4H-C5H/W3 C6H-C7H
8.0
7.6
7.2
6.8
ppm
b)
Q5/Q10 γNH2
Y13 C2,6H-C3,5H
W1 C6H C7H
W3 C4H-C5H
W1 C5H-C6H
W1 C4H-C5H/W3 C6H-C7H
8.0
7.6
7.2
6.8
ppm

In contrast to the result observed for the [L-Ala^9] analogue the relative intensity of the Met$^{12}_{\beta CH}$-Tyr$^{13}_{NH}$ cross-peak of the [D-Ala^9]α-factor decreases with peptide binding and disappears in the 8 mM DPPC:2 mM peptide TRNOESY spectrum (Figure 21). This result suggests that the C-terminus of the [D-Ala^9] analogue is constrained in the bound state relative to the [L-Ala^9] peptide. This conclusion is further supported by the fact that the Tyr^{13} $CH_{2,6}$-$CH_{3,5}$ NOE cross-peak in the [D-Ala^9]α-factor is stronger relative to the Trp^1 and Trp^3 intra-ring NOE connectivities in the presence of DPPC vesicles than is found for the [L-Ala^9] analogue (Figure 22). Furthermore, distortions to the Tyr^{13} $CH_{2,6}$-$CH_{3,5}$ NOE cross-peak due to the superposition of *zero*-quantum *J*-cross-peaks (117,118) are less pronounced for the [D-Ala^9]α-factor than the [L-Ala^9]α-factor at corresponding peptide concentrations (Figure 22). For both peptides the effects of *zero*-quantum coherence on the Tyr^{13} $CH_{2,6}$-$CH_{3,5}$ NOE cross-peak becomes less significant as the percentage of bound peptide increases. As both the decay rate of *zero*-quantum cross-peaks ($1/T_2^{(0)*}$) and the cross-relaxation rate are sensitive to τ_c (3,117,118) the above results indicate that the C-terminus of the [D-Ala^9] analogue is constrained to a greater extent than that of the [L-Ala^9] peptide when both are in the bound state.

Conformational Analysis of the Cyclic α-Factor Analogues in Aqueous Solution:

Aqueous samples of the cyclo^{7,10}[Cys^{7},Cys^{10},Nle^{12}]-, cyclo^{7,10}[Cys^{7},D-Ala^{9},Cys^{10},Nle^{12}]-, and cyclo^{7,10}[Cys^{7},L-Ala^{9},Cys^{10},Nle^{12}]α-factor analogues were prepared at pH 2.9 as these peptides had poor solubility at higher pH values. The maximum solubility of the cyclo^{7,10}[Cys^{7},D-Val^{9},Cys^{10},Nle^{12}]α-factor was less than 1 mM at all pH's. Therefore, two-dimensional NMR spectroscopy was not attempted for this peptide in aqueous solution. In the 400 ms NOESY spectrum of the cyclo^{7,10}[Cys^{7},D-Ala^{9},Cys^{10},Nle^{12}] peptide in aqueous solution all of the expected sequential αCH_i-NH_{i+1} cross-peaks are present, except for the Ala$^{9}_{\alpha CH}$-Cys$^{10}_{NH}$ connectivity (Figure 23). The absence of the Ala$^{9}_{\alpha CH}$-Cys$^{10}_{NH}$ cross-peak is presumably due to the extremely weak NOE interaction between these two resonances. In contrast, the Pro$^{8}_{\alpha CH}$-Ala$^{9}_{NH}$ cross-peak has a very strong intensity, which combined with the absence of the Ala$^{9}_{\alpha CH}$-Cys$^{10}_{NH}$ cross-peak suggests that residues 7-10 adopt a Type II β-turn conformation (3,83,145).

In an attempt to observe the cross-peak between residue 9 and 10 for cyclo^{7,10}[Cys^{7},L-Ala^{9},Cys^{10},Nle^{12}] and cyclo^{7,10}[Cys^{7},Cys^{10},Nle^{12}] analogues, ROESY and NOESY spectra of these peptides in aqueous solution were acquired with twice (128) the number of acquisitions per

FIGURE 23: The αCH-NH region of the 400 ms NOESY spectrum of the cyclo^{7,10}[Cys^{7},D-Ala^{9},Cys^{10},Nle^{12}]α-factor in water (25°C; pH 2.9).

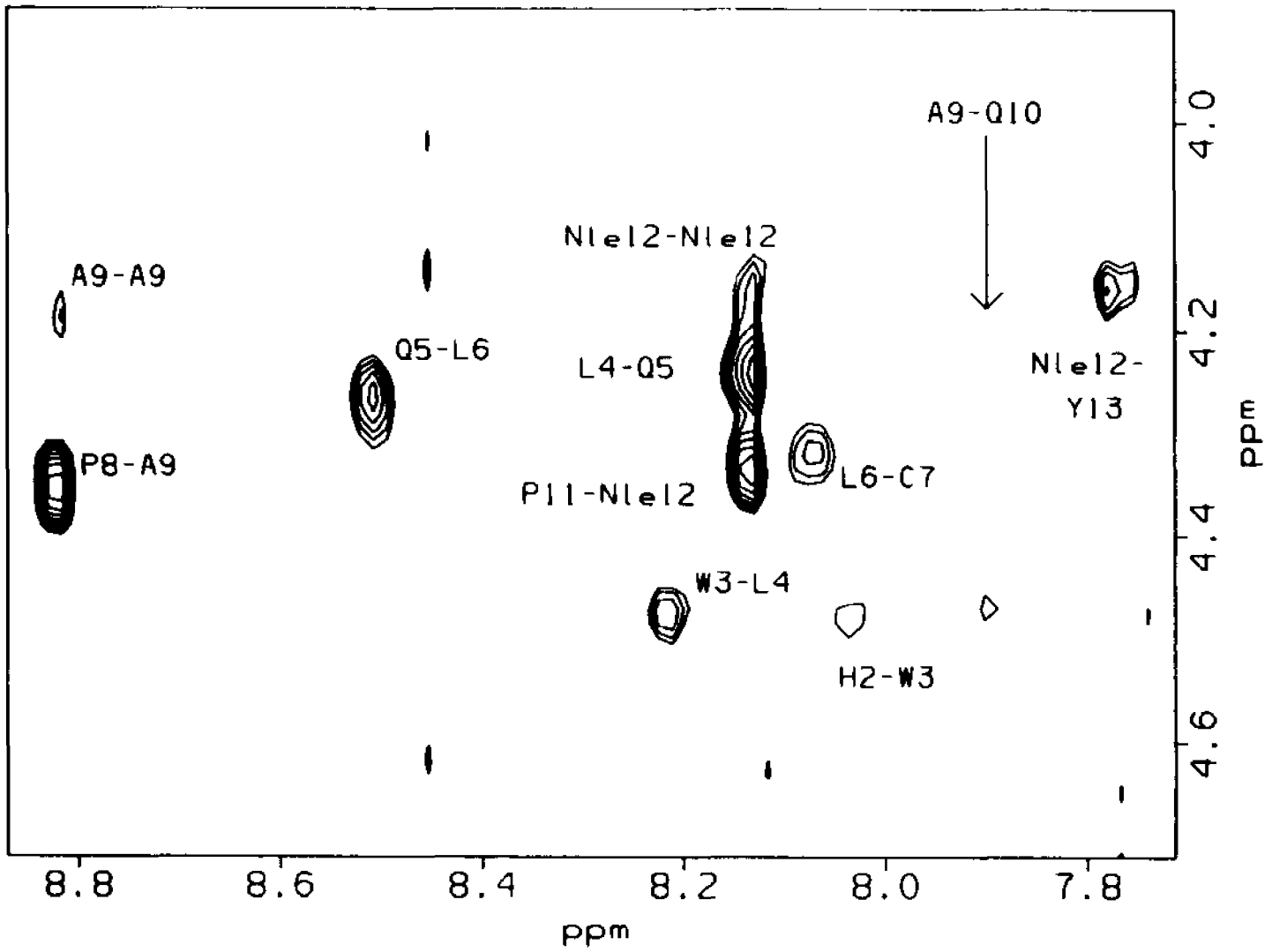
A9-Q10
Nle12-Nle12
A9-A9
Q5-L6
L4-Q5
Nle12-
Y13
P8-A9
L6-C7
P11-Nle12
W3-L4
H2-W3
4.0
4.2
4.4
4.6
ppm
8.8
8.6
8.4
8.2
8.0
7.8
ppm

t_1 increment relative to the spectrum acquired for the cyclo^{7,10}[Cys^7,D-Ala^9,Cys^{10},Nle^{12}]α-factor. Even with the increased signal averaging the Ala^9$_{\alpha CH}$-Cys^{10}$_{NH}$ connectivity in the cyclo^{7,10}[Cys^7,L-Ala^9,Cys^{10},Nle^{12}]α-factor is extremely weak (data not shown). For the cyclo^{7,10}[Cys^7,L-Ala^9,Cys^{10}, Nle^{12}]α-factor at 25°C there is severe spectral overlap between the Leu^4$_{\alpha CH}$-Gln^5$_{NH}$, Leu^6$_{\alpha CH}$-Cys^7$_{NH}$ and Pro^8$_{\alpha CH}$-Ala^9$_{NH}$ cross-peaks (data not shown). In order to alleviate the spectral overlap and allow the intensity of the Pro^8$_{\alpha CH}$-Ala^9$_{NH}$ connectivity to be determined, a ROESY spectrum of the cyclo^{7,10}[Cys^7,L-Ala^9, Cys^{10},Nle^{12}] peptide was acquired at 10°C. At this temperature there still remained some overlap between the Leu^6$_{\alpha CH}$-Cys^7$_{NH}$ and Pro^8$_{\alpha CH}$-Ala^9$_{NH}$ connectivities (Figure 24). However, it is apparent that the Pro^8$_{\alpha CH}$-Ala^9$_{NH}$ cross-peak has a weak intensity since there is no indication of a ROESY peak at the chemical shifts of the Pro^8 αCH and Ala^9 NH resonances. The weak intensities of the Pro^8$_{\alpha CH}$-Ala^9$_{NH}$ and Ala^9$_{\alpha CH}$-Cys^{10}$_{NH}$ cross-peaks are consistent with a Type I/III β-turn centered on residues 8 and 9 of the cyclo^{7,10}[Cys^7,L-Ala^9,Cys^{10},Nle^{12}]α-factor (3,83,145).

In the 400 ms NOESY of the cyclo^{7,10}[Cys^7,Cys^{10},Nle^{12}] analogue all of the expected αCH_i-NH_{i+1} cross-peaks are observed (Figure 25). In addition, a connectivity between one of the δ-protons of Pro^8 and the amide proton of Gly^9 is observed (Figure 25). Several authors have

FIGURE 24: The αCH-NH region of the 250 ms ROESY spectrum of the cyclo^{7,10}[Cys^{7},L-Ala^{9}, Cys^{10},Nle^{12}]α-factor in water (10°C; pH 2.9).

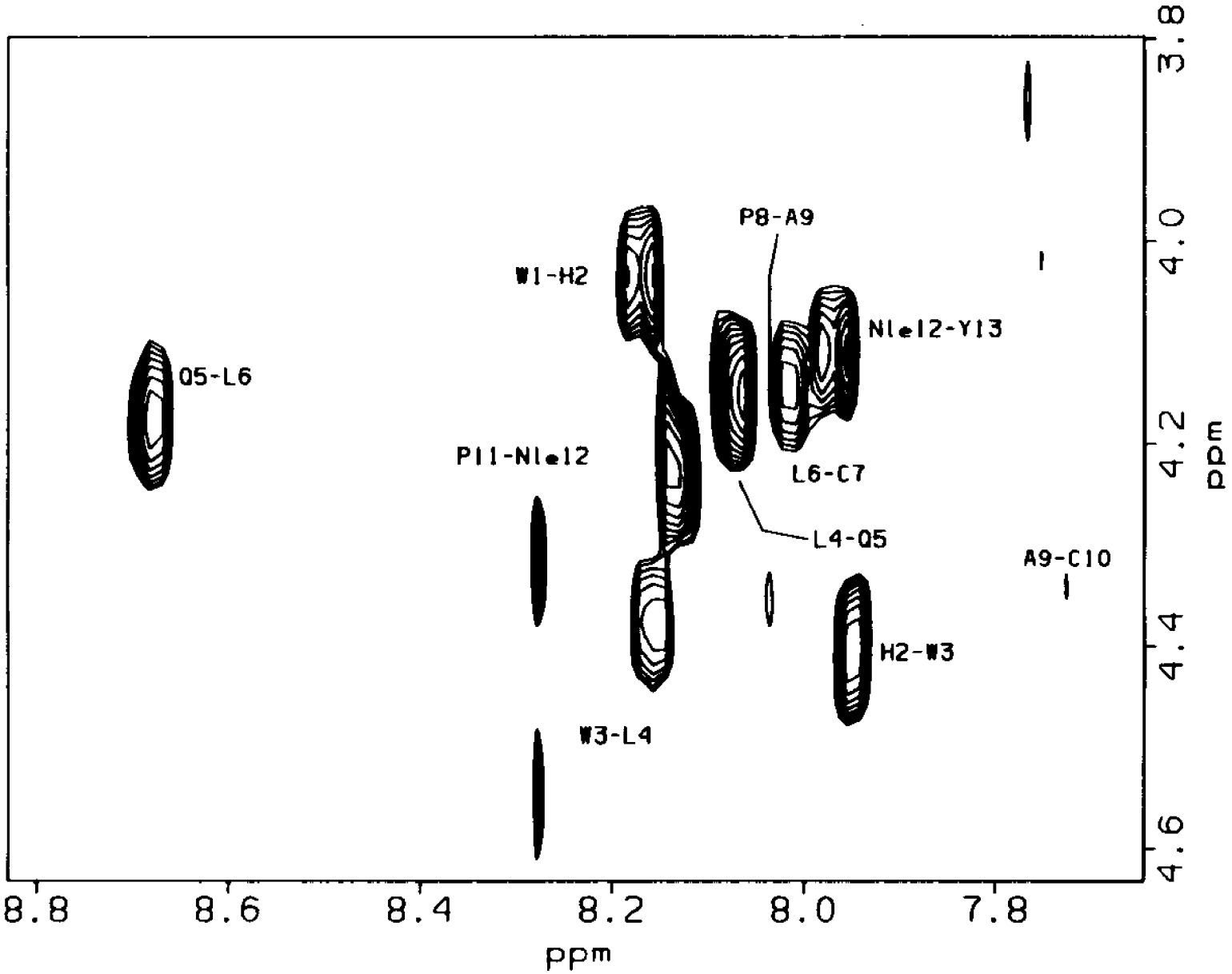
W1-H2
P8-A9
Nle12-Y13
Q5-L6
P11-Nle12
L6-C7
L4-Q5
A9-C10
H2-W3
W3-L4
8.8
8.6
8.4
8.2
8.0
7.8
ppm
3.8
4.0
4.2
4.4
4.6
ppm

used a ProδCH$_i$-NH$_{i+1}$ as a qualitative indicator for a Type I/III β-turn (145,159). This cross-peak is analogous to the NH$_{i+1}$-NH$_{i+2}$ connectivity expected for Type I/III β-turns (3,83,145,159). The intensity for this NOE interaction is expected to be highly sensitive to the ϕ and ψ of Pro^8 and reported ProδCH$_i$-NH$_{i+1}$ internuclear distances for a Type I β-turn range from 1.9 Å (145) to 3.26 Å (159), whereas for a Type II β-turn the ProδCH$_i$-NH$_{i+1}$ internuclear distance is expected to be > 5.0 Å (159). Therefore the Pro$^8\delta$CH-Gly^{9}NH cross-peak indicates that the cyclo^{7,10}[Cys^7,Cys^{10},Nle^{12}]α-factor adopts a Type I β-turn. It may be recalled that a Pro$^8\delta$CH-Gly^{9}NH cross-peak was not observed for the cyclo^{7,10}[Cys^7,L-Ala^9,Cys^{10},Nle^{12}]α-factor, which is identified as adopting a Type I β-turn. However, since the ProδCH$_i$-NH$_{i+1}$ internuclear distance can be > 3.0 Å this connectivity may not be observed at the peptide concentrations used. The Pro$^8{}_{\alpha CH}$-Gly$^9{}_{NH}$ connectivity in the cyclo^{7,10}[Cys^7,Cys^{10}, Nle^{12}]α-factor is significantly stronger than would be expected for a Type I/III β-turn (3,83,145). The intensity of this cross-peak is consistent with both Type II and γ-turn conformations (3,83,145). Therefore, it would appear that the cyclo^{7,10}[Cys^7,Cys^{10},Nle^{12}]α-factor is interconverting between two or possibly more conformers. The Gly^9 α-protons of the cyclo^{7,10}[Cys^7,Cys^{10}, Nle^{12}]α-factor peptide in aqueous solution are degenerate. In

many peptides the α-protons of glycine have slightly different chemical shifts and the absence of two distinct chemical shifts for the α-protons of glycyl residues has been associated with conformational averaging (160). Therefore, the degeneracy of the Gly^9 α-protons in the $cyclo^{7,10}[Cys^7, Cys^{10}, Nle^{12}]$α-factor peptide is consistent with the hypothesis that in water residues 7-10 of this peptide adopt at least two distinct conformations.

A strong NH-NH connectivity is observed between the ninth and tenth residues of the $cyclo^{7,10}[Cys^7, D\text{-}Ala^9, Cys^{10}, Nle^{12}]$-, $cyclo^{7,10}[Cys^7, L\text{-}Ala^9, Cys^{10}, Nle^{12}]$-, and $cyclo^{7,10}[Cys^7, Cys^{10}, Nle^{12}]$α-factor analogues (shown for the $cyclo^{7,10}[Cys^7, Cys^{10}, Nle^{12}]$α-factor in Figure 26). This cross-peak and the weaker $Leu^6{}_{NH}$-$Cys^7{}_{NH}$ connectivity are the only NH-NH connectivities observed for these peptides in aqueous solution. The observation of a strong NH-NH cross-peak between residues nine and ten supports the previous conclusions that the $cyclo^{7,10}[Cys^7, D\text{-}Ala^9, Cys^{10}, Nle^{12}]$- and $cyclo^{7,10}[Cys^7, L\text{-}Ala^9, Cys^{10}, Nle^{12}]$α-factor analogues adopt β-turn conformations, and that the $cyclo^{7,10}[Cys^7, Cys^{10}, Nle^{12}]$ α-factor adopts a Type I/III β-turn as one its low energy conformations. The non-sequential $Pro^8{}_{\alpha CH}$-$Cys^{10}{}_{NH}$ cross-peak, expected for a β-turn conformation is not observed for any of the peptides in aqueous solution. The protons in such a cross-peak are expected to have internuclear separations of 3.3-3.6 Å.

FIGURE 25: The αCH-NH region of the 400 ms NOESY spectrum of the cyclo^{7,10}[Cys^{7},Cys^{10},Nle^{12}] α-factor in water (25°C; pH 2.9).

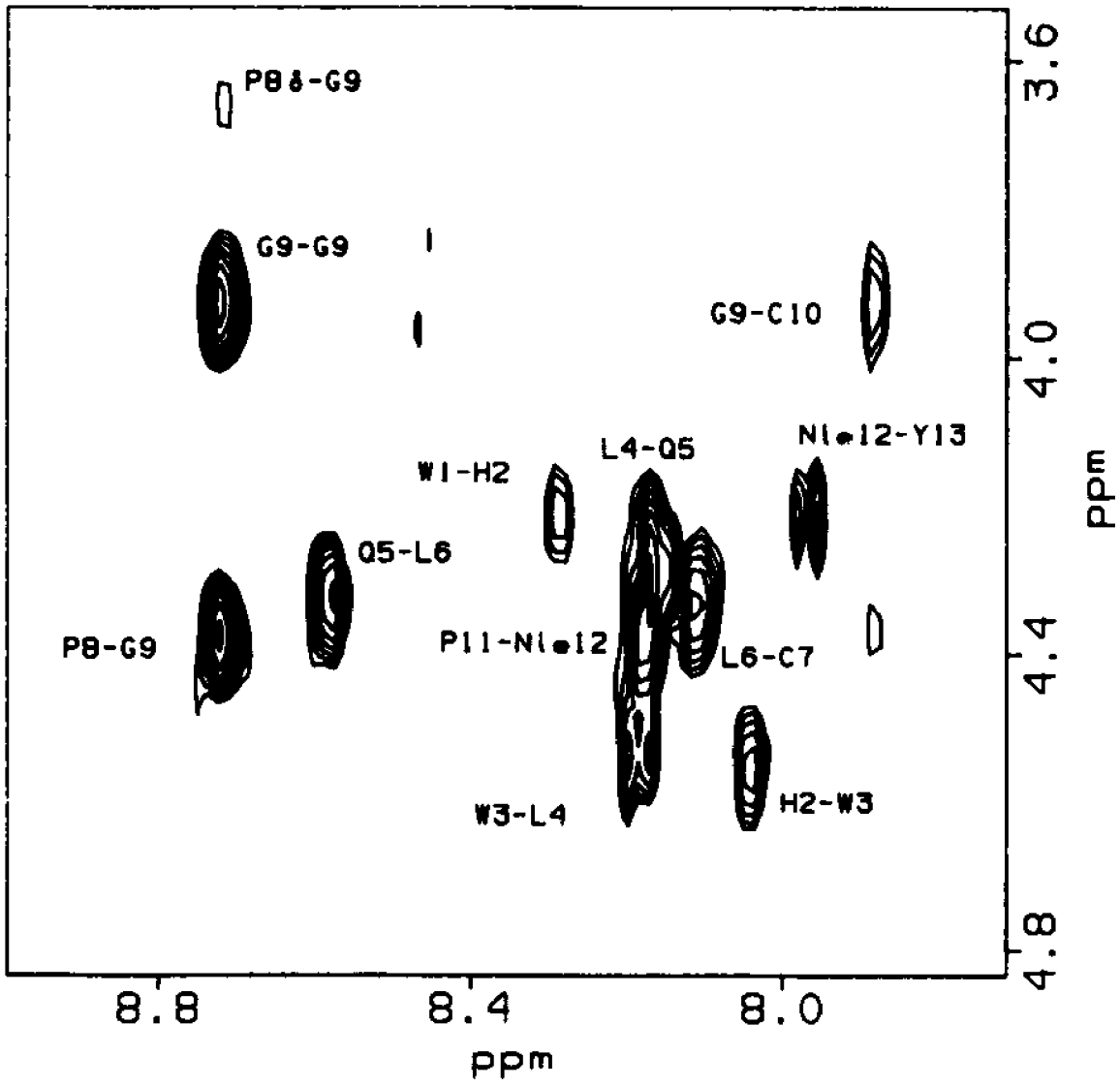
P8δ-G9
G9-G9
G9-C10
W1-H2
L4-Q5
Nε12-Y13
Q5-L6
P8-G9
P11-Nε12
L6-C7
W3-L4
H2-W3
3.6
4.0
4.4
4.8
ppm
8.8
8.4
8.0
ppm

FIGURE 26: The NH-NH region of the 400 ms NOESY spectrum of the cyclo^{7,10}[Cys^{7},Cys^{10}, Nle^{12}]α-factor in water (25°C; pH 2.9).

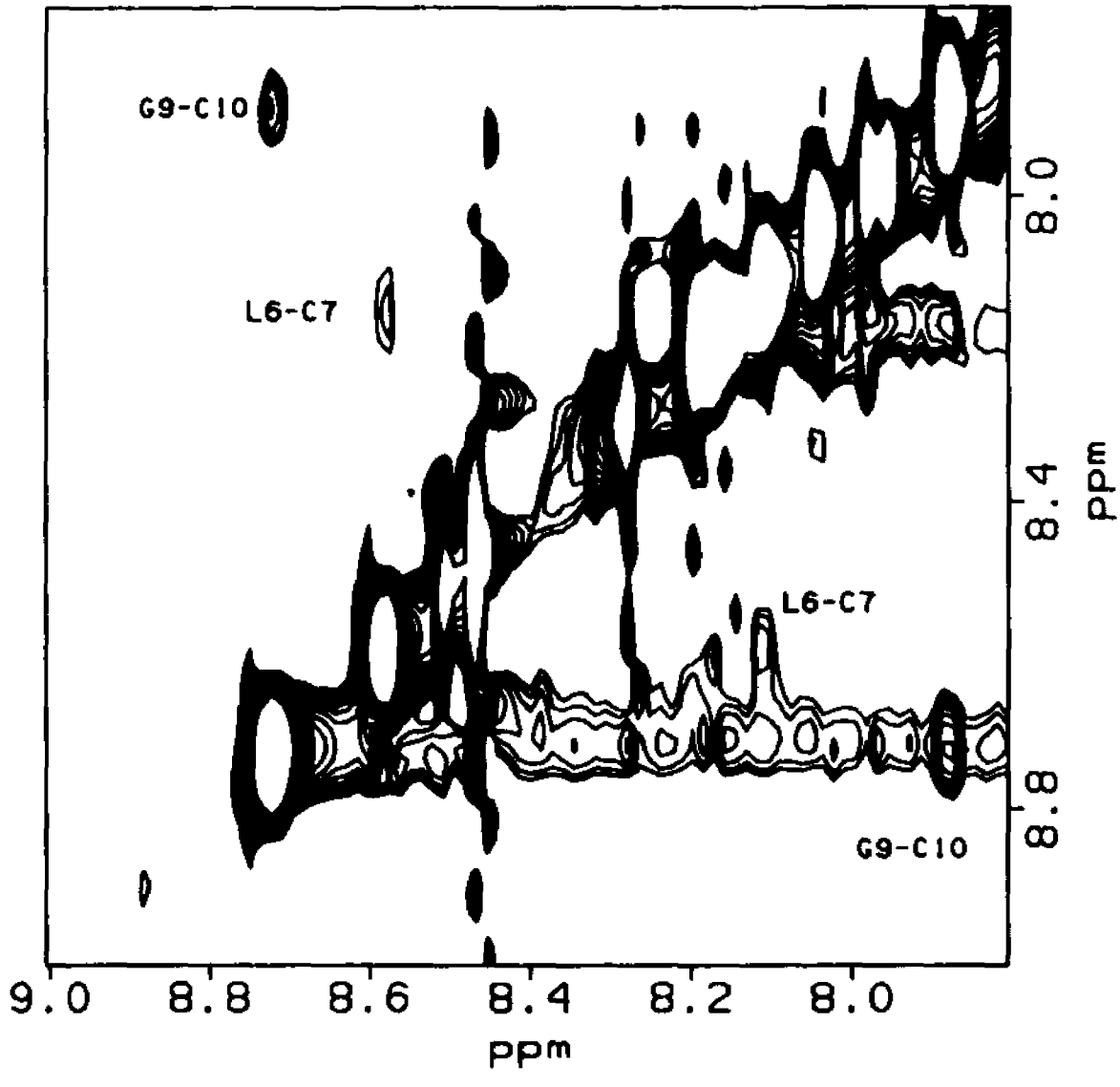
G9-C10
L6-C7
L6-C7
G9-C10
8.0
8.4
8.8
ppm
9.0
8.8
8.6
8.4
8.2
8.0
ppm

FIGURE 27: The NH-βCH region of the 400 ms NOESY spectrum of the cyclo^{7,10}[Cys^{7},Cys^{10}, Nle^{12}]α-factor in water (25°C; pH 2.9).

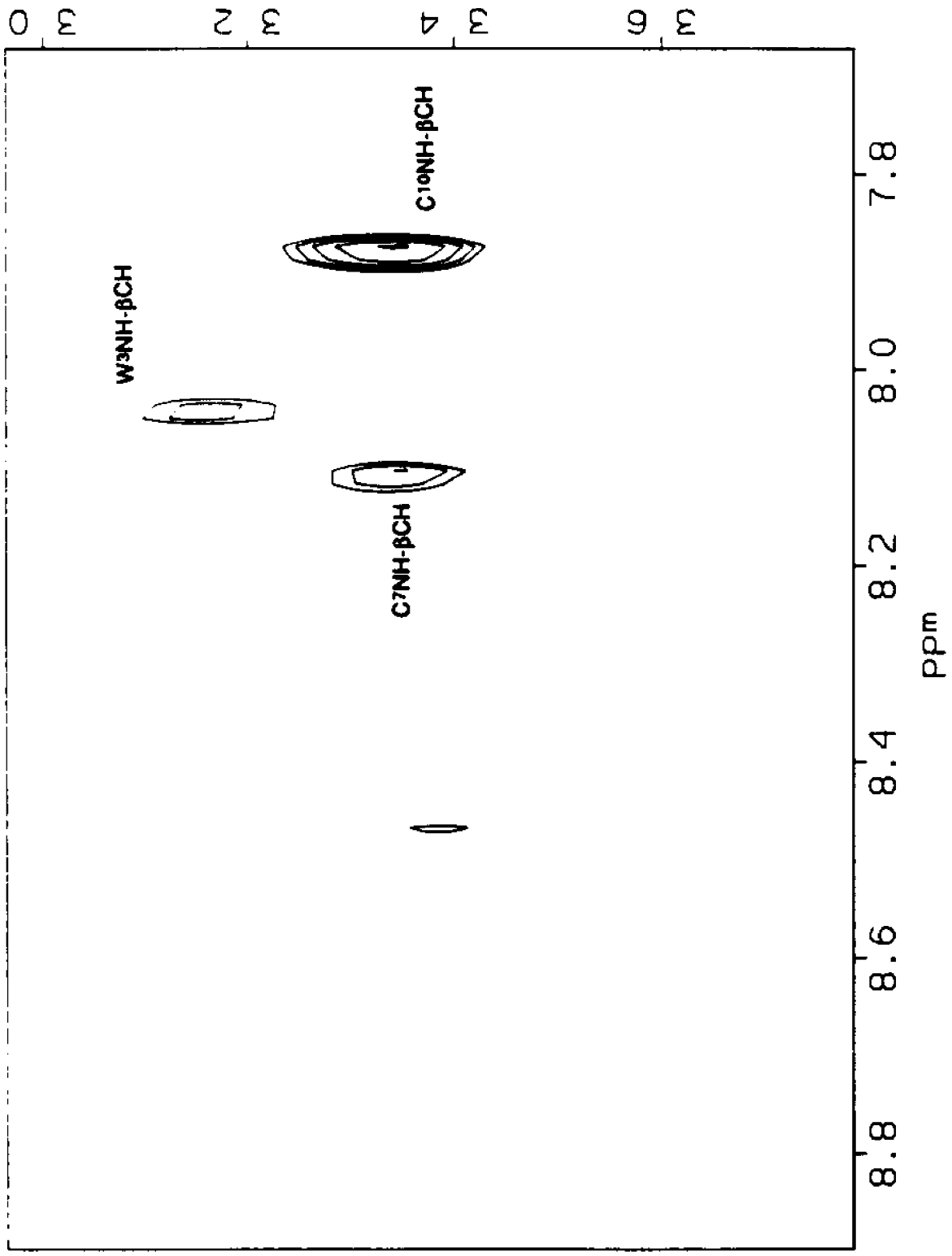
C19NH-βCH
W3NH-βCH
C7NH-βCH
ppm
7.8
8.0
8.2
8.4
8.6
8.8
3.6
3.4
3.2
3.0

Therefore, these interactions, like the $Ala^{9}_{\beta CH}$-Cys^{10}_{NH} cross-peak in the cyclo^{7,10}[Cys^{7},D-Ala^{9},Cys^{10},Nle^{12}] analogue, are presumably below our detection limit at the peptide concentrations used.

For all three of the cyclic analogues studied in aqueous solution cross-peaks were observed between the downfield β-proton of Cys^{7} and the amide proton of Cys^{7}, as well as, between the downfield β-proton of Cys^{10} and the amide proton of Cys^{10} (shown for the cyclo^{7,10}[Cys^{7}, Cys^{10},Nle^{12}]α-factor in Figure 27). These intraresidue NH-βCH connectivities combined with the absence of NH_i-βCH_i cross-peaks involving upfield β-protons of either cystine residue indicate that for both Cys^{7} and Cys^{10} the downfield β-proton is *gauche* to the amide proton while the upfield β-proton is *trans*. This result combined with the constraints imposed by 14 membered ring allows the downfield β-proton of Cys^{7} to be assigned as pro-R and the downfield proton of Cys^{10} to be assigned as pro-S. These results are in agreement with those obtained by Garcia-Echeverria *et al.* for a cyclo^{1,4}[Cys,Pro,D-Val,Cys] and cyclo^{1,4}[Pen,Pro,D-Val,Cys] tetrapeptides (85).

Conformational Analysis of the Cyclic α-Factor Analogues in DMSO/water Solution:

The high viscosity of cryoprotective solvent systems tends to stabilize low energy conformations (13) and it

was hoped that in DMSO/water (80:20) we would be able to observe interactions between the C- and N-terminal residues of the cyclo^{7,10}[Cys^{7},X^{9},Cys^{10},Nle^{12}]α-factor analogues. In the NOESY spectra of the cyclo^{7,10}[Cys^{7},X^{9}, Cys^{10},Nle^{12}] analogues in DMSO/water (Figures 28-31) all of the expected sequential αCH_i-NH_{i+1} connectivities are observed, except for the Ala$^{9}{}_{\alpha CH}$-Cys$^{10}{}_{NH}$ cross-peak in the cyclo^{7,10}[Cys^{7},D-Ala^{9},Cys^{10},Nle^{12}] peptide. The Ala^{9}αCH resonance of the cyclo^{7,10}[Cys^{7},D-Ala^{9},Cys^{10},Nle^{12}]α-factor in DMSO/water (80:20) is coincident with the water resonance. The absence of the Ala$^{9}{}_{\alpha CH}$-Cys$^{10}{}_{NH}$ cross-peak in the NOESY spectrum of the cyclo^{7,10}[Cys^{7},D-Ala^{9},Cys^{10}, Nle^{12}]α-factor is presumably due to the saturation of the Ala^{9}αCH resonance by the selective irradiation used to suppress the water resonance. In the NOESY spectra of the cyclo^{7,10}[Cys^{7},D-Ala^{9},Cys^{10},Nle^{12}] and cyclo^{7,10}[Cys^{7},D-Val^{9},Cys^{10},Nle^{12}] analogues (Figures 28 & 29, respectively) a very strong cross-peak is observed between the α-proton of Pro^{8} and the amide proton of residue 9 (Pro$^{8}{}_{\alpha CH}$-Ala$^{9}{}_{NH}$ and Pro$^{8}{}_{\alpha CH}$-Val$^{9}{}_{NH}$, respectively). In contrast, this cross-peak (Pro$^{8}{}_{\alpha CH}$-Ala$^{9}{}_{NH}$) is observed to be very weak for the cyclo^{7,10}[Cys^{7},L-Ala^{9},Cys^{10},Nle^{12}]α-factor (Figure 30). In addition, a Pro$^{8}{}_{\beta H}$-Ala$^{9}{}_{NH}$ connectivity is observed for the cyclo^{7,10}[Cys^{7},L-Ala^{9},Cys^{10},Nle^{12}] analogue. These results are consistent with the cyclo^{7,10}[Cys^{7},D-Ala^{9},Cys^{10}, Nle^{12}]- and cyclo^{7,10}[Cys^{7},D-Val^{9},Cys^{10},Nle^{12}]α-factor

FIGURE 28: The αCH-NH region of the 400 ms NOESY spectrum of the cyclo^{7,10}[Cys^{7},D-Ala^{9},Cys^{10},Nle^{12}]α-factor in DMSO/water (25°C).

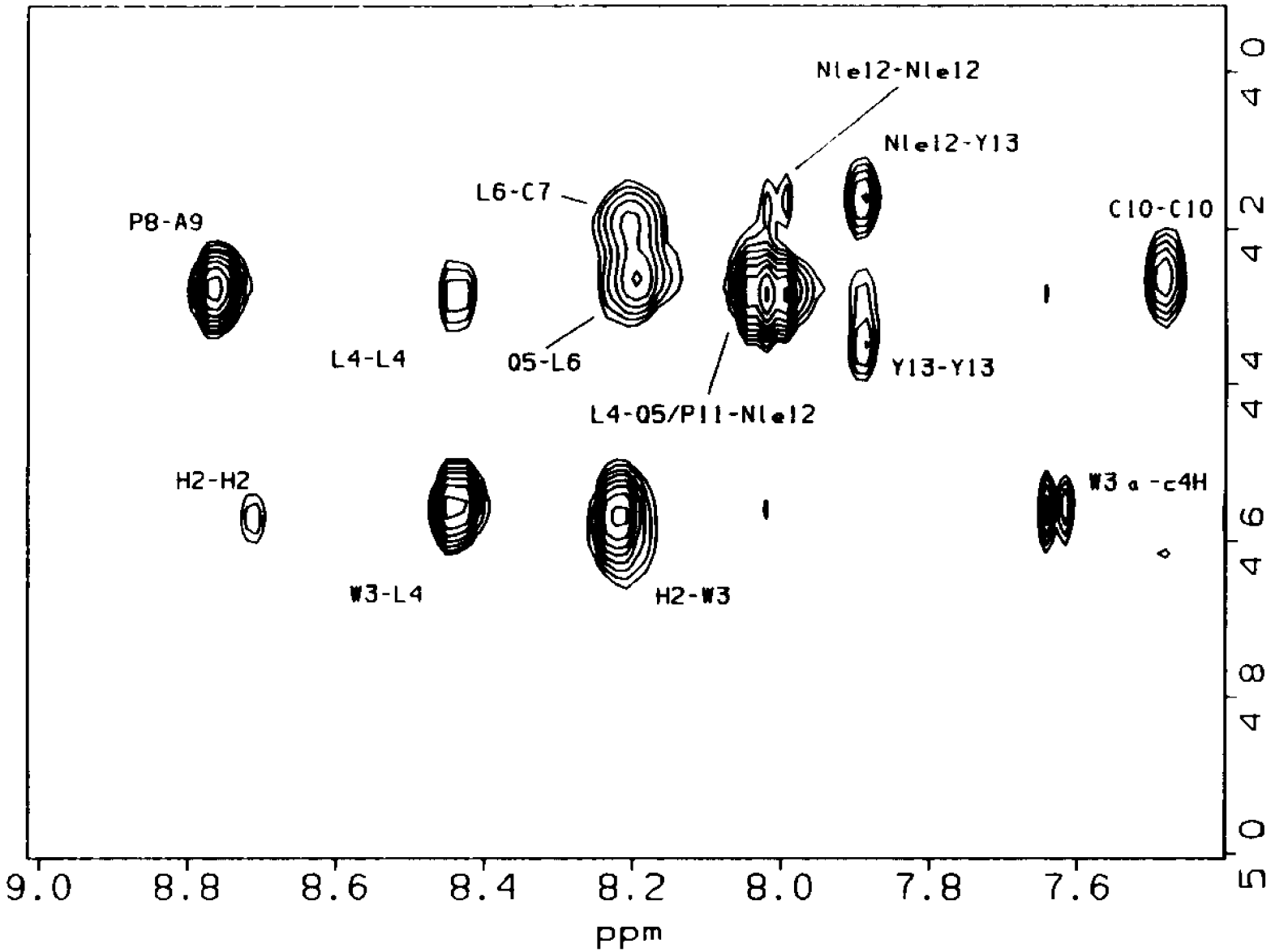
Nle12-Nle12
Nle12-Y13
L6-C7
P8-A9
C10-C10
L4-L4
Q5-L6
Y13-Y13
L4-Q5/P11-Nle12
H2-H2
W3 α -c4H
W3-L4
H2-W3
4.0
4.2
4.4
4.6
4.8
5.0
9.0
8.8
8.6
8.4
8.2
8.0
7.8
7.6
ppm

FIGURE 29: The αCH-NH region of the 400 ms NOESY spectrum of the cyclo^{7,10}[Cys^{7},D-Val^{9},Cys^{10},Nle^{12}]α-factor in DMSO/water (25°C).

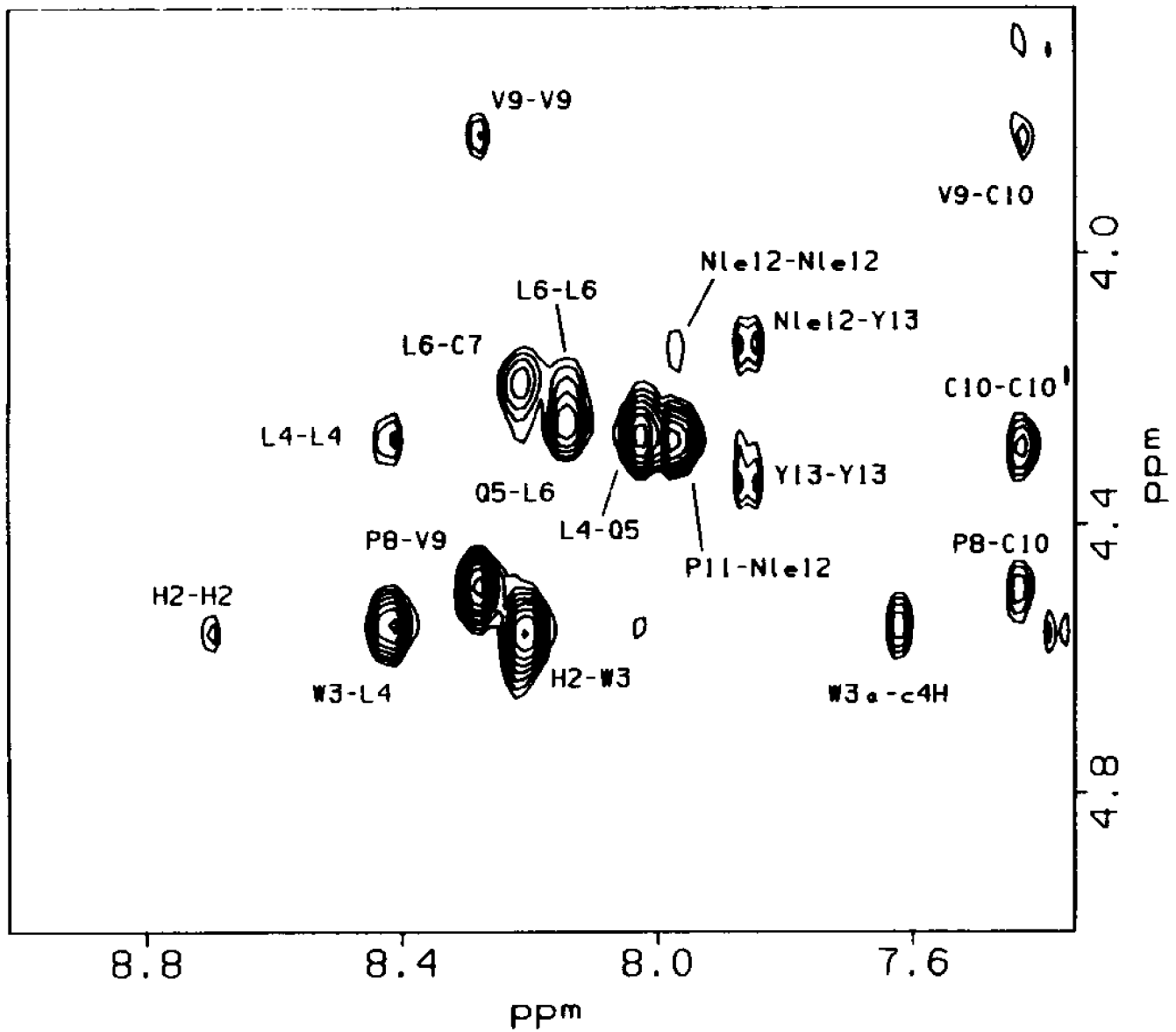
V9-V9
V9-C10
Nle12-Nle12
L6-L6
Nle12-Y13
L6-C7
C10-C10
L4-L4
Y13-Y13
Q5-L6
L4-Q5
P11-Nle12
P8-V9
P8-C10
H2-H2
W3-L4
H2-W3
W3ε-c4H
8.8
8.4
8.0
7.6
ppm
4.0
4.4
4.8
ppm

FIGURE 30: The αCH-NH region of the 400 ms NOESY spectrum of the cyclo^{7,10}[Cys^{7},L-Ala^{9}, Cys^{10},Nle^{12}]α-factor in DMSO/water. (25°C).

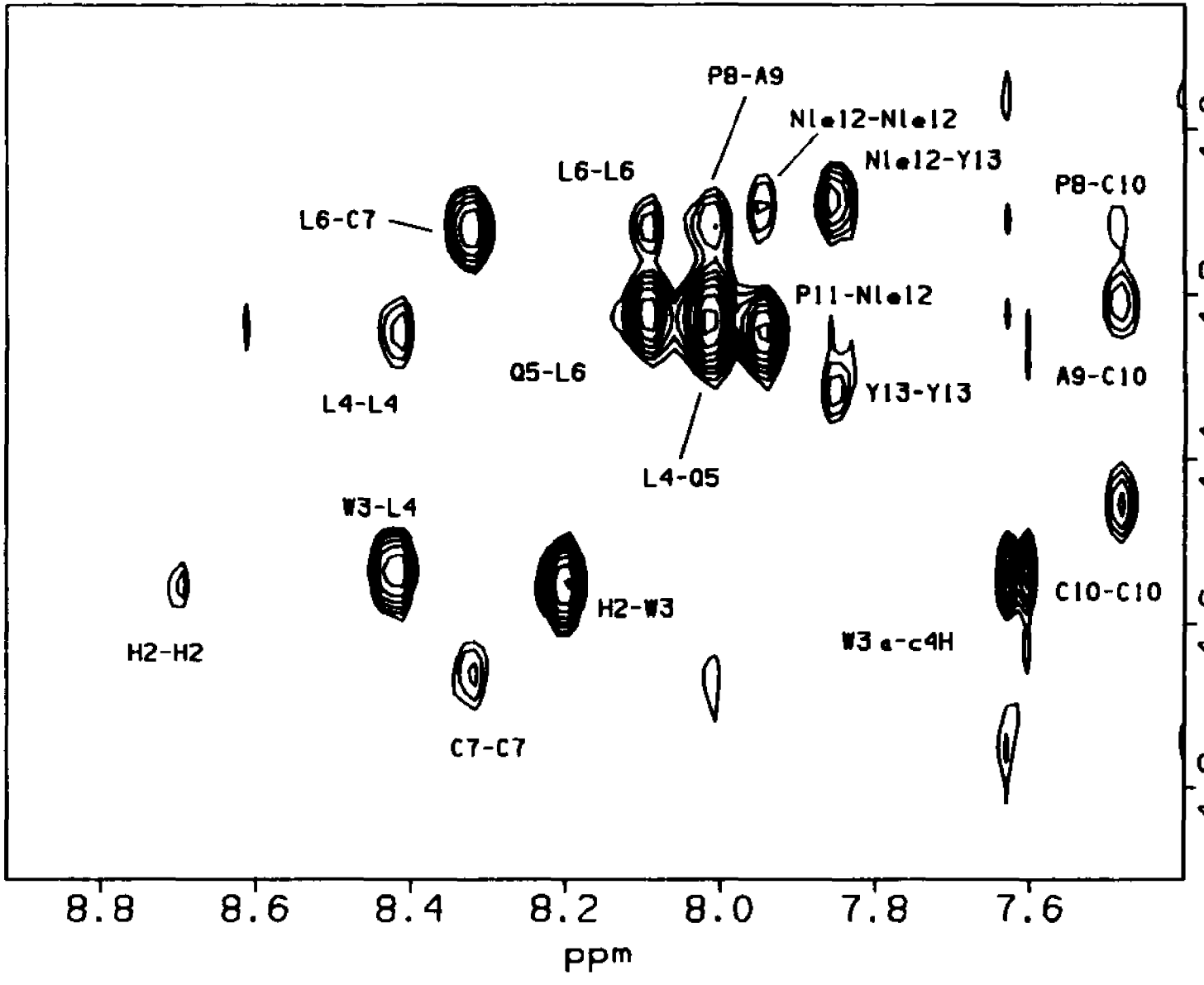
P8-A9
Nε12-Nε12
Nε12-Y13
L6-L6
P8-C10
L6-C7
P11-Nε12
Q5-L6
A9-C10
Y13-Y13
L4-L4
L4-Q5
W3-L4
C10-C10
H2-W3
H2-H2
W3 ε-c4H
C7-C7
8.8
8.6
8.4
8.2
8.0
7.8
7.6
ppm
4.0
4.2
4.4
4.6
4.8

FIGURE 31: The αCH-NH region of the 400 ms NOESY spectrum of the cyclo^{7,10}[Cys^{7},Cys^{10},Nle^{12}] α-factor in DMSO/water (25°C).

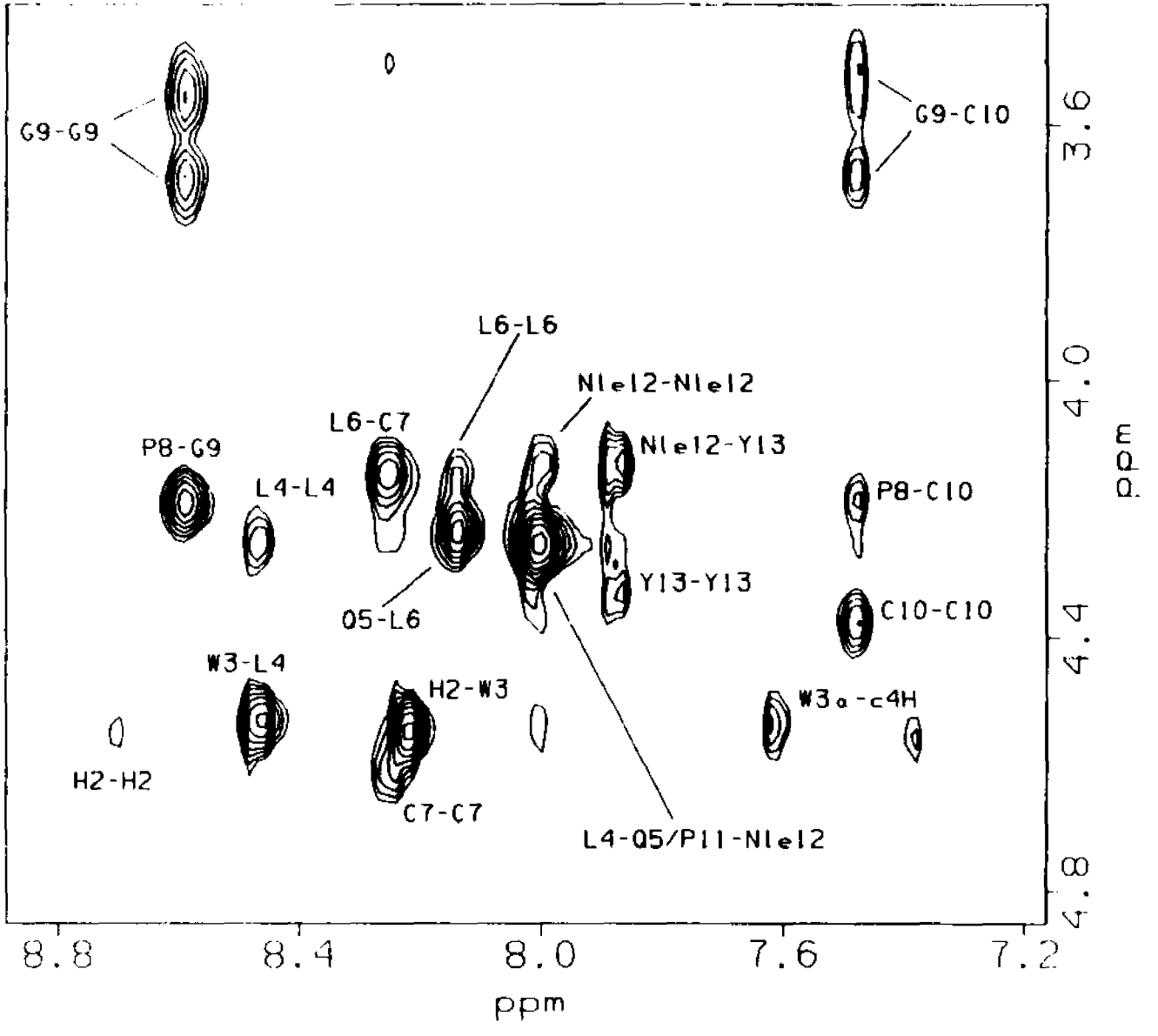
G9-G9
G9-C10
L6-L6
Nle12-Nle12
L6-C7
Nle12-Y13
P8-G9
L4-L4
P8-C10
Y13-Y13
Q5-L6
C10-C10
W3-L4
H2-W3
W3α-c4H
H2-H2
C7-C7
L4-Q5/P11-Nle12
8.8
8.4
8.0
7.6
7.2
ppm
3.6
4.0
4.4
4.8
ppm

peptides adopting Type II β-turn conformations, while the cyclo^{7,10}[Cys^{7},L-Ala^{9},Cys^{10},Nle^{12}] analogue adopts a Type I β-turn (3,83,145,159). For the cyclo^{7,10}[Cys^{7},D-Val^{9},Cys^{10}, Nle^{12}]- and cyclo^{7,10}[Cys^{7},L-Ala^{9},Cys^{10},Nle^{12}] analogues this conclusion is further supported by the presence of a non-sequential Pro$^{8}_{\alpha CH}$-Cys$^{10}_{NH}$ NOE connectivity (3,83,145). For the cyclo^{7,10}[Cys^{7},D-Ala^{9},Cys^{10},Nle^{12}]α-factor the Pro$^{8}_{\alpha CH}$-Cys$^{10}_{NH}$ cross-peak, if present, would be severely overlapped with the C$^{10}_{\alpha CH}$-C$^{10}_{NH}$ cross-peak.

For the cyclo^{7,10}[Cys^{7},Cys^{10},Nle^{12}]α-factor weak Gly$^{9}_{\alpha CH}$-C$^{10}_{NH}$ and Pro$^{8}_{\alpha CH}$-Cys$^{10}_{NH}$ NOESY cross-peaks are observed in DMSO/water (Figure 31). In addition, the Pro$^{8}_{\alpha CH}$-Gly$^{9}_{NH}$ NOESY connectivity has a very strong intensity and the Pro$^{8}_{\alpha CH}$-Gly$^{9}_{NH}$ cross-peak observed in aqueous solution is absent in DMSO/water solution. Interestingly, the degeneracy of the two Gly^{9}αCH resonances is broken in the DMSO/water solvent system and separate resonances are observed for each proton. The above results suggest that in DMSO/water the equilibrium distribution of the cyclo^{7,10}[Cys^{7},Cys^{10},Nle^{12}] analogue is shifted towards a Type II β-turn conformer (3,83,145).

In the 400 ms spectrum of the cyclo^{7,10}[Cys^{7},Cys^{10}, Nle^{12}]α-factor the Gly$^{9}_{NH}$-Cys$^{10}_{NH}$ connectivity has a significantly stronger intensity than all other NH-NH cross-peaks (Figure 32). Similar results were obtained for all of the other cyclic α-factor analogues in

FIGURE 32: The NH-NH region of the 400 ms NOESY spectrum of the cyclo^{7,10}[Cys^{7},Cys^{10},Nle^{12}] ✱-factor in DMSO/water (25°C).

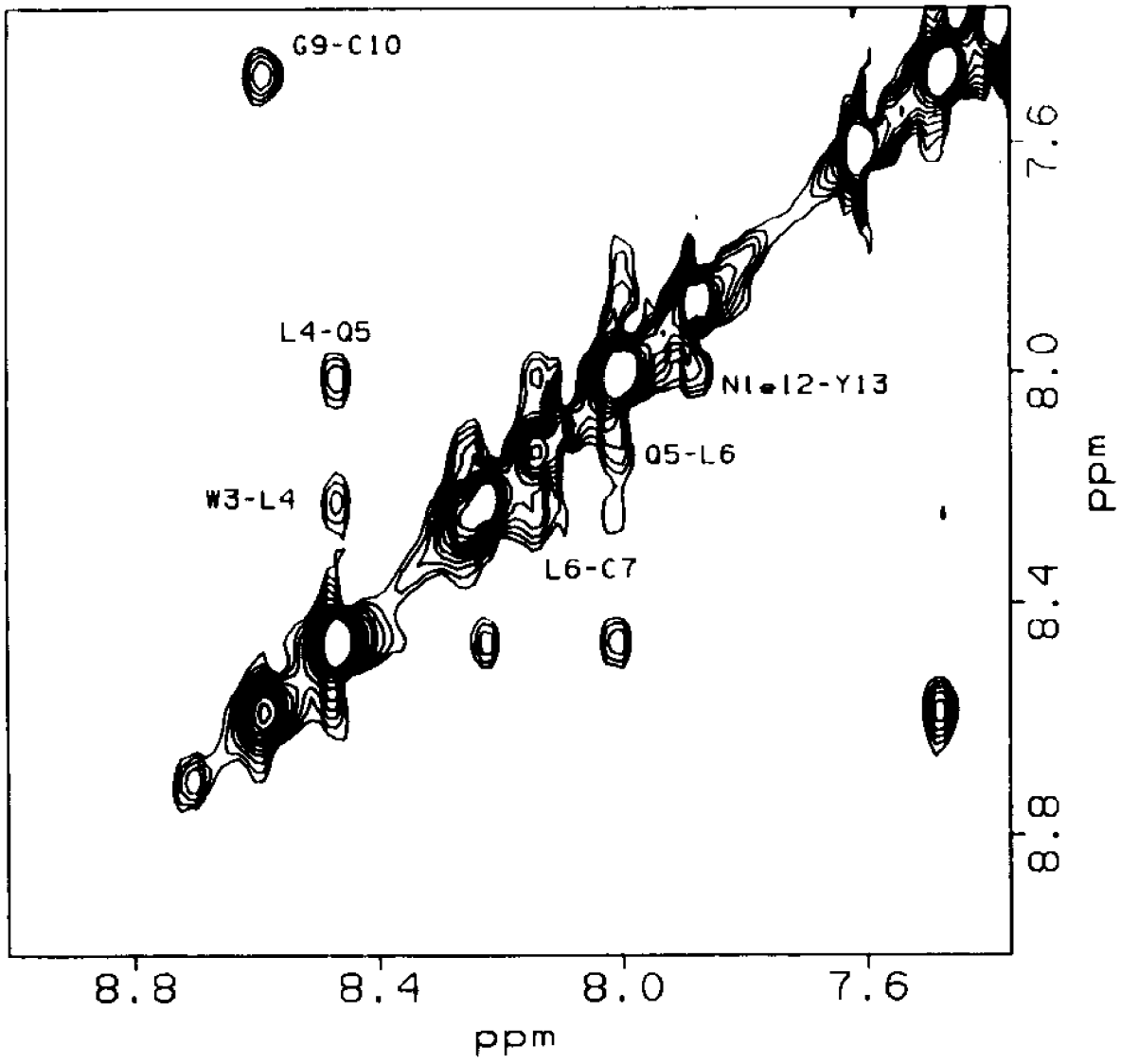
G9-C10
L4-Q5
W3-L4
N12-Y13
Q5-L6
L6-C7
8.8
8.4
8.0
7.6
ppm
8.8
8.4
8.0
7.6
ppm

DMSO/water. This result provides further support for the conclusion that the four cyclo^{7,10}[Cys^{7},X^{9},Cys^{10},Nle^{12}]α-factor peptides examined form β-turns centered on residues 8 and 9.

For all of the cyclic analogues studied in DMSO/water solution Cys^{7} and Cys^{10} exhibited stronger NH_i-βCH_i connectivities with the downfield β-proton than with the upfield β-resonance (data not shown). This result suggests that for both the Cys^{7} and Cys^{10} residues the downfield β-proton is *gauche* to the amide proton while the upfield β-proton is *trans*. As was the case in aqueous solution this result combined with the constraints imposed by 14 membered ring and β-turn conformation allows the downfield β-proton of Cys^{7} and Cys^{10} to be assigned as pro-R and Pro-S, respectively.

Interestingly, in DMSO/water and aqueous solutions the αCH resonances of residue 9 in the cyclo^{7,10}[Cys^{7},D-Ala^{9},Cys^{10},Nle^{12}]- and cyclo^{7,10}[Cys^{7},D-Val^{9},Cys^{10},Nle^{12}]α-factor analogues is shifted upfield (≈ 0.2-0.3 ppm) relative to the Ala^{9} αCH resonance in the cyclo^{7,10}[Cys^{7},L-Ala^{9},Cys^{10},Nle^{12}] peptide. A similar upfield shift is observed for the D-Val^{3} αCH resonance in the cyclo^{1,4}[Cys^{1},Pro^{2},D-Val^{3},Cys^{4}] tetrapeptide (85). It is possible that this upfield shift results from the Type II β-turn conformation.

In addition to the above qualitative analysis, the internuclear distances for NOE interactions of residues 7-10 were estimated for the cyclo^{7,10}[Cys^{7},Cys^{10},Nle^{12}] and cyclo^{7,10}[Cys^{7},L-Ala^{9},Cys^{10},Nle^{12}] analogues in DMSO/water using the cross-peak between the geminal β-protons of Pro^{8} and Pro^{11} to calibrate the relationship between NOE intensity and internuclear separation (equation 3). The cross-peak between the geminal β-protons of Pro^{8} and Pro^{11} for the cyclo^{7,10}[Cys^{7},Cys^{10},Nle^{12}]α-factor are shown in Figure 33. The internuclear distances obtained in this manner are presented in Table 10.

In the spectra of the cyclo^{7,10}[Cys^{7},D-Val^{9},Cys^{10}, Nle^{12}] analogue in DMSO/water it was not possible to find a suitable cross-peak of known internuclear distance for use in equation 3. For this peptide there was severe overlap between the β-protons of Pro^{8} and Pro^{11} and, as was the case for all the cyclic α-factor analogues in DMSO/water, the cross-peaks between the geminal δ-protons of Pro^{8} and Pro^{11} were not observed due to interference from the selective saturation used to suppress the water resonance. Despite their shorter internuclear distances, the connectivities between intraresidue aromatic resonances or between the γNH$_2$ resonances of Gln^{5} were significantly weaker than sequential αCH-NH connectivities. This result indicates that the sidechain resonances experience much shorter effective

FIGURE 33: Expansion of the 200 ms NOESY spectrum of the cyclo^{7,10}[Cys^{7},Cys^{10},Nle^{12}]α-factor in DMSO/water. Note the cross-peaks between the geminal β- and γ-protons of Pro^{8} and Pro^{11}.

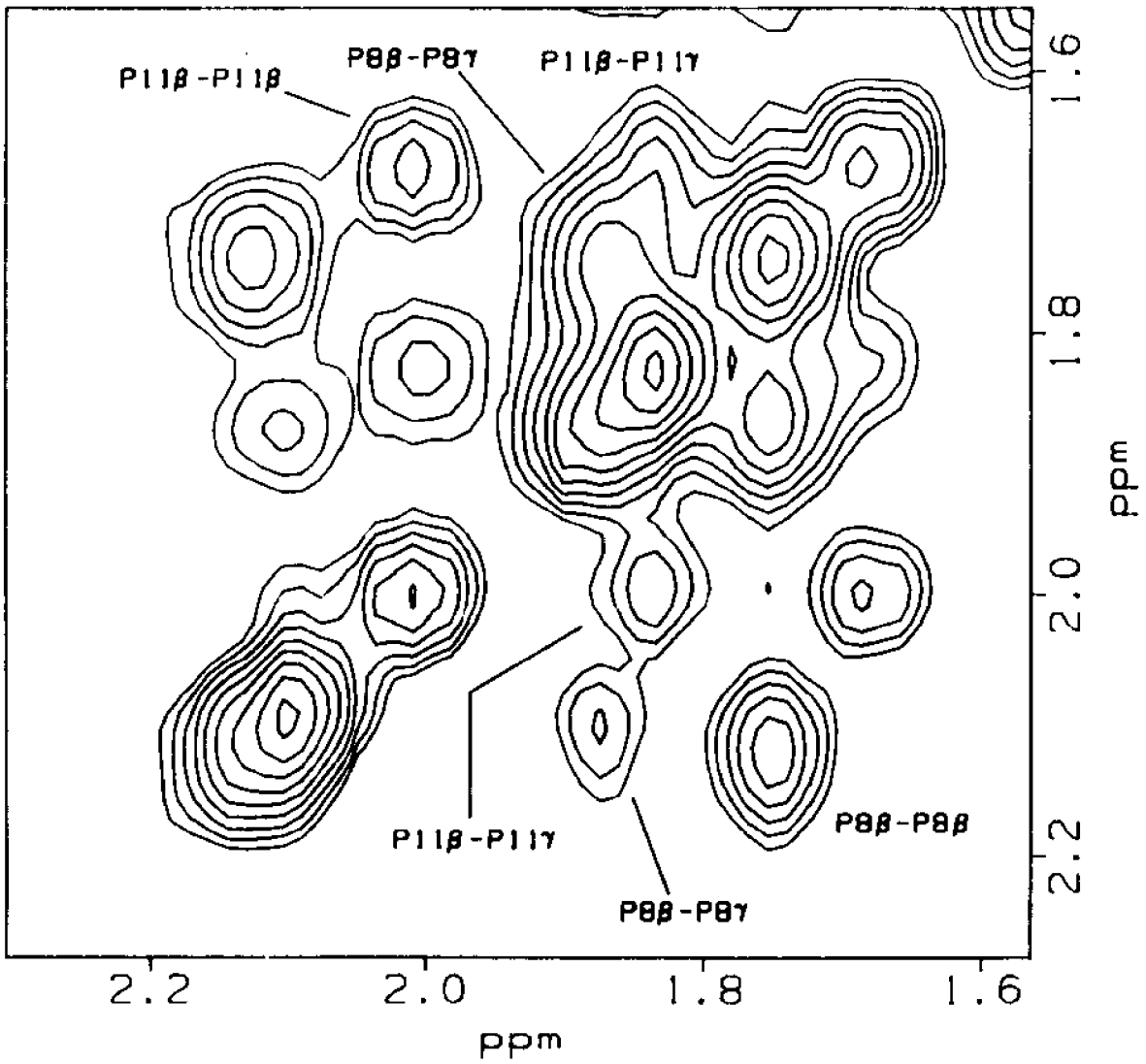
P11β-P11β
P8β-P8γ
P11β-P11γ
P11β-P11γ
P8β-P8β
P8β-P8γ
2.2
2.0
1.8
1.6
ppm
2.2
2.0
1.8
1.6
ppm

TABLE 10

Internuclear distances for the cyclic α-factor analogues measured (± 0.1 Å) from 100 (CGAF) and 200 ms (CLAF,CDVAF) NOESY spectra.

CDVAF		CLAF		CGAF	
$P^{8}_{\beta CH}$-V^{9}_{NH}	2.2 Å	$P^{8}_{\beta CH}$-A^{9}_{NH}	3.2 Å	$P^{8}_{\beta CH}$-G^{9}_{NH}	2.3 Å
$V^{9}_{\beta CH}$-V^{9}_{NH}	3.1 Å	$P^{8}_{\beta CH}$-A^{9}_{NH}	2.8 Å	$G^{9}_{\beta CH}$-G^{9}_{NH}	2.4 Å
$V^{9}_{\beta CH}$-C^{10}_{NH}	3.2 Å	$A^{9}_{\beta CH}$-C^{10}_{NH}	3.2 Å	$G^{9}_{\beta CH}$-C^{10}_{NH}	3.3 Å
$P^{8}_{\beta CH}$-C^{10}_{NH}	2.9 Å	$P^{8}_{\beta CH}$-C^{10}_{NH}	N.A.	$P^{8}_{\beta CH}$-C^{10}_{NH}	N.A.
V^{9}_{NH}-C^{10}_{NH}	2.6 Å	A^{9}_{NH}-C^{10}_{NH}	2.4 Å	G^{9}_{NH}-C^{10}_{NH}	2.4 Å
$C^{10}_{\beta CH}$-C^{10}_{NH}	2.8 Å *	$C^{10}_{\beta CH}$-C^{10}_{NH}	2.8 Å	$C^{10}_{\beta CH}$-C^{10}_{NH}	2.9 Å

*This internuclear separation was assumed and was used to estimate all other internuclear separation reported for the CDVAF peptide.

CDVAF = cyclo^{7,10}[Cys^{7},D-Val^{9},Cys^{10},Nle^{12}]α-factor
CLAF = cyclo^{7,10}[Cys^{7},L-Ala^{9},Cys^{10},Nle^{12}]α-factor
CGAF = cyclo^{7,10}[Cys^{7},Cys^{10},Nle^{12}]α-factor

TABLE 11

Internuclear distances for the cyclic α-factor analogues measured (± 0.1 Å) from 400 ms NOESY spectra.

CDVAF		CLAF		CGAF	
$P^{8}{}_{\beta CH}$-$V^{9}{}_{NH}$	2.2 Å	$P^{8}{}_{\beta CH}$-$A^{9}{}_{NH}$	3.3 Å	$P^{8}{}_{\beta CH}$-$G^{9}{}_{NH}$	2.4 Å
$V^{9}{}_{\beta CH}$-$V^{9}{}_{NH}$	3.1 Å	$P^{8}{}_{\beta CH}$-$A^{9}{}_{NH}$	2.9 Å	$G^{9}{}_{\alpha CH}$-$G^{9}{}_{NH}$	2.6 Å
$V^{9}{}_{\beta CH}$-$C^{10}{}_{NH}$	3.1 Å	$A^{9}{}_{\beta CH}$-$C^{10}{}_{NH}$	3.2 Å	$G^{9}{}_{\alpha CH}$-$C^{10}{}_{NH}$	3.5 Å
$P^{8}{}_{\beta CH}$-$C^{10}{}_{NH}$	3.0 Å	$P^{8}{}_{\beta CH}$-$C^{10}{}_{NH}$	3.5 Å	$P^{8}{}_{\beta CH}$-$C^{10}{}_{NH}$	3.1 Å
$V^{9}{}_{NH}$-$C^{10}{}_{NH}$	2.6 Å	$A^{9}{}_{NH}$-$C^{10}{}_{NH}$	2.4 Å	$G^{9}{}_{NH}$-$C^{10}{}_{NH}$	2.7 Å
$C^{10}{}_{\beta CH}$-$C^{10}{}_{NH}$	2.8 Å *	$C^{10}{}_{\beta CH}$-$C^{10}{}_{NH}$	2.8 Å	$C^{10}{}_{\beta CH}$-$C^{10}{}_{NH}$	2.9 Å

*This internuclear separation was assumed and was used to estimate all other internuclear separation reported for the CDVAF peptide.

CDVAF = cyclo^{7,10}[Cys^{7},D-Val^{9},Cys^{10},Nle^{12}]α-factor
CLAF = cyclo^{7,10}[Cys^{7},L-Ala^{9},Cys^{10},Nle^{12}]α-factor
CGAF = cyclo^{7,10}[Cys^{7},Cys^{10},Nle^{12}]α-factor

correlation times relative to the peptide backbone resonances. In addition, effects due to the superposition of *zero*-quantum coherence were observed in several of the cross-peaks arising between aromatic resonances, in particular those of the Tyr^{13} phenolic ring. Thus, we did not use these NOESY interactions for estimating internuclear separations. In order to estimate the internuclear distances for cyclo^{7,10}[Cys^{7},D-Val^{9},Cys^{10},Nle^{12}]α-factor (Table 10) we assumed a $Cys^{10}{}_{\alpha CH}$-$Cys^{10}{}_{NH}$ internuclear distance (i.e the distance in the i+3 residue of the putative turn) of 2.8 ± 0.2 Å. This value corresponds to the range of intraresidue αCH-NH internuclear distances over the sterically allowed values for the phi angle in L-residues (-60 - -180°) (83,116). Due to the limited range of αCH_i-NH_i internuclear distances in the allowed region Saulitis and Leipins have suggested that αCH_i-NH_i cross-peaks in L-amino acids can be used as a reference for estimating internuclear distances from NOE data (116). Of particular relevance is the fact that this value is in agreement with the Cys^{10} αCH_i-NH_i internuclear distances obtained for the cyclo^{7,10}[Cys^{7},Cys^{10},Nle^{12}]- and cyclo^{7,10}[Cys^{7},L-Ala^{9},Cys^{10},Nle^{12}]α-factor analogues (see Table 10) and for two cyclic model compounds (the cyclo^{1,4}[Cys^{1},Pro^{2},D-Val^{3},Cys^{4}] and cyclo^{1,4}[Pen^{1},Pro^{2},D-Val^{3},Cys^{4}] tetrapeptides) studied by Garcia-Echeverria *et al.* (85).

In the NOESY spectrum of the cyclo^{7,10}[Cys^{7},D-Ala^{9},Cys^{10},Nle^{12}] analogue in DMSO/water the β-protons of Pro^{8} and Pro^{11} were poorly resolved. In addition, there was severe spectral overlap of the Pro^{8}$_{\beta CH}$-Cys^{10}$_{NH}$ and Cys^{10}$_{\beta CH}$-Cys^{10}$_{NH}$ cross-peaks. Therefore, it was not possible to use the geminal β-protons of either Pro^{8} or Pro^{11} or the Cys^{10}$_{\beta CH}$-Cys^{10}$_{NH}$ cross-peaks to estimate internuclear distances for the cyclo^{7,10}[Cys^{7},D-Ala^{9}, Cys^{10},Nle^{12}] analogue. Although the cross-peaks used to calibrate internuclear separation in the cyclo^{7,10}[Cys^{7}, Cys^{10},Nle^{12}]-, cyclo^{7,10}[Cys^{7},L-Ala^{9},Cys^{10},Nle^{12}]-, and cyclo^{7,10}[Cys^{7},D-Val^{9},Cys^{10},Nle^{12}]α-factor analogues involve proton pairs that are *J*-coupled no evidence of *zero*-quantum coherence transfer was observed. All of the internuclear distances reported for the cyclo^{7,10}[Cys^{7}, Cys^{10},Nle^{12}] and cyclo^{7,10}[Cys^{7},L-Ala^{9},Cys^{10},Nle^{12}] analogues in Table 10 are within ± 0.2 Å of the values reported for standard Type I and Type II β-turns (see Table 7) and support the conclusions that the cyclo^{7,10}[Cys^{7},Cys^{10}, Nle^{12}]α-factor adopts primarily a Type II β-turn conformation in DMSO/water, whereas the cyclo^{7,10}[Cys^{7},L-Ala^{9},Cys^{10},Nle^{12}]α-factor assumes a Type I β-turn. For the cyclo^{7,10}[Cys^{7},D-Val^{9},Cys^{10},Nle^{12}]α-factor analogue the Val^{9}αCH-Val^{9}NH internuclear distance (3.1 Å) is significantly larger than the value reported in Table 7 for the *i*+2 residue in a β-turn. It should be noted

however that the values in Table 7 correspond to L-residues only. Based on molecular modeling the Val^9αCH-Val^9NH internuclear distance of 3.1 Å is consistent with the D-valine having a ϕ angle of approximately 80-100°, which is in the range expected for a Type II β-turn (83). The $Pro^8_{\alpha CH}$-Cys^{10}_{NH} internuclear distance (2.9 Å) is somewhat shorter than the reported value of 3.3 Å reported for a standard Type II β-turn (see Table 7;3,83) or 3.7 Å reported for a cyclo^{1,4}[Cys^1, Pro^2,D-Val^3,Cys^4] tetrapeptide which was determined to adopt a Type II β-turn (85). The short $Pro^8_{\alpha CH}$-Cys^{10}_{NH} internuclear distance combined with the Val^9αCH-Val^9NH internuclear distance suggests (based on molecular modeling) that the Pro^8 ψ angle is approximately 140.8° and the D-Val^9 ϕ and ψ angles are 98.8 and -18.2 respectively. These backbone torsion angles and the $Pro^8_{\alpha CH}$-Cys^{10}_{NH} internuclear distance are consistent with the corresponding values reported for a cyclo^{1,4}[Pen^1,Pro^2,D-Val^3,Cys^4] tetrapeptide in CD_3CN, which was determined to adopt a Type II β-turn (85).

In order to reduce the possibility of spin-diffusion the values reported in Table 10 were obtained from NOESY spectra acquired with mixing times of 100 for the cyclo^{7,10}[Cys^7,Cys^{10},Nle^{12}]α-factor and 200 ms for the cyclo^{7,10}[Cys^7,L-Ala^9,Cys^{10},Nle^{12}] and cyclo^{7,10}[Cys^7,D-Val^9,Cys^{10},Nle^{12}]α-factor analogues. The values reported in Table 10 for the cyclo^{7,10}[Cys^7,L-Ala^9,Cys^{10},Nle^{12}] and

cyclo^{7,10}[Cys^{7},D-Val^{9},Cys^{10},Nle^{12}]α-factor analogues are within ± 0.1 Å (the estimated experimental error) of those obtained for these peptides from 400 ms NOESY spectra (see Table 11). This result suggests that even at the longer mixing time spin diffusion does not significantly affect the relative NOE intensities (i.e. internuclear distance information) for these two peptides.

In a Type II β-turn spanning residues 7-10 the two Gly^{9} αCH$_{i}$-NH$_{i}$ internuclear distances would be expected to be very different (3,83). For one of the Gly^{9} αCH$_{i}$-NH$_{i}$ interactions the internuclear separation would be expected to be 2.2 Å, while for the other Gly^{9} αCH$_{i}$-NH$_{i}$ interaction it would be expected to be 3.2 Å (3,83). Therefore, the strong and nearly equal intensities of the two Gly$^{9}_{\alpha CH}$-Gly$^{9}_{NH}$ connectivities in the 400 ms spectrum of the cyclo^{7,10}[Cys^{7},Cys^{10},Nle^{12}]α-factor (Figure 31) suggests that spin-diffusion was occurring through the geminal α-protons of Gly^{9}. In contrast, only one strong Gly$^{9}_{\alpha CH}$-Gly$^{9}_{NH}$ connectivity was observed in the 100 ms NOESY spectrum (the spectrum used to determine internuclear separation) of this peptide (Figure 34). This result indicates that spin-diffusion through this pathway is not significant at this shorter mixing time.

The $^{3}J_{\alpha NH}$ coupling constants for the cyclo^{7,10}[Cys^{7},X^{9},Cys^{10},Nle^{12}]α-factor analogues in aqueous and DMSO/water

FIGURE 34: The αCH-NH region of the 100 ms NOESY spectrum of the cyclo^{7,10}[Cys^{7},Cys^{10},Nle^{12}] α-factor in DMSO/water (25°C).

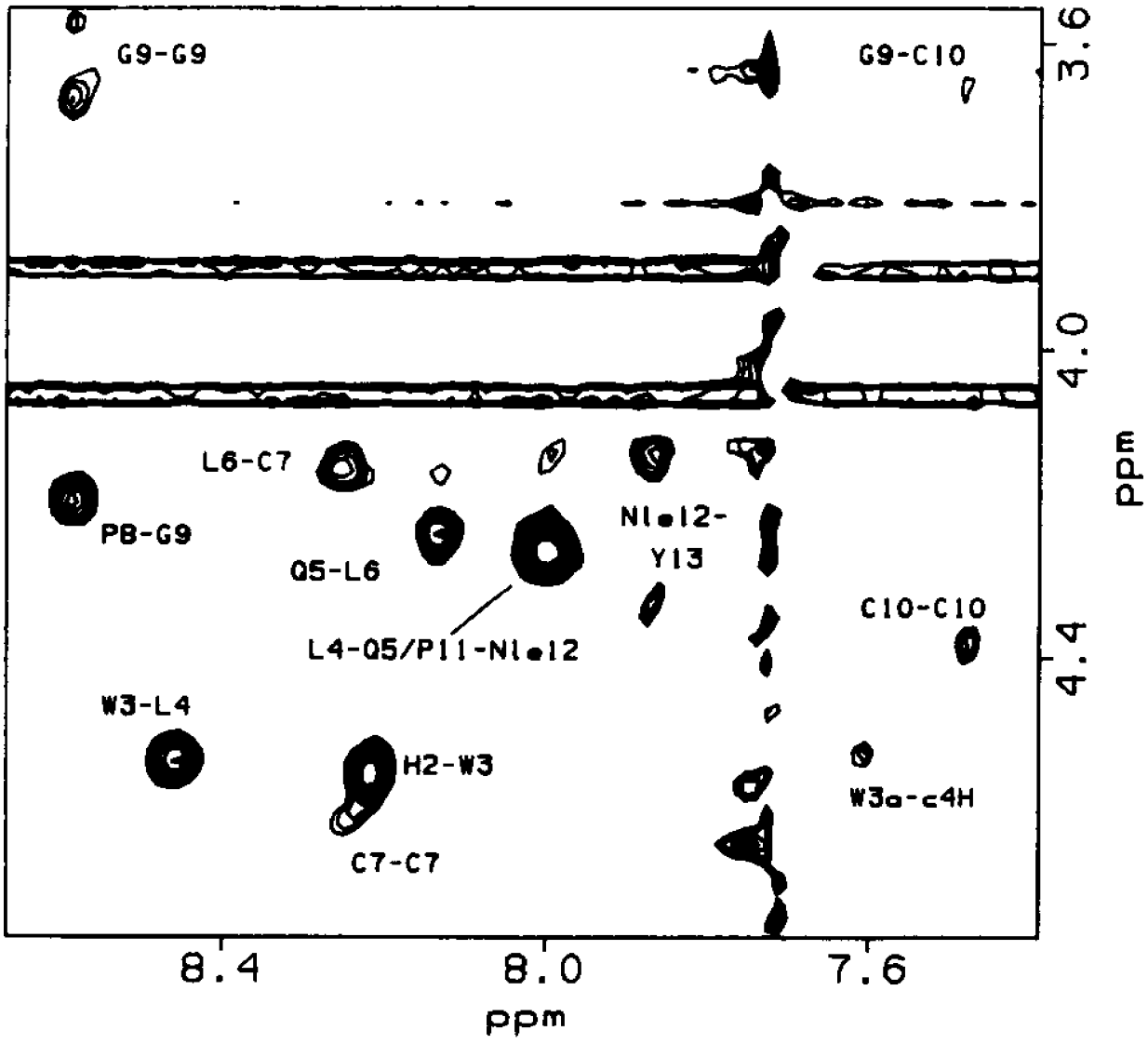
G9-G9
G9-C10
L6-C7
P8-G9
Q5-L6
N1•12-
Y13
L4-Q5/P11-N1•12
C10-C10
W3-L4
H2-W3
C7-C7
W3α-c4H
3.6
4.0
4.4
ppm
8.4
8.0
7.6
ppm

solutions are reported in Tables 12 and 13, respectively. $^3J_{\alpha NH}$ coupling constants which could not be measured from high resolution one-dimensional spectra, due to spectral overlap, were estimated from DQF-COSY spectra zero-filled to a digital resolution of 1.38 Hz/pt in the F_2 dimension. All of the $^3J_{\alpha NH}$ coupling constants for the cyclic α-factor peptides in both aqueous and DMSO/water solution are in the range normally associated for highly flexible peptides (148,149). However, the $^3J_{\alpha NH}$ coupling constants observed for D-Ala^9 in the cyclo^{7,10}[Cys^7,D-Ala^9,Cys^{10},Nle^{12}]α-factor in aqueous and DMSO/water solution (6.1 Hz and 6.2 Hz, respectively) and for D-Val^9 in the cyclo^{7,10}[Cys^7,D-Val^9,Cys^{10},Nle^{12}]α-factor in DMSO/water solution (6.5 Hz) are consistent with the values expected for a D-residue in the i+2 position of a Type II β-turn (83,161). The $^3J_{\alpha NH}$ coupling constant observed for L-Ala^9 in the cyclo^{7,10}[Cys^7,L-Ala^9,Cys^{10}, Nle^{12}]α-factor in aqueous solution (8 Hz) is only slightly smaller than the value expected (approximately 9 Hz) for the i+2 residue of a Type I β-turn (83,161). It was not possible to measure the $^3J_{\alpha NH}$ coupling constants for the Gly^9 amide in the cyclo^{7,10}[Cys^7,Cys^{10},Nle^{12}]α-factor as the triplet was poorly resolved in both aqueous and DMSO/water solutions and it was not possible to obtain these $^3J_{\alpha NH}$ coupling constants from DQF-COSY spectra as the geminal coupling

TABLE 12

$^3J_{\alpha N}$ coupling constants for the cyclic α-factor analogue peptides in water, pH 2.9.

Residue	CDAF		CLAF		CGAF
Trp^3	6[a]		7.0		6.9
Leu^4	7.2[b]		7.4		7.5
Gln^5	7		6		6
Leu^6	6.7		7.8		6.8
Cys^7	7		7.8		7.0
D-Ala^9	6.1	L-Ala^9	8	Gly^9	---
Cys^{10}	6.9		---		6.9
Nle^{12}	8		7		7
Tyr^{13}	7.7		8.1		8.0

[a] $^3J_{\alpha NH}$ values measured from DQF-COSY spectra are reported to the nearest Hz.

[b] $^3J_{\alpha NH}$ values measured from high resolution 1-dimensional spectra are reported to the nearest 0.1 Hz.

CDAF = cyclo^{7,10}[Cys^7,D-Ala^9,Cys^{10},Nle^{12}]α-factor
CLAF = cyclo^{7,10}[Cys^7,L-Ala^9,Cys^{10},Nle^{12}]α-factor
CGAF = cyclo^{7,10}[Cys^7,Cys^{10},Nle^{12}]α-factor

TABLE 13

$^3J_{\alpha N}$ coupling constants for the cyclic α-factor analogue peptides in DMSO/water.

Residue	CDAF	CLAF	CGAF	CDVAF
His^2	7.1[a]	7.3	7.2	7.7
Trp^3	---	7.9	6	---
Leu^4	7.3	7.0	7.4	7.6
Gln^5	7.9	---	8.5	7.7
Leu^6	9 [b]	8.5	8.6	8.9
Cys^7	---	8.7	9	---
D-Ala^9	6.2	L-Ala^9 ---	Gly^9 ---	D-Val^9 6.5
Cys^{10}	6	---	6	6
Nle^{12}	9.1	8.8	10	9.3
Tyr^{13}	8.5	8.2	8.7	8.7

[a] $^3J_{\alpha NH}$ values measured from high resolution 1-dimensional spectra are reported to the nearest 0.1 Hz.

[b] $^3J_{\alpha NH}$ values measured from DQF-COSY spectra are reported to the nearest Hz.

CDVAF = cyclo^{7,10}[Cys^7,D-Val^9,Cys^{10},Nle^{12}]α-factor
CDAF = cyclo^{7,10}[Cys^7,D-Ala^9,Cys^{10},Nle^{12}]α-factor
CLAF = cyclo^{7,10}[Cys^7,L-Ala^9,Cys^{10},Nle^{12}]α-factor
CGAF = cyclo^{7,10}[Cys^7,Cys^{10},Nle^{12}]α-factor

TABLE 14

Amide proton temperature coefficients for cyclic α-factor analogue peptides in water, pH 2.9. Values reported in ppb/K.

Residue	CDAF		CLAF		CGAF
Trp^{3}	-6.6		-6.1		-5.2
Leu^{4}	-6.7		-6.7		-5.4
Gln^{5}	-5.7		-5.9		-4.7
Leu^{6}	-10		-14		-11
Cys^{7}	-6.5		-3.8		-4.0
$D\text{-}Ala^{9}$	-8.3	$L\text{-}Ala^{9}$	-4.9	Gly^{9}	-5.5
Cys^{10}	-3.1		-3.6		-2.1
Nle^{12}	-8.1		-8.5		-7.2
Tyr^{13}	-7.7		-12		-8.5

CDAF = $cyclo^{7,10}[Cys^{7}, D\text{-}Ala^{9}, Cys^{10}, Nle^{12}]$α-factor
CLAF = $cyclo^{7,10}[Cys^{7}, L\text{-}Ala^{9}, Cys^{10}, Nle^{12}]$α-factor
CGAF = $cyclo^{7,10}[Cys^{7}, Cys^{10}, Nle^{12}]$α-factor

TABLE 15

Amide proton temperature coefficients for cyclic α-factor analogue peptides in DMSO/water. Values reported in ppb/K.

Residue	CDAF		CLAF		CGAF		CDVAF
His^{2}	-5.1		-4.8		-4.5		-4.5
Trp^{3}	-5.4		-4.9		-5.3		-4.7
Leu^{4}	-7.1		-6.8		-6.5		-7.0
Gln^{5}	-4.6		-4.6		-4.5		-4.4
Leu^{6}	-10		-9.8		-9.7		-9.6
Cys^{7}	-5.4		-2.8		-2.5		-4.7
D-Ala^{9}	-5.2	L-Ala^{9}	-4.6	Gly^{9}	-4.5	D-Val^{9}	-4.2
Cys^{10}	-1.2		-1.5		-0.9		-1.0
Nle^{12}	-6.1		-5.9		-5.0		-5.5
Tyr^{13}	-8.5		-8.2		-8.3		-8.4

CDVAF = cyclo^{7,10}[Cys^{7}, D-Val^{9}, Cys^{10}, Nle^{12}]α-factor
CDAF = cyclo^{7,10}[Cys^{7}, D-Ala^{9}, Cys^{10}, Nle^{12}]α-factor
CLAF = cyclo^{7,10}[Cys^{7}, L-Ala^{9}, Cys^{10}, Nle^{12}]α-factor
CGAF = cyclo^{7,10}[Cys^{7}, Cys^{10}, Nle^{12}]α-factor

FIGURE 35: Hypothetical β-sheet formation involving residues 4-7 and 10-13, showing expected hydrogen bonds and NOE connectivities.

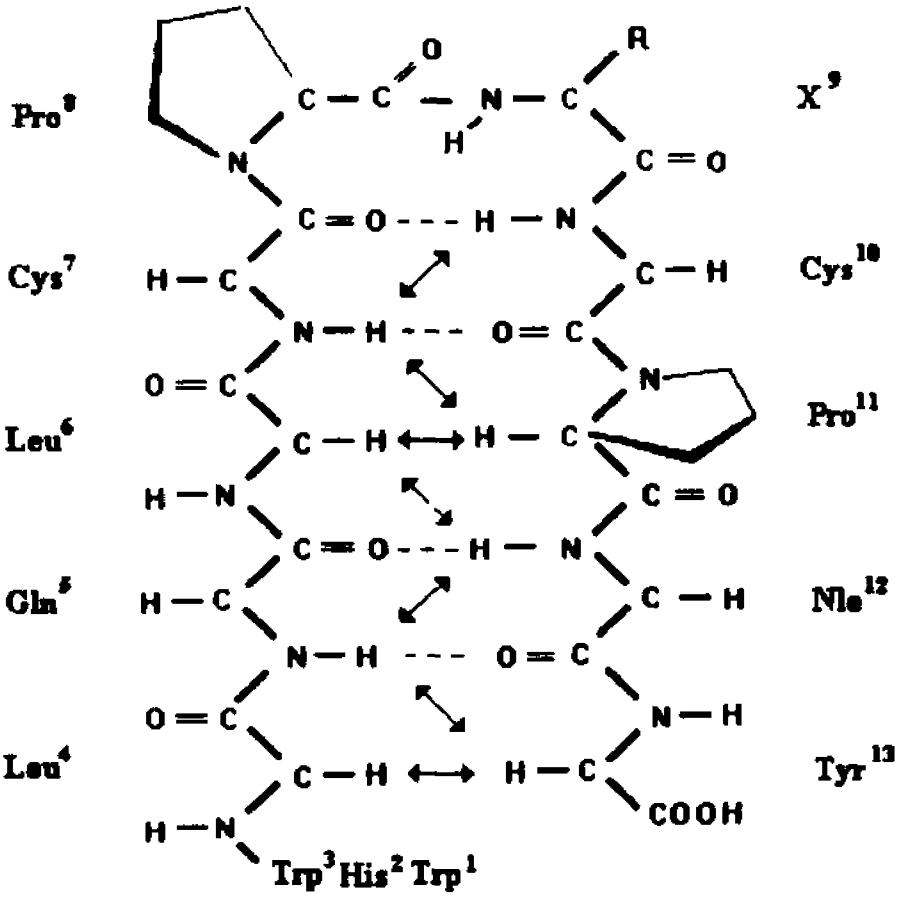
Pro⁸
X⁹
Cys⁷
Cys¹⁰
Leu⁶
Pro¹¹
Gln⁵
Nle¹²
Leu⁴
Tyr¹³
COOH
Trp³ His² Trp¹

of the α-protons distorts and complicates the COSY cross-peak splitting pattern.

The NH temperature coefficients for the cyclic α-factor analogues was measured over the range 19-49°C in aqueous solution (Table 14) and 5-35°C in DMSO/water (Table 15). For the peptides examined in aqueous solution the NH $d\delta/dT$ of the Cys^{10} amide resonance (-2.1 - -3.6 ppb/k) are significantly lower than the NH $d\delta/dT$ observed for other residues. This result suggests that the Cys^{10} amide proton in these peptides is shielded from the solvent and may be involved in intramolecular hydrogen bonding. Even lower NH $d\delta/dT$ for the Cys^{10} NH resonance are found in DMSO/water solution (-0.9 - -1.5 ppb/K). The very low temperature coefficients found for the Cys^{10} amide resonance for all of the cyclic α-factor analogues in DMSO/water are in the range that has been associated with strong intramolecular hydrogen bonding in both DMSO and aqueous solutions (145,148,149). Therefore, it is expected that the low temperature coefficients observed for the Cys^{10} amide resonance in DMSO/water is indicative of intramolecular hydrogen bonding in this solvent.

The amide temperature coefficients measured for the Leu^{4}, Leu^{6}, and Tyr^{13} are somewhat higher than those observed for the Gln^{5}, Cys^{7}, Cys^{10}, and Nle^{12} residues. The NH temperature coefficients for Cys^{7} are particularly

low for the cyclo^{7,10}[Cys^{7},L-Ala^{9},Cys^{10},Nle^{12}]- and cyclo^{7,10}[Cys^{7},Cys^{10},Nle^{12}]α-factor. This pattern of alternating high and low NH temperature coefficients might be consistent with the presence of a transient β-sheet conformation involving residues 4-7 and residues 10-13 (see Figure 35). This structural feature was suggested by the results of VCD spectroscopic studies on the cyclo^{7,10}[Cys^{7},D-Ala^{9},Cys^{10},Nle^{12}] and cyclo^{7,10}[Cys^{7},L-Ala^{9},Cys^{10},Nle^{12}] analogues in DMSO/water (*vide infra*).

Vibrational Circular Dichroism:

In addition to NMR spectroscopy I have also utilized vibrational circular dichroism (VCD) to study the [L-Ala^{9}]-, the cyclo^{7,10}[Cys^{7},D-Ala^{9},Cys^{10},Nle^{12}]-, and the cyclo^{7,10}[Cys^{7},L-Ala^{9},Cys^{10},Nle^{12}]α-factors, and an analogue in which the Pro^{8} and Gly^{9} residues have been replaced by 5-amino pentanoic acid, in a DMSO/water mixture. These studies were carried out in collaboration with Mr. Arthur Barlow and Dr. Max Diem. The infrared absorption and VCD spectrum of the [L-Ala^{9}]-, cyclo^{7,10}[Cys^{7},D-Ala^{9},Cys^{10}, Nle^{12}]-, cyclo^{7,10}[Cys^{7},L-Ala^{9},Cys^{10},Nle^{12}]α-factor analogues in the amide I' region are presented in Figure 36. In the absorption spectrum of the [L-Ala^{9}]α-factor a broad peak centered about 1660 cm^{-1} and a distinct shoulder around 1695 cm^{-1} is observed. The VCD spectrum of [L-Ala^{9}] exhibits a weak negative-positive couplet under the

FIGURE 36: VCD (top) and absorption (bottom) spectra for the linear [L-Ala^{9}]α-factor (heavy dotted line), cyclo^{7,10}[Cys^{7},L-Ala^{9},Cys^{10},Nle^{12}]α-factor (dotted line), cyclo^{7,10}[Cys^{7},D-Ala^{9},Cys^{10}, Nle^{12}]α-factor (solid line) in DMSO/water.

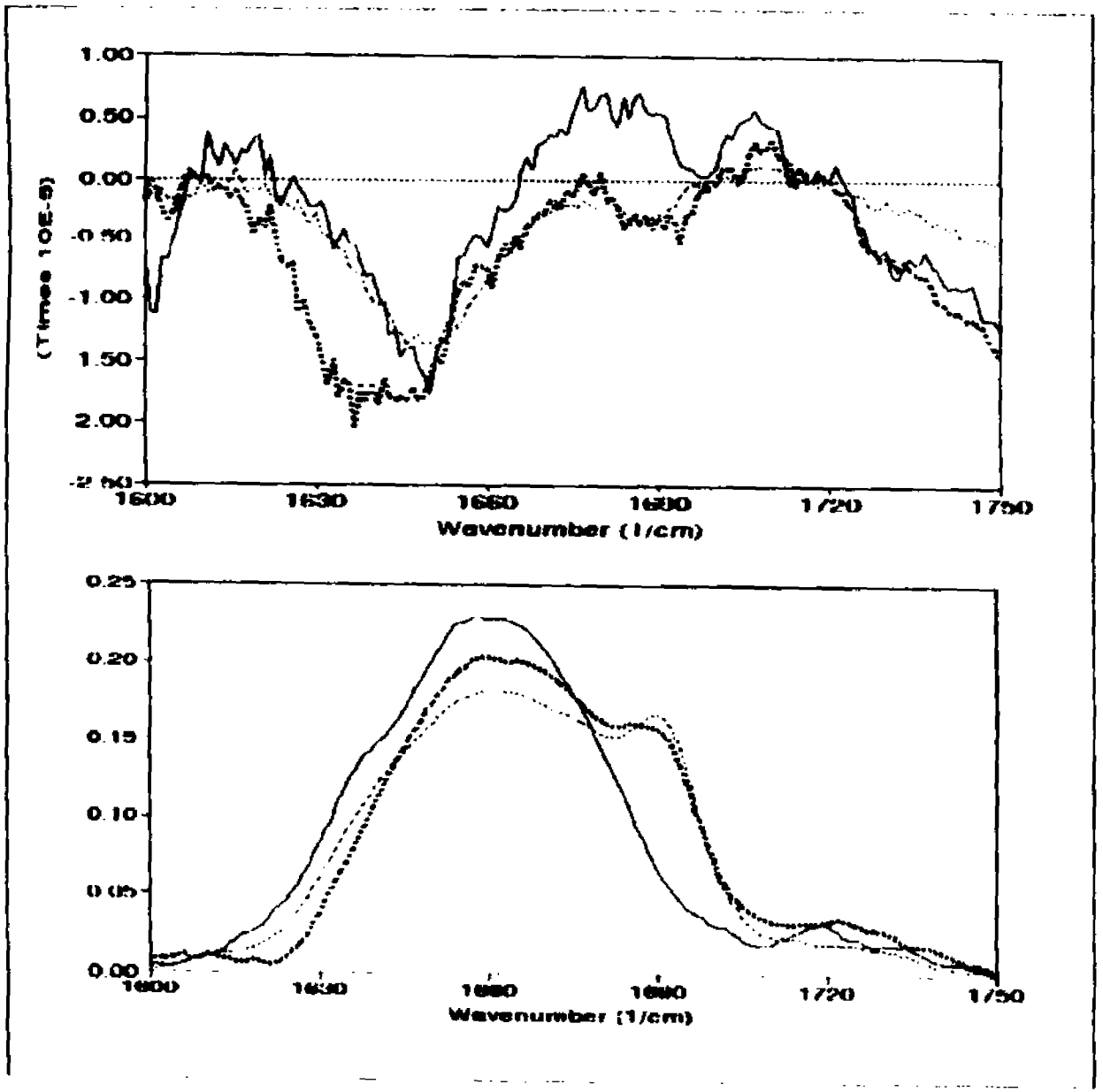
1.00
0.50
0.00
-0.50
-1.00
1.50
2.00
(Times 10E-5)
1600
1630
1660
1690
1720
1750
Wavenumber (1/cm)
0.25
0.20
0.15
0.10
0.05
0.00
1600
1630
1660
1690
1720
1750
Wavenumber (1/cm)

FIGURE 37: VCD (top) and absorption (bottom) spectra for the des-Pro^{8},Gly^{9}cyclo^{7,10}[Cys^{7},5-amino pentanoic acid,Cys^{10},Nle^{12}]α-factor in DMSO/water.

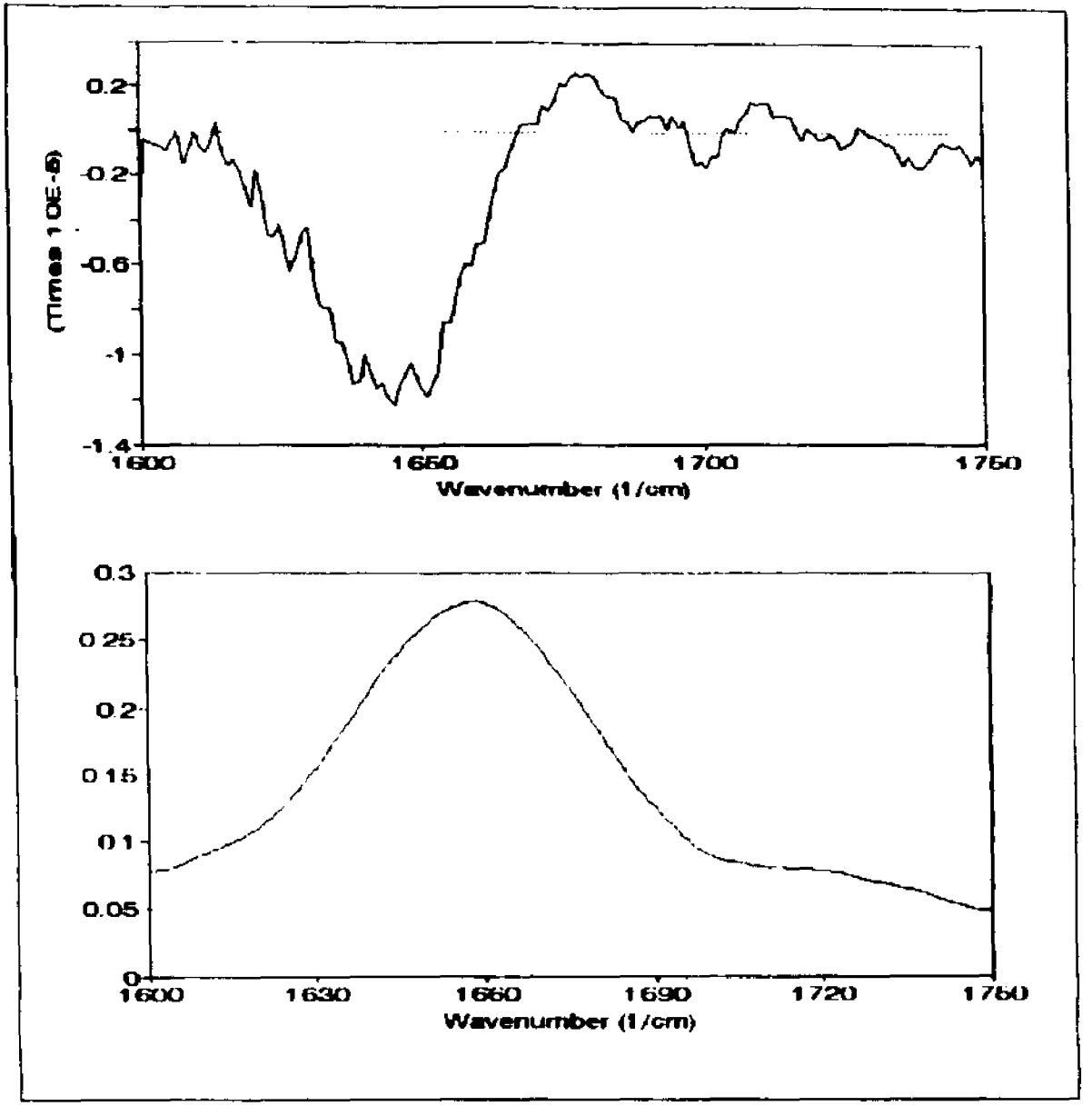
0.2
-0.2
-0.6
-1
-1.4
(Times 1.0E-6)
1600
1650
1700
1750
Wavenumber (1/cm)
0.3
0.25
0.2
0.15
0.1
0.05
0
1600
1630
1660
1690
1720
1750
Wavenumber (1/cm)

absorption peak at 1695 cm^{-1}. In addition a broad negative signal with a minimum at a lower frequency (1640 cm^{-1}) than that of the main absorption peak is observed.

The absorption spectrum of the cyclo^{7,10}[Cys^{7},L-Ala^{9}, Cys^{10},Nle^{12}] analogue is very similar to that for the [L-Ala^{9}]α-factor. Apparently the substitution of Lys^{7} and Gln^{10} by two cysteine residues and the disulfide bridge does not significantly change the absorption spectrum in the amide I' region. The VCD spectrum of the cyclo^{7,10}[Cys^{7},L-Ala^{9},Cys^{10},Nle^{12}]α-factor is very similar to that obtained for the [L-Ala^{9}] peptide, with both the high frequency couplet and the lower frequency negative peak present. However, the main negative feature in the VCD spectrum of the cyclo^{7,10}[Cys^{7},L-Ala^{9},Cys^{10},Nle^{12}]α-factor has a much narrower width and is shifted to higher wavenumber (1650 cm^{-1}) relative to that found for the [L-Ala^{9}] analogue.

The spectral features of both the absorption and VCD spectra of the cyclo^{7,10}[Cys^{7},D-Ala^{9},Cys^{10},Nle^{12}]α-factor in the amide I' region (Figure 36) are significantly different from those of the [L-Ala^{9}] and cyclo^{7,10}[Cys^{7},L-Ala^{9},Cys^{10},Nle^{12}] analogues. In addition to the main absorption peak at 1660 cm^{-1} a poorly resolved low frequency shoulder (at approximately 1640 cm^{-1}) is observed in the absorption spectrum of the cyclo^{7,10}[Cys^{7},D-Ala^{9},Cys^{10},Nle^{12}]α-factor. The high

frequency shoulder observed for both the cyclo^{7,10}[Cys^{7},L-Ala^{9},Cys^{10},Nle^{12}] and [L-Ala^{9}] analogues is not found for the cyclo^{7,10}[Cys^{7},D-Ala^{9},Cys^{10},Nle^{12}]α-factor. The VCD of the cyclo^{7,10}[Cys^{7},D-Ala^{9},Cys^{10},Nle^{12}]α-factor exhibits a positive signal around 1680 cm^{-1} and a negative minimum at 1650 cm^{-1}.

The spectral differences observed for the cyclo^{7,10}[Cys^{7},D-Ala^{9},Cys^{10},Nle^{12}]α-factor relative to the linear [L-Ala^{9}]α-factor and the cyclo^{7,10}[Cys^{7},L-Ala^{9}, Cys^{10},Nle^{12}] analogue are presumably due to the different conformational preferences of these peptides and not from the chirality of alanine. This conclusion is based on the fact that VCD signals observed in the amide I' region are almost exclusively due to the dipolar coupling of the stretching vibrations of the carbonyl groups (23,24). Therefore, changes in the chirality of a residue will not affect the VCD spectrum unless this change also affects the conformation of the peptide. The strong negative peak common to all three peptides can be described qualitatively as being associated with β-sheet conformations (20,21,24). Therefore, this feature is presumably due to the interaction of residues 4-6 at the N-terminus with residues 11-13 at the C-terminus (see Figure 35).

The substitution of Pro^{8} and Ala^{9} (or D-Ala^{9}) by 5-aminopentanoic acid in the des-Pro^{8},des-Gly^{9}-

cyclo^{7,10}[Cys^{7},5-aminopentanoic acid,Cys^{10},Nle^{12}]α-factor analogue removes the carbonyl groups that are involved in the β-turn while maintaining the size of the ring. Thus, it is expected that transitions that would arise from the cyclic region will not be observed for this analogue. The absorption spectrum of the des-Pro^{8},des-Gly^{9}-cyclo^{7,10}[Cys^{7},5-aminopentanoic acid,Cys^{10},Nle^{12}]α-factor analogue in the amide I' region is devoid of either the high-or low frequency shoulders observed for the other peptides (Figure 37). This result suggests that both these spectral features are associated with the amino acids involved in the β-turns. As with the other analogues studied the main spectral feature observed in the VCD of the des-Pro^{8},des-Gly^{9}-cyclo^{7,10}[Cys^{7},5-aminopentanoic acid,Cys^{10},Nle^{12}] analogue is a broad negative signal at 1660 cm^{-1} (Figure 37).

The similarity of VCD spectra of the linear [L-Ala^{9}]α-factor and cyclo^{7,10}[Cys^{7},L-Ala^{9},Cys^{10},Nle^{12}]α-factor suggests that the linear peptide adopts a Type I β-turn in DMSO/water. This hypothesis is further supported by the presence of the shoulder at 1695 cm^{-1} in the absorption spectrum of the linear [L-Ala^{9}]α-factor. This peak is observed in the absorption spectrum of the cyclo^{7,10}[Cys^{7},L-Ala^{9},Cys^{10},Nle^{12}]α-factor, but is absent in the absorption spectrum of the cyclo^{7,10}[Cys^{7},D-Ala^{9},Cys^{10}, Nle^{12}]α-factor and cyclic analogue in which residues 8

and 9 are replaced by 5-amino pentanoic acid. Thus, it appears that this spectral feature is associated with the Type I β-turn conformation. These results suggest that DMSO/water may stabilize a Type I β-turn in the linear [L-Ala^9] peptide.

CHAPTER V

Results on the a-Factor and a-Factor Analogues in DMSO:

Assignments of the a-Factor and a-Factor Analogues

The a-factor and five a-factor analogues (see Figure 4) were studied in DMSO using NMR spectroscopy. The resonance assignments for these peptides was accomplished using a protocol similar to that used for the α-factor analogues (see Chapter IV). The ^1H resonances of the two Ile residues, Lys^4, Gly^5, Val^6, Pro^{10}, and Ala^{11} were assigned by identification of their unique spin-spin connectivity patterns in the DQF-COSY spectrum. The Phe^7, Trp^8, Asp^9, and Cys^{12} residues all have identical spin systems (not including the aromatic resonances, which were assigned directly from the DQF-COSY spectra). Therefore, the sequential assignment of these residues was accomplished through the use of αCH_i-NH_{i+1} NOE connectivities. Assignment of the Ile^2 and Ile^3 spin systems was also made in this manner. The absence of a cross-peak arising from the Tyr^1 NH_3 in the DQF-COSY spectrum allowed direct assignment of the α- and β-proton resonances of the Tyr^1 residue. Assignments for the S-Alkyl groups were made primarily through the analysis of one-dimensional spectra. The chemical shifts for corresponding resonances in all a-factor peptides

TABLE 16
1H Assignments for a-factor in DMSO.

Residue	NH	αCH	βCH	γCH	δCH	εCH	Other
Tyr[1]	----	3.94	2.93 2.75				$C_{2,6}H$ 7.00 $C_{3,5}H$ 6.67 OH 9.31
Ile[2]	8.45	4.31	1.68	1.47 1.05 0.80	0.80		
Ile[3]	8.09	4.19	1.74	1.44 1.10 0.81	0.80		
Lys[4]	7.97	4.26	1.65 1.52	1.29	1.51	2.71	εNH_2 7.70
Gly[5]	8.04	3.80 3.65					
Val[6]	7.69	4.14	1.90	0.71			
Phe[7]	8.05	4.52	2.96 2.75				ring protons: 7.24,7.18, 7.11
Trp[8]	7.98	4.56	3.09 2.93				ring protons 7.54,6.96, 7.05,7.31, 7.11 indole NH 10.80
Asp[9]	8.41	4.76	2.70 2.36				
Pro[10]	----	4.24	1.83	1.74 1.59	3.41 3.22		
Ala[11]	7.79	4.23	1.20				
Cys[12]	8.06	4.39	2.80 2.68				$S-C_{15}H_{25}$ 5.15,5.08, 5.04,3.14, 2.04,2.00, 1.61,1.54 OCH_3 3.62

TABLE 17

1H Assignments for the nonmethylated a-factor in DMSO.

Residue	NH	αCH	βCH	γCH	δCH	εCH	Other
Tyr[1]	----	3.94	2.94 2.75				$C_{2,6}H$ 7.00 $C_{3,5}H$ 6.67 OH 9.32
Ile[2]	8.46	4.30	1.68	1.46 1.03 0.80	0.80		
Ile[3]	8.08	4.19	1.73	1.43 1.07 0.81	0.79		
Lys[4]	7.98	4.26	1.52	1.28	1.50	2.71	εNH_2 7.68
Gly[5]	8.06	3.80 3.65					
Val[6]	7.68	4.12	1.89	0.70			
Phe[7]	8.05	4.51	2.97 2.75				ring protons: 7.24,7.18, 7.11
Trp[8]	7.97	4.55	3.08 2.94				ring protons 7.54,6.96, 7.05,7.31, 7.11 indole NH 10.80
Asp[9]	8.41	4.76	2.69 2.37				
Pro[10]	----	4.24	1.84	1.74 1.59	3.41 3.23		
Ala[11]	7.82	4.23	1.19				
Cys[12]	7.87	4.28	2.83 2.67				$S\text{-}C_{15}H_{25}$ 5.13,5.04, 5.02,3.13, 2.02,2.00, 1.58,1.52

TABLE 18

1H Assignments for the S-geranyl a-factor in DMSO.

Residue	NH	αCH	βCH	γCH	δCH	εCH	Other
Tyr[1]	----	3.99	2.93 2.77				$C_{2,6}H$ 7.00 $C_{3,5}H$ 6.66 OH 9.30
Ile[2]	8.49	4.30	1.68	1.47 1.05 0.80	0.81		
Ile[3]	8.09	4.19	1.74	1.44 1.08 0.80	0.81		
Lys[4]	7.97	4.26	1.64 1.49	1.29	1.50	2.70	εNH_2 7.70
Gly[5]	8.03	3.79 3.64					
Val[6]	7.69	4.15	1.90	0.70			
Phe[7]	8.05	4.53	2.97 2.74				ring protons: 7.24,7.17, 7.11
Trp[8]	7.99	4.56	3.08 2.92				ring protons 7.54,6.96, 7.05,7.31, 7.10 indole NH 10.79
Asp[9]	8.41	4.76	2.70 2.37				
Pro[10]	----	4.23	1.82	1.74 1.57	3.39 3.19		
Ala[11]	7.75	4.22	1.19				
Cys[12]	8.05	4.38	2.79 2.68				$S\text{-}C_{10}H_{17}$ 5.14,5.07, 5.03,3.14, 2.03,2.00, 1.61,1.54 OCH_3 3.64

TABLE 12

1H Assignments for the S-hexadecyl a-factor in DMSO.

Residue	NH	αCH	βCH	γCH	δCH	εCH	Other
Tyr[1]	----	4.01	2.95 2.79				$C_{2,6}H$ 7.02 $C_{3,5}H$ 6.68 OH 9.32
Ile[2]	8.51	4.33	1.68	1.46 1.06 0.81	0.82		
Ile[3]	8.11	4.21	1.74	1.46 1.09 0.81	0.82		
Lys[4]	7.98	4.27	1.52	1.29	1.50	2.73	εNH_2 7.71
Gly[5]	8.04	3.80 3.66					
Val[6]	7.71	4.16	1.91	0.72			
Phe[7]	8.06	4.54	2.98 2.76				ring protons: 7.22,7.21, 7.15
Trp[8]	8.01	4.57	3.09 2.94				ring protons 7.55,6.97, 7.05,7.32, 7.12 indole NH 10.82
Asp[9]	8.43	4.77	2.72 2.39				
Pro[10]	----	4.25	1.83	1.76 1.60	3.41 3.21		
Ala[11]	7.74	4.23	1.20				
Cys[12]	8.03	4.39	2.86 2.76				$S\text{-}C_{16}H_{33}$ 2.46,1.50, 1.23 OCH_3 3.61

TABLE 20

1H Assignments for the S-methyl a-factor in DMSO.

Residue	NH	αCH	βCH	γCH	δCH	εCH	Other
Tyr[1]	----	3.99	2.95 2.78				$C_{2,6}H$ 7.01 $C_{3,5}H$ 6.68 OH 9.34
Ile[2]	8.49	4.32	1.68	1.48 1.06 0.83	0.82		
Ile[3]	8.10	4.21	1.73	1.44 1.09 0.83	0.82		
Lys[4]	7.98	4.27	1.63	1.29	1.50	2.73	εNH_2 7.73
Gly[5]	8.03	3.81 3.65					
Val[6]	7.70	4.15	1.90	0.72			
Phe[7]	8.05	4.54	2.95 2.75				ring protons: 7.22,7.21, 7.15
Trp[8]	7.99	4.57	3.09 2.94				ring protons 7.55,6.98, 7.05,7.32, 7.12 indole NH 10.82
Asp[9]	8.42	4.77	2.72 2.38				
Pro[10]	----	4.24	1.84	1.80 1.61	3.42 3.23		
Ala[11]	7.75	4.23	1.21				
Cys[12]	8.03	4.42	2.80 2.75				S-CH_3 2.07 OCH_3 3.65

TABLE 21

1H Assignments for the nonfarnesylated, nonmethylated a-factor in DMSO.

Residue	NH	αCH	βCH	γCH	δCH	εCH	Other
Tyr[1]	----	4.01	2.95 2.78				$C_{2,6}H$ 7.02 $C_{3,5}H$ 6.67 OH 9.31
Ile[2]	8.49	4.32	1.68	1.46 1.06 0.80	0.78		
Ile[3]	8.10	4.20	1.74	1.45 1.08 0.80	0.78		
Lys[4]	7.97	4.26	1.66 1.52	1.29	1.50	2.71	εNH_2 7.65
Gly[5]	8.03	3.80 3.65					
Val[6]	7.70	4.16	1.91	0.71			
Phe[7]	8.05	4.53	2.98 2.73				ring protons: 7.22,7.20, 7.15
Trp[8]	8.01	4.56	3.08 2.93				ring protons 7.55,6.96, 7.05,7.32, 7.12 indole NH 10.79
Asp[9]	8.42	4.76	2.71 2.36				
Pro[10]	----	4.25	1.84	1.76 1.59	3.39 3.22		
Ala[11]	7.81	4.22	1.21				
Cys[12]	7.99	4.45	2.94 2.77				S-H 2.08

(Tables 16-21) were within 0.05 ppm, with the exception of those resonances of Cys^{12} from the nonmethylated a-factor (NH 7.87; αCH 4.28; βCH 2.83, 2.67 ppm) and nonmethylated, nonfarnesylated a-factor (NH 7.99; αCH 4.45; βCH 2.94, 2.77 ppm) analogues, which showed a greater variation.

The $^3J_{\alpha NH}$ coupling constants and NH temperature coefficients for the a-factor and a-factor peptides are reported in Tables 22 and 23, respectively. The high degree of spectral overlap found in these peptides dictated that two-dimensional techniques be used to obtain the $^3J_{\alpha NH}$ coupling constants and the NH temperature coefficients. The $^3J_{\alpha NH}$ coupling constants were estimated from the anti-phase splitting of DQF-COSY cross-peaks from spectra that were zero-filled to a digital resolution of 1.38 Hz/pt. in the F_2 dimension. The $^3J_{\alpha NH}$ coupling constants for Gly^5 in the a-factor and a-factor analogues could not be measured from the Gly^5 NH-αCH COSY cross-peaks due to the additional splitting from the geminal coupling of the two α-protons. All $^3J_{\alpha NH}$ coupling constants for the a-factor peptides were in the range (7-9 Hz) expected for peptides undergoing rapid conformational averaging (148,149). The NH temperature coefficients were measured using absolute value COSY spectra acquired over a temperature range of 19-49°C. The NH temperature coefficients obtained for the a-factor

TABLE 22

$^3J_{\alpha NH}$ coupling constants for the a-factor and a-factor analogues (in DMSO at 25°C) obtained from DQF-COSY spectra zero-filled to a digital resolution of 1.38 Hz/pt. Values reported in Hz.

Residue	aF	SM-aF	HD-aF	FA-aF	SG-aF	SH-aF
Ile^2	9	8	8	8	8	8
Ile^3	8	8	8	8	8	8
Lys^4	8	7	7	7	7	8
Gly^5	---	---	---	---	---	---
Val^6	9	9	9	8	9	8
Phe^7	8	8	8	8	7	8
Trp^8	7	7	7	7	7	7
Asp^9	8	7	8	7	7	8
Ala^{11}	7	8	7	7	7	7
Cys^{12}	7	7	7	7	7	7

aF = a-Factor
SM-aF = S-Methyl a-Factor
HD-aF = S-Hexadecanyl a-Factor
FA-aF = nonmethylated a-Factor
SG-aF = S-Geranyl a-Factor
SH-aF = nonfarnesylated,nonmethylated a-factor

TABLE 23

Amide proton temperature coefficients for a-factor and a-factor analogue peptides in DMSO.
Values reported in ppb/K.

NH	aF	SM-aF	HD-aF	FA-aF	SG-aF	SH-aF
Ile^{2}	-4.9	-4.5	-4.4	-5.6	-4.1	-3.9
Ile^{3}	-5.7	-5.4	-5.2	-5.5	-4.8	-4.9
Lys^{4}	-4.8	-4.7	-4.4	-4.5	-4.2	-4.2
Gly^{5}	-4.4	-3.9	-3.8	-4.1	-3.8	-3.8
Val^{6}	-4.4	-4.2	-4.3	-4.2	-4.5	-4.1
Phe^{7}	-4.6	-4.5	-4.6	-4.7	-4.1	-4.3
Tyr^{8}	-4.9	-5.9	-6.0	-5.5	-5.5	-5.6
Asp^{9}	-6.1	-6.2	-6.0	-6.2	-5.9	-5.7
Ala^{11}	-5.6	-5.0	-4.6	-5.0	-4.8	-4.4
Cys^{12}	-5.5	-5.0	-5.1	-4.3	-4.9	-5.6

aF = a-Factor
SM-aF = S-Methyl a-Factor
SH-aF = S-Hexadecanyl a-Factor
FA-aF = nonmethylated a-Factor
SG-aF = S-Geranyl a-Factor
SH-aF = nonfarnesylated,nonmethylated a-Factor

and a-factor analogues were significantly greater than the value (-2 ppb/K) usually associated with intramolecular hydrogen-bonding in DMSO solution (148,149).

In the NOESY spectra of all a-factor peptides strong αCH_i-NH_{i+1} connectivities are observed between all residues, except Asp^9 and Pro^{10} (Figure 38). For these two residues the analogous αCH_i-δCH_{i+1} connectivities were observed. In addition to the sequential αCH_i-NH_{i+1} NOE connectivities a weak cross-peak between the a-proton of Val^6 and the amide proton of Trp^8 was observed.

The NH-NH region of the 400 ms NOESY spectrum of a-factor is shown in Figure 39. Many of the possible sequential NH-NH connectivities are present. Due to the clustering of amide chemical shifts, several of the NH-NH cross-peaks overlap or are hidden by the diagonal. In the spectra of the a-factor and the nonmethylated a-factor analogue a second non-sequential cross-peak is observed, which is either due to a Val^6-Trp^8 or Lys^4-Val^6 interaction. This cross-peak is not observed in the spectra of the other a-factor peptides presumably due to the spectral overlap with the stronger Val^6-Phe^7 cross-peak.

As stated above a strong cross-peak was observed between the Asp^9 a-proton and the d-protons of Pro^{10}. The presence of this cross-peak indicates that the Asp^9-Pro^{10}

FIGURE 38: αCH-NH region of the 400 ms NOESY spectrum of α-factor in DMSO. Note the $V^{6}_{\alpha CH}$-W^{8}_{NH} connectivity.

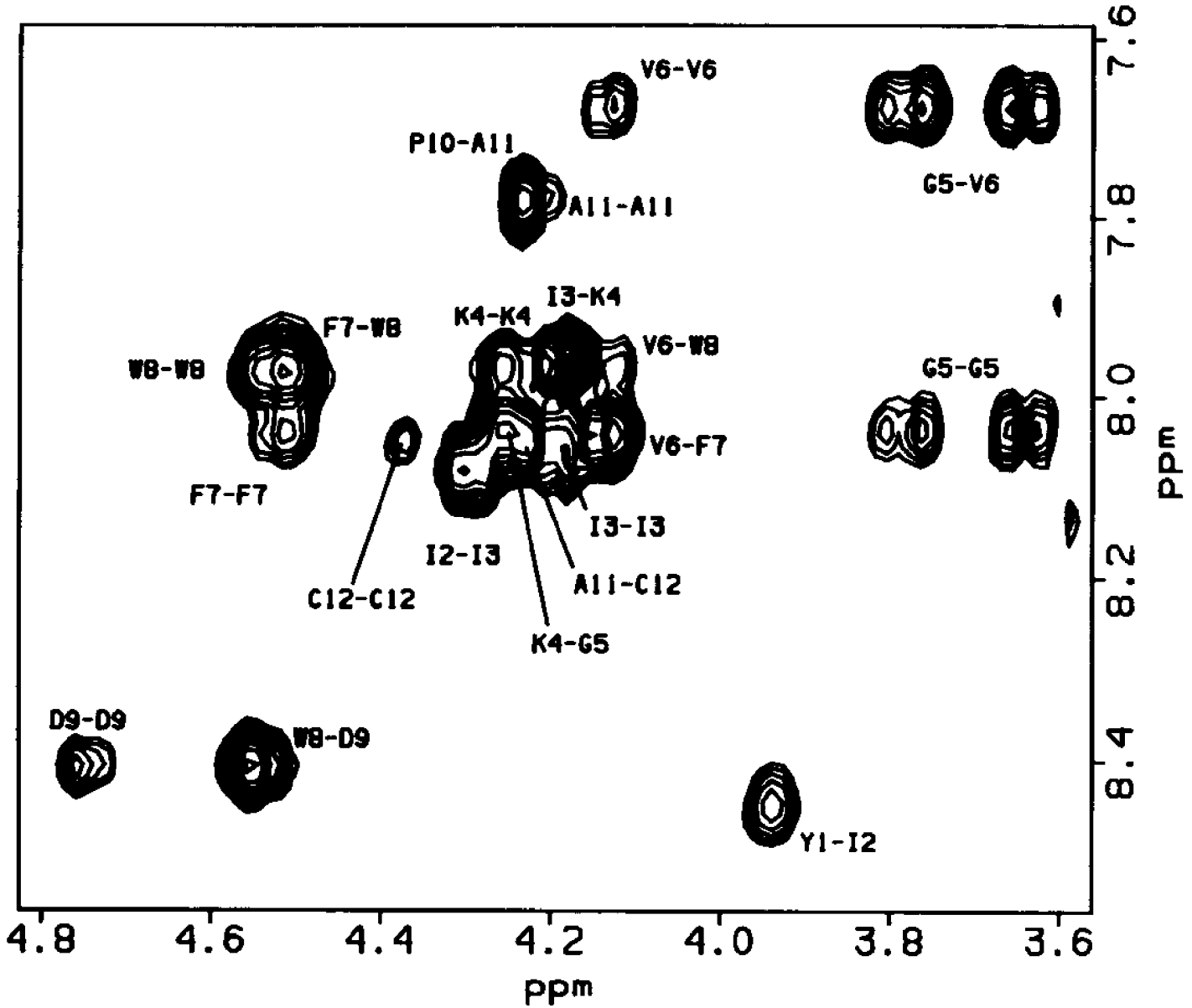
V6-V6
P10-A11
A11-A11
G5-V6
I3-K4
K4-K4
F7-W8
V6-W8
W8-W8
G5-G5
V6-F7
F7-F7
I3-I3
I2-I3
A11-C12
C12-C12
K4-G5
D9-D9
W8-D9
Y1-I2
7.6
7.8
8.0
8.2
8.4
ppm
4.8
4.6
4.4
4.2
4.0
3.8
3.6
ppm

FIGURE 39: NH-NH region of the 400 ms NOESY spectrum of ■-factor in DMSO. Note the V^{6}_{NH}-W^{8}_{NH} connectivity. Cross-peaks are labeled D9 and A11 are due to chemical exchange between the *cis-trans* isomers of the Pro^{10} amide bond.

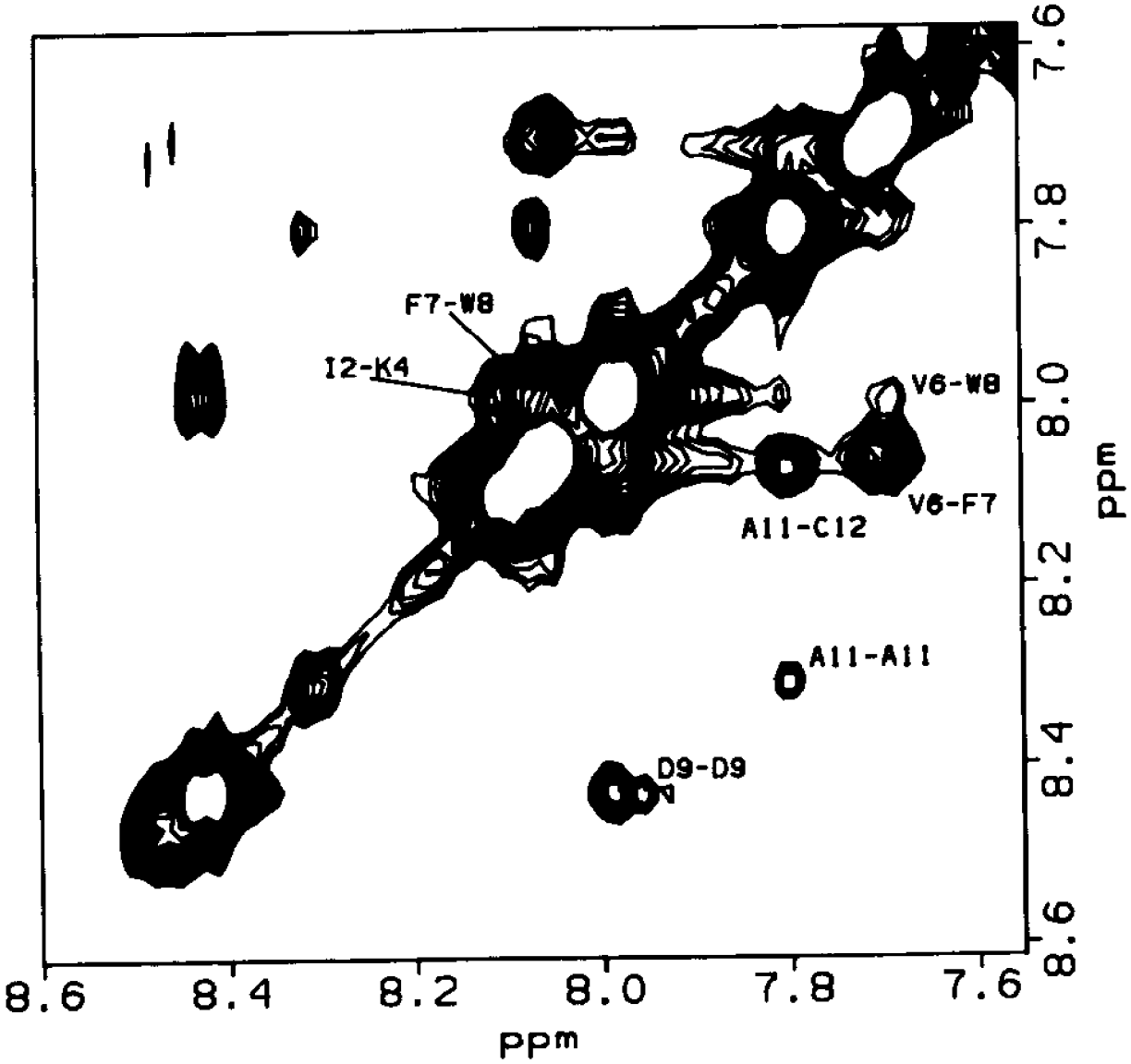
F7-W8
I2-K4
V6-W8
V6-F7
A11-C12
A11-A11
D9-D9
8.6
8.4
8.2
8.0
7.8
7.6
ppm
ppm

bond is predominantly *trans* (83). However, evidence for cis-*trans* isomerization of the Asp^{9}-Pro^{10} bond was observed in the one-dimensional spectrum as well as in the NOESY spectrum of a-factor. In the NOESY spectra of a-factor a cross-peak was observed between the Asp^{9} NH resonances and a resonance at 7.94 ppm and between the Ala^{11} NH resonance and a resonance at 8.32 ppm. The resonances at 7.94 ppm and 8.32 ppm did not correspond to any of the resonance assignments made for a-factor. However, they did correspond to extremely small intensity resonances in the one-dimensional spectrum (the resonance at 7.94 ppm was resolvable only between 40-50°C). Therefore, it was believed that the above cross-peaks might be due to the slow interconversion of *cis* and *trans* isomers of the Asp^{9}-Pro^{10} bond. In order to ascertain if this was the case, saturation transfer experiments (Chapter II) were performed at 50°C for the resonance at 7.94 ppm and at 53°C for the resonance at 8.32 ppm. A slightly greater saturation transfer effect for the resonance at 8.32 ppm was observed at 53°C relative to that observed at 50°C. The results for the saturation transfer experiments on the resonance at 8.32 ppm are presented in Figure 40. It is often necessary to perform saturation transfer experiments at elevated temperatures in order for the interconversion between *cis* and *trans* isomers to be fast relative to the spin-lattice

FIGURE 40: Results of saturation transfer experiments at 53°C on the *cis* and *trans* resonances of the Ala^{11} amide proton. In a) no irradiation was applied. In b) the *cis* Ala^{11} amide resonance (denoted by arrow) at 3275 Hz (8.32 ppm) is irradiated and decrease in the *trans* A^{11} NH proton resonance (denoted by triangle) at 3056 Hz (7.79 ppm) is observed. In c) The *trans* Ala^{11} NH proton resonance (denoted by arrow) is irradiated and a decrease in the *cis* Ala^{11} NH proton resonance (denoted by triangle) is observed.

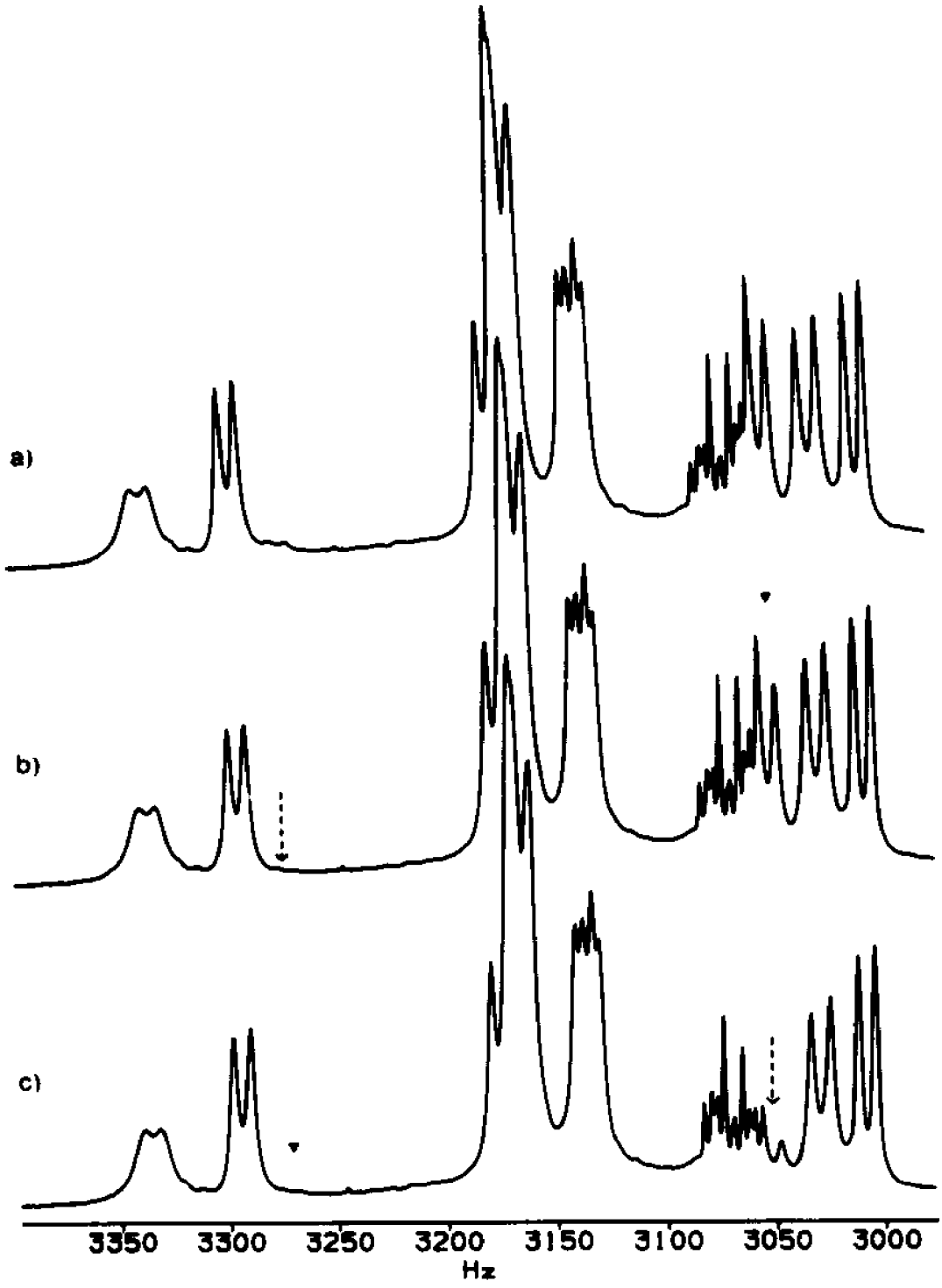
a)
b)
c)
3350
3300
3250
3200
3150
3100
3050
3000
Hz

relaxation, thereby, allowing the saturation transfer effect to be observed. At lower temperatures (25°C and 35°C) the effects of saturation transfer were not observed. The fact that saturation transfer effects were observed only at elevated temperatures (50°C and 53°C) removed the possibility that an NOE was mistaken for a transfer of saturation, as the NOE would be expected to become more positive with increasing temperature (3). The results of these experiments demonstrated that the resonances at 7.94 ppm and 8.32 ppm are due to the Asp^{9} and Ala^{11} amide resonances, respectively, of the *cis* isomer. From integration by cutting and weighing of the *cis* and *trans* Ala^{11} NH resonance, it was estimated that the amount of *cis* isomers was approximately 4% at 25 C. Additional low intensity resonances and exchange cross-peaks were also observed for the other α-factor analogues indicating that *cis-trans* isomerism of the Pro^{10} amide bond was occurring in these peptides as well.

CHAPTER VI

DISCUSSION:

Cyclic and Linear α-factor Analogues

The work of Jelicks *et al.* (77,78) suggested that a Type II β-turn spanning residues 7-10 is present in the biologically active conformation of the α-factor. In order to provide further support for this hypothesis Dr. Naider's research group has synthesized and studied a number of α-factor analogues in which the residues corresponding to positions 7-10 in the native pheromone are expected to adopt a Type II β-turn. Of the new analogues investigated, those with side chain cyclization were of particular interest as they are conformationally more constrained than are corresponding linear peptides. It was anticipated that the reduced flexibility of these peptides would simplify interpretation of their activity and of spectral data obtained. Furthermore, several cyclo^{1,4}[Cys^1,Pro^2,X^3,Cys^4] tetrapeptides have been studied by NMR spectroscopy (84-86). Garcia-Echeverria *et al.* (84,85) have found that both the cyclo^{1,4}[Cys^1,Pro^2,D-Val^3,Cys^4] tetrapeptide in water and the cyclo^{1,4}[Pen^1,Pro^2,D-Val^3,Cys^4] tetrapeptide in MeCN-d_3 adopt Type II β-turns. Rao *et al.* (86) have shown that in both DMSO-d_6 and CCl_3D the cyclo^{1,4}[Cys^1,Pro^2,D-Ala^3,Cys^4] tetrapeptide

adopts a Type II β-turn, while the cyclo^{1,4}[Cys^{1},Pro^{2},L-Ala^{3},Cys^{4}] tetrapeptide adopts a Type I β-turn. Therefore, it was expected that residues 7-10 of the cyclo^{7,10}[Cys^{7},X^{9},Cys^{10},Nle^{12}]α-factor analogues (where X = Gly, L-Ala, D-Ala, or D-Val) would adopt β-turn conformations.

The results and conclusions for the cyclic and linear α-factor analogues examined in this thesis are presented in Tables 24-31. The two cyclic α-factor analogues which contained a Pro-D-residue sequence, the cyclo^{7,10}[Cys^{7},D-Ala^{9},Cys^{10},Nle^{12}]α-factor and cyclo^{7,10}[Cys^{7},D-Val^{9},Cys^{10}, Nle^{12}]α-factor, were found to adopt a Type II β-turn spanning residues 7-10. In both DMSO/water and aqueous solution the cyclo^{7,10}[Cys^{7},D-Ala^{9},Cys^{10},Nle^{12}]α-factor exhibited strong Pro$^{8}_{\alpha CH}$-Ala$^{9}_{NH}$ and Ala$^{9}_{NH}$-Cys$^{10}_{NH}$ NOESY cross-peaks. The cyclo^{7,10}[Cys^{7},D-Val^{9},Cys^{10},Nle^{12}]α-factor in DMSO/water exhibited strong Pro$^{8}_{\alpha CH}$-Val$^{9}_{NH}$ and Val$^{9}_{NH}$-Cys$^{10}_{NH}$ NOESY connectivities, as well as, a weak Val$^{9}_{\alpha CH}$-Cys$^{10}_{NH}$ NOESY cross-peak and a non-sequential Pro$^{8}_{\alpha CH}$-Cys$^{10}_{NH}$ NOESY connectivity.

The cyclo^{7,10}[Cys^{7},L-Ala^{9},Cys^{10},Nle^{12}]α-factor, which contains a L-residue in position 9, was found to adopt a Type I β-turn centered on residues 8 and 9 in both DMSO/water and aqueous solution. In both DMSO/water and aqueous solution weak Pro$^{8}_{\alpha CH}$-Ala$^{9}_{NH}$ and Ala$^{9}_{\alpha CH}$-Cys$^{10}_{NH}$ NOESY connectivities were observed, as was a strong Ala$^{9}_{NH}$-

TABLE 24

The cyclo^{7,10}[Cys^{7},D-Ala^{9},Cys^{10},Nle^{12}]α-factor in water and DMSO/water (80:20):

Observations in aqueous solution:

1) Strong Pro$^{8}{}_{\alpha CH}$-Ala$^{9}{}_{NH}$ and Ala$^{9}{}_{NH}$-Cys$^{10}{}_{NH}$ NOESY connectivities.

2) Ala$^{9}{}_{\alpha CH}$-Cys$^{10}{}_{NH}$ NOESY cross-peak absent.

3) No NH_i-NH_{i+1} NOESY connectivities, other than the Ala$^{9}{}_{NH}$-Cys$^{10}{}_{NH}$ NOESY cross-peak, are present.

4) Temperature coefficient of Cys^{10} NH was -3.1 ppb/K

Observations in DMSO/water (80:20):

1) Strong Pro$^{8}{}_{\alpha CH}$-Ala$^{9}{}_{NH}$ and Ala$^{9}{}_{NH}$-Cys$^{10}{}_{NH}$ NOESY connectivities.

2) Temperature coefficient of Cys^{10} NH was -1.2 ppb/K

Conclusions:

The cyclo^{7,10}[Cys^{7},D-Ala^{9},Cys^{10},Nle^{12}]α-factor adopts a Type II β-turn spanning residues 7-10 in both water and DMSO/water (80:20).

TABLE 25

The cyclo^{7,10}[Cys^{7},D-Val^{9},Cys^{10},Nle^{12}]α-factor in DMSO/water (80:20):

Observations:

1) Strong Pro$^{8}_{\alpha CH}$-Val$^{9}_{NH}$ and Val$^{9}_{NH}$-Cys$^{10}_{NH}$ NOESY connectivities.

2) Weak Val$^{9}_{\alpha CH}$-Cys$^{10}_{NH}$ NOESY cross-peak.

3) Non-sequential Pro$^{8}_{\alpha CH}$-Cys$^{10}_{NH}$ NOESY connectivity.

4) Internuclear distances obtained from NOESY spectra (see Table 10) consistent with Type II β-turn spanning residues 7-10.

5) Temperature coefficient of Cys^{10} NH was -1.0 ppb/K

Conclusions:

The cyclo^{7,10}[Cys^{7},D-Val^{9},Cys^{10},Nle^{12}]α-factor adopts a Type II β-turn spanning residues 7-10 in DMSO/water (80:20).

TABLE 26

The cyclo^{7,10}[Cys^{7},L-Ala^{9},Cys^{10},Nle^{12}]α-factor in water and DMSO/water (80:20):

Observations in aqueous solution:

1) Weak Pro$^{8}_{\alpha CH}$-Ala$^{9}_{NH}$ and Ala$^{9}_{\alpha CH}$-Cys$^{10}_{NH}$ NOESY connectivities.

2) Strong Ala$^{9}_{NH}$-Cys$^{10}_{NH}$ NOESY connectivity.

3) No NH_i-NH_{i+1} NOESY connectivities, other than the Ala$^{9}_{NH}$-Cys$^{10}_{NH}$ NOESY cross-peak, are present.

4) Temperature coefficient of Cys^{10} NH was -3.6 ppb/K

Observations in DMSO/water (80:20):

1) Weak Pro$^{8}_{\alpha CH}$-Ala$^{9}_{NH}$ and Ala$^{9}_{\alpha CH}$-Cys$^{10}_{NH}$ NOESY connectivities.

2) Strong Ala$^{9}_{NH}$-Cys$^{10}_{NH}$ NOESY connectivity.

3) Non-sequential Pro$^{8}_{\alpha CH}$-Cys$^{10}_{NH}$ NOESY connectivity.

4) Internuclear distances obtained from NOESY spectra (see Table 10) consistent with Type I β-turn spanning residues 7-10.

5) Temperature coefficient of Cys^{10} NH was -1.5 ppb/K

Conclusions:

The cyclo^{7,10}[Cys^{7},L-Ala^{9},Cys^{10},Nle^{12}]α-factor adopts a Type I β-turn spanning residues 7-10 in both water and DMSO/water (80:20).

TABLE 27

The cyclo^{7,10}[Cys^{7},Cys^{10},Nle^{12}]α-factor in water and DMSO/water (80:20):

Observations in aqueous solution:

1) Weak Pro$^{8}_{\beta CH}$-Gly$^{9}_{NH}$ NOESY cross-peak.

2) Strong Pro$^{8}_{\beta CH}$-Gly$^{9}_{NH}$ and Gly$^{9}_{NH}$-Cys$^{10}_{NH}$ NOESY connectivities.

3) No NH_i-NH_{i+1} NOESY connectivities, other than the Ala$^{9}_{NH}$-Cys$^{10}_{NH}$ NOESY cross-peak, are present.

4) α-protons of Gly^{9} have degenerate chemical shifts.

5) Temperature coefficient of Cys^{10} NH was -2.1 ppb/K

Observations in DMSO/water (80:20):

1) Strong Pro$^{8}_{\beta CH}$-Gly$^{9}_{NH}$ and Gly$^{9}_{NH}$-Cys$^{10}_{NH}$ NOESY connectivities.

2) Weak Gly$^{9}_{\alpha CH}$-Cys$^{10}_{NH}$ NOESY cross-peak.

3) Non-sequential Pro$^{8}_{\alpha CH}$-Cys$^{10}_{NH}$ NOESY connectivity.

4) Pro$^{8}_{\beta CH}$-Gly$^{9}_{NH}$ NOESY cross-peak absent.

5) Internuclear distances obtained from NOESY Spectra (see Table 10) consistent with Type II β-turn spanning residues 7-10.

6) Temperature coefficient of Cys^{10} NH was -0.9 ppb/K

Conclusions:

1) The cyclo^{7,10}[Cys^{7},Cys^{10},Nle^{12}]α-factor adopts two or more conformations in water. One of these being a Type I β-turn spanning residues 7-10.

2) In DMSO/water (80:20) the cyclo^{7,10}[Cys^{7},Cys^{10},Nle^{12}]α-factor adopts a Type II β-turn spanning residues 7-10.

TABLE 28

The [D-Ala^9]α-factor in water and DMSO:

Observations in aqueous solution:

1) Strong Pro$^8{}_{\alpha CH}$-Ala$^9{}_{NH}$ and Ala$^9{}_{NH}$-Gln$^{10}{}_{NH}$ NOESY connectivities.

2) Weak Ala$^9{}_{\alpha CH}$-Gln$^{10}{}_{NH}$ NOESY cross-peak.

3) No NH_i-NH_{i+1} NOESY connectivities, other than the Ala$^9{}_{NH}$-Gln$^{10}{}_{NH}$ NOESY cross-peak, are present.

4) Temperature coefficient of Gln^{10} NH was -3.6 ppb/K

Observations in DMSO:

1) Strong Pro$^8{}_{\alpha CH}$-Ala$^9{}_{NH}$ and Ala$^9{}_{NH}$-Gln$^{10}{}_{NH}$ NOESY connectivities.

2) Weak Ala$^9{}_{\alpha CH}$-Gln$^{10}{}_{NH}$ NOESY cross-peak.

3) Temperature coefficient of Gln^{10} NH was -3.3 ppb/K

Conclusions:

The [D-Ala^9]α-factor adopts a Type II β-turn spanning residues 7-10 in both water and DMSO.

TABLE 29

The [L-Ala^9]α-factor in water and DMSO:

Observations in aqueous solution:

1) All αCH_i-NH_{i+1} NOESY connectivities have similar intensities.

2) No NH_i-NH_{i+1} NOESY connectivities are present.

3) Temperature coefficient of Gln^{10} NH was -8.2 ppb/K

Observations in DMSO:

1) All αCH_i-NH_{i+1} NOESY connectivities have similar intensities.

2) All NH_i-NH_{i+1} NOESY connectivities have similar intensities and are significantly weaker than the αCH_i-NH_{i+1} NOESY connectivities.

3) Temperature coefficient of Gln^{10} NH was -5.0 ppb/K

Conclusions:

The [L-Ala^9]α-factor is unstructured in both water and DMSO.

TABLE 30
The [D-Ala^9]- and [L-Ala^9]α-Factor in the Presence of Lipid:

Observations:

1) The [D-Ala^9]α-factor exhibited strong $Pro^{8}_{\alpha CH}$-Ala^{9}_{NH} and Ala^{9}_{NH}-Gln^{10}_{NH} NOESY cross-peaks.

2) The [D-Ala^9]α-factor exhibited a weak $Ala^{9}_{\alpha CH}$-Gln^{10}_{NH} NOESY cross-peak.

3) The [L-Ala^9]α-factor exhibited strong $Pro^{8}_{\alpha CH}$-Ala^{9}_{NH} and Ala^{9}_{NH}-Gln^{10}_{NH} NOESY cross-peaks.

4) The N-terminal NH resonances of the [D-Ala^9]- and [L-Ala^9]α-factor exhibit a greater increase in the selective spin-lattice relaxation and cross-relaxation rates with increasing lipid/peptide ratio relative to the C-terminal NH resonances.

5) The $Met^{12}_{\alpha CH}$-Tyr^{13}_{NH} cross-peak is observed in the 8 mM DPPC:4 mM [D-Ala^9]α-factor TRNOESY spectrum, but not in the 8 mM DPPC:2 mM [D-Ala^9]α-factor TRNOESY spectrum

6) The $Tyr^{13}_{C2,6H}$-$Tyr^{13}_{C3,5H}$ cross-peak in the spectrum of the [D-Ala^9]α-factor is stronger relative to the intra-ring connectivities of Trp^1 and Trp^3 than the corresponding cross-peak in the spectrum of the [L-Ala^9]α-factor.

Conclusions:

1) The N-terminal residues of the [D-Ala^9]- and [L-Ala^9]α-factor analogues have a stronger interaction with the lipid than do the C-terminal residues.

2) The C-terminus of the [D-Ala^9]α-factor appears to be constrained to a greater extent upon interaction with the lipid relative to the C-terminus of the [L-Ala^9]α-factor

3) The [D-Ala^9]α-factor maintains a Type II β-turn conformation upon interaction with lipid vesicles.

TABLE 31

VCD and Absorption Spectra of α-Factor Analogues in DMSO/water (80:20):

Observations:

1) The cyclic and linear analogues examined exhibited a strong absorption peak at ≈1660 cm^{-1}.

2) The cyclo^{7,10}[Cys^{7},L-Ala^{9},Cys^{10},Nle^{12}]α-factor exhibited a negative-positive VCD couplet at ≈ 1650 cm^{-1}, a negative VCD peak at ≈ 1650 cm^{-1}, and a distinct shoulder at ≈ 1695 cm^{-1} in the absorption spectrum.

3) The cyclo^{7,10}[Cys^{7},D-Ala^{9},Cys^{10},Nle^{12}]α-factor exhibited a positive VCD signal at ≈1680 cm^{-1}, a negative VCD peak at ≈ 1650 cm^{-1}, and a shoulder at ≈ 1640 cm^{-1} in the absorption spectrum.

4) The linear [L-Ala^{9}]α-factor exhibited a strong negative VCD peak at ≈1640 cm^{-1}, a negative-positive VCD couplet centered near 1695 cm^{-1}, and a shoulder at ≈ 1695 cm^{-1} in the absorption spectrum.

5) Absorption peaks at 1695 cm^{-1} and 1640 cm^{-1} were not observed for the analogue which incorporated 5-aminopentanoic acid in place of Pro^{8} and Ala^{9}.

Conclusions:

1) The cyclic and linear analogues examined may adopt a transient β-sheet conformation in DMSO/water (80:20).

2) It may be possible to identify Type I and Type II β-turns using VCD spectroscopy.

3) The absorption peaks at 1695 cm^{-1} and 1640 cm^{-1} appear to be associated with Type I and Type II β-turn conformations.

4) The linear [L-Ala^{9}]α-factor may adopt a Type I β-turn in DMSO/water (80:20) analogous to the cyclo^{7,10}[Cys^{7},L-Ala^{9},Cys^{10},Nle^{12}]α-factor.

Cys^{10}_{NH} NOESY connectivity. Furthermore, weak $Pro^{8}_{\beta CH}$-Cys^{10}_{NH} and $Pro^{8}_{\beta CH}$-Ala^{9}_{NH} connectivities were present in the NOESY spectrum of the cyclo^{7,10}[Cys^{7},L-Ala^{9},Cys^{10},Nle^{12}] analogue in DMSO/water. The results found in this study for the cyclo^{7,10}[Cys^{7},D-Ala^{9},Cys^{10},Nle^{12}]-, cyclo^{7,10}[Cys^{7}, Cys^{10},D-Val^{9},Nle^{12}]-, and cyclo^{7,10}[Cys^{7},L-Ala^{9},Cys^{10},Nle^{12}]α-factor analogues are in agreement with the conclusions of Garcia-Echeverria *et al.* (84,85) and Rao *et al.* (86) for the cyclo^{1,4}[Cys^{1},Pro^{2},X^{3},Cys^{4}] tetrapeptides.

The observation of a $Pro^{8}_{\beta CH}$-Gly^{9}_{NH} connectivity for the cyclo^{7,10}[Cys^{7},Cys^{10},Nle^{12}]α-factor indicated that residues 7-10 of this peptide adopt a Type I/III β-turn in water (145,159). However, several spectral features, in particular the intensity of the $Pro^{8}_{\beta CH}$-Gly^{9}_{NH} connectivity (which is significantly stronger than would be expected for a Type I/III β-turn) and the degeneracy of the Gly^{9} α-protons, suggest that at least two distinct conformations are adopted by residues 7-10 of this peptide (83,160).

Interestingly, the cyclo^{7,10}[Cys^{7},Cys^{10},Nle^{12}]α-factor in DMSO/water appears to adopt a Type II β-turn, since this peptide exhibited strong $Pro^{8}_{\beta CH}$-Gly^{9}_{NH} and Gly^{9}_{NH}-Cys^{10}_{NH} connectivities and a non-sequential $Pro^{8}_{\beta CH}$-Cys^{10}_{NH} cross-peak. Furthermore, a distinct resonance was observed for each of the Gly^{9} α-protons and the $Pro^{8}_{\beta CH}$-Gly^{9}_{NH} connectivity which was observed in water was

absent. These results combined with the quantitative results discussed below suggest that other conformations, such as a Type I/III β-turn or a γ-turn, are not significantly populated in DMSO/water (80:20) (83,160).

The presence of a β-turn in the cyclo^{7,10}[Cys^{7},X^{9}, Cys^{10},Nle^{12}]α-factor analogues was further supported by the low temperature coefficients observed for the Cys^{10} amide proton. In aqueous solution the Cys^{10} NH temperature coefficients for the cyclo^{7,10}[Cys^{7},D-Ala^{9}, Cys^{10},Nle^{12}]-, cyclo^{7,10}[Cys^{7},Cys^{10},Nle^{12}]-, and cyclo^{7,10}[Cys^{7}, L-Ala^{9},Cys^{10},Nle^{12}]α-factor analogues were significantly smaller than those measured for the other amide protons in these peptides (see Table 14) and were in the range (2.0-5.0 ppb/K) associated with intermediate hydrogen-bonding in aqueous solution (145,149). In DMSO/water the NH temperature coefficients for Cys^{10} NH in the cyclic α-factor analogues vary from 0.9-1.5 ppb/K, which is in the range expected for strong hydrogen-bonding in both DMSO and water (145,148,149). The Cys^{10} amide temperature coefficients for the cyclo^{7,10}[Cys^{7},X^{9},Cys^{10},Nle^{12}]α-factor analogues suggest that the Cys^{10} amide proton is involved in intramolecular hydrogen-bonding and are consistent with β-turn conformations spanning residues 7-10 of these peptides.

The signal/noise for the NOESY spectra of the cyclic α-factor analogues in water was too low to permit

determination of internuclear distances. However, the signal/noise was high enough to allow internuclear distances to be estimated from spectra collected in DMSO/water (80:20). The internuclear distances determined from 400 ms NOESY spectra for the cyclo^{7,10}[Cys^{7},L-Ala^{9},Cys^{10},Nle^{12}]- and cyclo^{7,10}[Cys^{7},D-Val^{9},Cys^{10},Nle^{12}]α-factor analogues were within experimental error (estimated to be ± 0.1 Å) of the corresponding internuclear distances obtained from 200 ms spectra of these peptides. In the 100 ms NOESY spectrum of the cyclo^{7,10}[Cys^{7},Cys^{10},Nle^{12}]α-factor in DMSO/water only one strong Gly$^{9}_{\alpha CH}$-Gly$^{9}_{NH}$ NOESY connectivity was observed. Therefore it appears that spin diffusion was not significant at the mixing times used to estimate the internuclear separations.

The results of the quantitative analysis of the NOESY spectra for the cyclo^{7,10}[Cys^{7},L-Ala^{9},Cys^{10},Nle^{12}]- and cyclo^{7,10}[Cys^{7},Cys^{10},Nle^{12}]α-factors using the NOE connectivity between the geminal β-protons of Pro^{8} and Pro^{11} as standards and for the cyclo^{7,10}[Cys^{7},D-Val^{9},Cys^{10}, Nle^{12}]α-factor using the assumption that the Cys$^{10}_{\alpha CH}$-Cys$^{10}_{NH}$ internuclear distance was 2.8 ± 0.2 Å (116) support the conclusions made above concerning the conformation of residues 7-10 in these peptides. In particular, the cyclo^{7,10}[Cys^{7}, Cys^{10},Nle^{12}]α-factor appears to adopt a single conformation (Type II β-turn) in DMSO/water

solution (see Table 10). The internuclear distances obtained for the cyclo^{7,10}[Cys^{7},L-Ala^{9},Cys^{10},Nle^{12}] and cyclo^{7,10}[Cys^{7},Cys^{10}, Nle^{12}] analogues are within (± 0.2 Å) of those reported for standard Type I and Type II β-turns, respectively (3,83; see Table 7). The internuclear distances obtained for the cyclo^{7,10}[Cys^{7},D-Val^{9},Cys^{10}, Nle^{12}]α-factor, with the exception of the Pro$^{8}_{\alpha CH}$-Cys$^{10}_{NH}$ and Val^{9}αCH-Val^{9}NH internuclear distances, are consistent with the standard values reported for a type II β-turn (3,83) as well as those values reported for the cyclo^{1,4}[Cys^{1},Pro^{2},D-Val^{3},Cys^{4}] tetrapeptide studied in water (85). The Pro$^{8}_{\alpha CH}$-Cys$^{10}_{NH}$ internuclear distance obtained for the cyclo^{7,10}[Cys^{7},D-Val^{9},Cys^{10},Nle^{12}]α-factor is significantly shorter (2.9 Å) than the standard values reported for a Type II β-turn (3.3 Å) (3,83) or the values reported for the cyclo^{1,4}[Cys^{1},Pro^{2},D-Val^{3},Cys^{4}] tetrapeptide (3.7 Å) (85). The Val^{9}αCH-Val^{9}NH internuclear distance is longer than would be expected from Table 7. Molecular modeling of the Cys-Pro-D-Val-Cys portion of the cyclo^{7,10}[Cys^{7},D-Val^{9},Cys^{10},Nle^{12}]α-factor using the experimentally obtained internuclear distances suggested that the Pro^{8} φ,ψ angles are approximately -58.9° and 148.2°, respectively, and the D-Val^{9} φ,ψ angles are approximately 75.3° and -6.0°, respectively. These values are consistent with the values reported for the corresponding torsion angles in the cyclo^{1,4}[Pen^{1},Pro^{2},D-

Val^3,Cys^4] tetrapeptide (Pro^2♦,♦; -59.99,134.74; D-Val^3♦,♦;102.87,-17.96) in d_3-MeCN (85). However, they are significantly different from the torsion angles reported for the cyclo^{1,4}[Cys^1,Pro^2,D-Val^3,Cys^4] tetrapeptide (Pro^2♦,♦; -47.09,108.97; D-Val^3♦,♦;71.36, 13.46) in water (85). Therefore, it appears that the Cys-Pro-D-Val-Cys segment undergoes a slight conformational change (relative to the cyclo^{1,4}[Cys^1, Pro^2,D-Val^3,Cys^4] tetrapeptide in water) either as a result of being incorporated into a larger peptide or due to a solvent effect. The latter possibility seems particularly likely in light of the apparent shift in conformer distribution observed for the cyclo^{7,10}[Cys^7, Cys^{10},Nle^{12}]■-factor in DMSO/water relative to aqueous solution.

The [D-Ala^9]- and [L-Ala^9]■-factor analogues are linear peptides and are expected to be much more flexible relative to the cyclic ■-factor analogues. Therefore, the internuclear separations for these peptides were not estimated from NOESY spectra. However, the qualitative analysis of the NOESY spectra of the [D-Ala^9]■-factor in both DMSO and aqueous solution suggested that the [D-Ala^9]■-factor adopts a transient Type II β-turn centered about Pro^8 and Ala^9. In both solvents strong Pro$^8{}_{\blacksquare CH}$-Ala$^9{}_{NH}$ and Ala$^9{}_{NH}$-Gln$^{10}{}_{NH}$ NOESY connectivities, as well as, a weak

$Ala^{9}_{\alpha CH}$-Gln^{10}_{NH} NOESY connectivity were observed for the [D-Ala^{9}]α-factor. In water the presence of the Type II β-turn is further supported by the small temperature coefficient of the Gln^{10} NH (-3.6 ppb/K) and the $^{3}J_{\alpha NH}$ (6.3 Hz) of D-Ala^{9}. These two spectral parameters are very similar to the corresponding parameters in the cyclo^{7,10}[Cys^{7},D-Ala^{9},Cys^{10},Nle^{12}]α-factor, suggesting that the Type II β-turn conformation is highly populated in water. Furthermore, the weak intensity observed for the $Ala^{9}_{\alpha CH}$-Gln^{10}_{NH} cross-peak suggests that conformations where residues 7-10 are extended are not highly populated as the intensity of this cross-peak would be dominated by the shorter internuclear distances (≈ 2.2 Å) associated with these conformations (3,83).

The temperature coefficient for the Gln^{10} NH resonance of the [D-Ala^{9}] analogue in DMSO (-3.3 ppb/K) is significantly higher than coefficients reported for strongly hydrogen bonded amide resonances in this solvent (148,149). This suggests that either the Type II β-turn is less populated in this solvent than in water (145) or that in DMSO the hydrogen bond is less important for the stability of the β-turn conformation (76).

In NOESY and ROESY spectra of the [L-Ala^{9}]α-factor in aqueous solution no NH-NH connectivities are observed. The absence of NH-NH connectivities in the spectra of the [L-Ala^{9}]α-factor in water suggests that folded

conformations are not highly populated in this solvent (3,83). Furthermore, in aqueous solution the C-terminus of the of the [L-Ala^9]α-factor appears to have a significantly shorter effective correlation time than the C-terminus of the [D-Ala^9]α-factor analogue as judged by the absence of the Met$^{12}{}_{\alpha CH}$-Tyr$^{13}{}_{NH}$ cross-peak in the 400 ms NOESY spectrum of the [L-Ala^9]α-factor. Therefore it appears that the [L-Ala^9]α-factor is less structured in aqueous solution than the [D-Ala^9]α-factor. The NOESY connectivities observed for the [L-Ala^9]α-factor in DMSO, in particular the strong Ala$^9{}_{\alpha CH}$-Gln$^{10}{}_{NH}$ cross-peak, indicate that residues 7-10 in this peptide do not adopt a β-turn conformation. None of the NH temperature coefficients for the [L-Ala^9]α-factor in either DMSO or water were reflective of intramolecular hydrogen bonding. In addition all of the $^3J_{\alpha NH}$ coupling constants observed for the [L-Ala^9]α-factor are in the range expected for predominately unstructured peptides (148,149). These results are consistent with the conclusion that the [L-Ala^9]α-factor is predominately unstructured in both DMSO and aqueous solutions.

Nearly all of the possible sequential NH_i-NH_{i+1} connectivities are observed in the NOESY spectrum of the linear α-factor analogues in DMSO and of the cyclic α-factor analogues in DMSO/water. The presence of a series

of NH_i-NH_{i+1} connectivities is consistent with an α-helical structure (3,83) and would suggest that these peptides adopt such a structure in DMSO or DMSO/water. For an α-helical structure the NH_i-NH_{i+1} connectivities would be expected to be stronger than the sequential αCH_i-NH_{i+1} cross-peaks (3,83). However, for all the linear and cyclic α-factor analogues the sequential αCH_i-NH_{i+1} connectivities are significantly stronger than the sequential NH_i-NH_{i+1} connectivities. Furthermore, no non-sequential cross-peaks, other than the $Pro^{8}{}_{\alpha CH}$-$Cys^{10}{}_{NH}$ NOE connectivity, were observed in the cyclic α-factor analogues in DMSO/water. The $^{3}J_{\alpha NH}$ coupling constants for the linear and cyclic α-factor analogues are significantly larger than the 3-4 Hz expected for α-helical structures (83). Finally, none of the α-factor analogues exhibit the series of low NH temperature coefficients which would reflect the presence of the intra-molecular hydrogen-bonding necessary to stabilize a helical conformation. Therefore, the sequential NH_i-NH_{i+1} connectivities appear to be associated with a predominantly disordered peptide. Sequential NH_i-NH_{i+1} connectivities have been observed by both Wright *et al.* (147) and Scherf *et al.* (162) in predominately unstructured peptides. The presence of numerous NH_i-NH_{i+1} connectivities in DMSO and DMSO/water which are not observed in water is presumably due to the fact that both

DMSO and DMSO\water are more viscous than water. Therefore, the peptides probably experience longer effective correlation times in DMSO or in the DMSO/water mixture compared to water.

The main spectral feature observed in the VCD spectra of both the cyclo^{7,10}[Cys^{7},D-Ala^{9},Cys^{10},Nle^{12}] and cyclo^{7,10}[Cys^{7},L-Ala^{9},Cys^{10},Nle^{12}]α-factor analogues in DMSO/water was strong negative peak at approximately 1660 cm^{-1}. Similar spectral features in other peptides, such as poly-lysine (21,24) and EGF (20), have been associated with β-sheet structures. In the cyclo^{7,10}[Cys^{7},D-Ala^{9}, Cys^{10},Nle^{12}] and cyclo^{7,10}[Cys^{7},L-Ala^{9},Cys^{10},Nle^{12}]α-factor analogues this conformational feature would presumably involve residues 4-7 and 10-13 (see Figure 34). The presence of an anti-parallel β-sheet conformation is not supported by non-sequential NOE connectivities. However, this is not entirely surprising as the non-sequential Leu$^{4}{}_{\alpha CH}$-Tyr$^{13}{}_{\alpha CH}$ and Leu$^{6}{}_{\alpha CH}$-Nle$^{12}{}_{\alpha CH}$ connectivities corresponding to short (2.2 Å) distances in this structure would be hidden by the diagonal or the noise surrounding the water signal and many of the expected non-sequential αCH_i-NH_j connectivities would be hidden by sequential αCH_i-NH_{i+1} cross-peaks. Furthermore, the expected non-sequential αCH_i-NH_j and NH_i-NH_j connectivities would have internuclear distances of approximately 3.2 Å (3,83; see Table 7). This relatively

large internuclear separation combined with the probable transient nature of this conformation would lead to extremely weak intensities for the non-sequential αCH_i-NH_j and NH_i-NH_j connectivities. The smaller amide temperature coefficients observed for residues for 5, 7, 10, 12 relative to residues 4, 6, 13 in the cyclo^{7,10}[Cys^7,D-Ala^9,Cys^{10},Nle^{12}] and cyclo^{7,10}[Cys^7,L-Ala^9,Cys^{10},Nle^{12}]α-factor analogues are consistent with a transient β-sheet conformation. However the NH temperature coefficients for residues 5, 7, 12 are not sufficiently small to indicate intramolecular hydrogen-bonding (The NH temperature coefficient for Cys^{10} is very low, however, and this proton is presumably involved in a hydrogen-bond which stabilizes the β-turn).

Both the cyclo^{7,10}[Cys^7,L-Ala^9,Cys^{10},Nle^{12}]- and cyclo^{7,10}[Cys^7,D-Ala^9,Cys^{10},Nle^{12}]α-factor exhibited shoulders in the absorbance spectrum (1695 cm^{-1} and 1640 cm^{-1} for the cyclo^{7,10}[Cys^7,L-Ala^9,Cys^{10},Nle^{12}] and cyclo^{7,10}[Cys^7, D-Ala^9,Cys^{10},Nle^{12}]α-factor analogues, respectively), which were not observed for the analogue that incorporated 5-aminopentanoic acid in place of Pro^8 and Ala^9. Therefore, these absorption peaks appear to be associated with β-turn conformations. In addition to the above spectral features the cyclo^{7,10}[Cys^7,L-Ala^9, Cys^{10},Nle^{12}]α-factor exhibited a negative-positive couplet in the VCD at approximately 1695 cm^{-1} and the

cyclo^{7,10}[Cys^{7},D-Ala^{9},Cys^{10},Nle^{12}]α-factor exhibited a positive VCD signal at approximately 1680 cm^{-1}. These spectral differences observed for the cyclo^{7,10}[Cys^{7},L-Ala^{9},Cys^{10},Nle^{12}]- and cyclo^{7,10}[Cys^{7},D-Ala^{9},Cys^{10},Nle^{12}]α-factor suggest that Type I and Type II β-turns can be identified using VCD spectroscopy. In order to substantiate these conclusions VCD and infrared studies should be performed on a number of small model compounds of known conformation, such as the cyclo^{1,4}[Cys^{1},Pro^{2},L-Ala^{3},Cys^{4}] and cyclo^{1,4}[Cys^{1},Pro^{2},D-Ala^{3},Cys^{4}] tetrapeptides.

The VCD and absorption spectra of the of the linear [L-Ala^{9}]α-factor were very similar to those observed for the cyclo^{7,10}[Cys^{7},L-Ala^{9},Cys^{10},Nle^{12}]α-factor, including the strong negative VCD peak at 1640 cm^{-1}, the negative-positive VCD couplet centered near 1695 cm^{-1}, and the shoulder at 1695 cm^{-1} in the absorption spectrum. The similar spectral features observed for these two peptides suggest that the linear [L-Ala^{9}]α-factor adopts a Type I β-turn in DMSO/water analogous to the cyclo^{7,10}[Cys^{7},L-Ala^{9},Cys^{10},Nle^{12}]α-factor. There are two possible reasons to explain the absence of evidence for the presence of a β-turn conformation in the NMR spectra of the linear [L-Ala^{9}] peptide in both DMSO and water. It is possible that the β-turn conformer is in equilibrium with a number of energetically similar conformers. Therefore, given

that NMR parameters reflect population weighted averages, the population of the β-turn conformer may be below the detection limit of NMR techniques. This hypothesis requires that the other conformers present do not significantly affect the VCD spectrum. The second, possibly more plausible, explanation is that a Type I β-turn conformation in the linear [L-Ala^9]α-factor is stabilized in DMSO/water solution. In order to distinguish between these two possibilities the linear [L-Ala^9]α-factor in DMSO/water should be studied by NMR spectroscopy.

The presence of two peaks in the ^{31}P NMR spectrum in an approximately 2:1 ratio upon the addition of $PrCl_3$, indicated that the DPPC solution used for the TRNOESY experiments consisted predominantly of unilamellar lipid vesicles. The results of ^{31}P spectra of the DPPC vesicles upon addition of the [D-Ala^9]- and [L-Ala^9]α-factor analogues suggests that the α-factor analogues induced the lipid vesicles to become leaky. There are several possible mechanisms for the leakage phenomenon. The peptides may trigger an isothermal phase transition of the lipid bilayer to a nonlamellar phase as was found for the gramicidin-PE interaction (163). The peptides may insert into the bilayer causing a defect in the lipid packing or the peptides may form a transmembrane pore as

does melittin (164,165), GALA (151), and the α-toxin of *Staphylococcus aureas* (166). The continued presence of the upfield ^{31}P resonance suggests that the peptides do not induce all of the lipid vesicles to become leaky. This observation is consistent with the pore formation mechanism proposed for GALA (151), in which 8-12 individual peptide molecules associate to form a transmembrane pore. Since the peptide/lipid ratio was higher in my study of the [D-Ala^9]- and [L-Ala^9]α-factors relative to that used in the GALA investigation (151) it appears that the interactions required to form transmembrane pores are rare for these yeast pheromones. Furthermore, the peptide molecules would not be expected to readily dissociate from the lipid bilayer once they are associated with a transbilayer pore and the observation of TRNOESY cross-peaks in the presence of lipid indicates that the majority of the [D-Ala^9]- and [L-Ala^9]α-factor is in fast exchange between the lipid-bound and free states (119,120).

Relative to the resonances located at the C-terminus the N-terminal NH resonances of the [D-Ala^9] and [L-Ala^9] analogues exhibit a greater increase in the selective spin-lattice relaxation rate, as judged from the diagonal signal intensity from TRNOESY spectra, and cross-relaxation rate with increasing lipid/peptide ratio. This result suggests that the N-terminal residues of

these peptides have a stronger interaction with the lipid than do the C-terminal residues. It is possible that the N-terminus of both analogues interacts directly with the lipid bilayer, while the C-terminus does not directly interact with the lipid. This conclusion is consistent with the findings of Jelicks *et al.* (77) and Wakamatsu *et al.* (80,81) for α-factor in the presence of lipid.

Based on the disappearance of the $Met^{12}{}_{\alpha CH}$-$Tyr^{13}{}_{NH}$ cross-peak in the 8 mM DPPC:2 mM peptide TRNOESY spectrum of [D-Ala^9]α-factor it appears that the C-terminus of the [D-Ala^9]α-factor is constrained to a greater extent upon interaction of the peptide with the lipid than the C-terminus of the [L-Ala^9] analogue. This conclusion is supported by the fact that the $Tyr^{13}{}_{C2,6H}$-$Tyr^{13}{}_{C3,5H}$ cross-peak in the [D-Ala^9]α-factor was observed to be stronger relative to the intra-ring connectivities of Trp^1 and Trp^3, and is affected less by the supposition of *zero*-quantum coherence than is the corresponding cross-peak in the [L-Ala^9] analogue. A possible explanation for this observation is that for the [D-Ala^9]α-factor the Tyr^{13} residue comes into direct contact with the lipid bilayer. Implicit in this model is the hypothesis that the [D-Ala^9]α-factor maintains the β-turn conformation upon interaction with the lipid bilayer.

Interpretation of the TRNOESY data for the [D-Ala^9] and [L-Ala^9] analogues in terms of peptide conformation

is complicated by the line broadening and increased spectral overlap observed for these peptides in the presence of lipid vesicles. However, strong $Pro^{8}_{\alpha CH}$-Ala^{9}_{NH} and Ala^{9}_{NH}-Gln^{10}_{NH} cross-peaks and a weak $Ala^{9}_{\alpha CH}$-Gln^{10}_{NH} cross-peak are observed in the TRNOESY spectrum of the [D-Ala^{9}]α-factor. These results are consistent with the maintenance of a Type II β-turn upon interaction with the lipid (3,83,145). The possibility that other conformers, with different internal mobilities, contribute to the observed TRNOE signal does not allow conclusions to be made as to the whether the lipid stabilizes the β-turn conformation.

The TRNOE connectivities observed for the [L-Ala^{9}]α-factor in the presence of lipid are consistent (strong $Pro^{8}_{\alpha CH}$-Ala^{9}_{NH} and Ala^{9}_{NH}-Gln^{10}_{NH} cross-peaks) with a β-turn conformation spanning residues 7-10 (3,83). However, it may be possible that several conformations exist for the lipid-bound [L-Ala^{9}]α-factor. In such a case the TRNOESY cross-peaks may not only reflect the major bound conformation (see section II). The apparently greater mobility of the C-terminus of the [L-Ala^{9}]α-factor relative to that of the [D-Ala^{9}]α-factor suggests that the [L-Ala^{9}]α-factor is less structured when bound to lipid vesicles than is the [D-Ala^{9}]α-factor.

We do not observe any of the non-sequential NOE connectivities that were reported by Jelicks *et al.* (77).

We attribute this to the following; 1) Perdeuterated lipid was used in the present study, which minimized magnetization transfer (spin-diffusion) through the lipid. 2) The experiments performed in this study were carried out using a much shorter mixing time (75 ms compared to 400 ms used by Jelicks *et al.*) which also reduced possible spin diffusion. Finally, the conclusions of Jelicks *et al.* suggest that α-factor adopts a compact N-terminus in the presence of lipid vesicles (77), while those of Wakamatsu *et al.* (80,81), suggest that the N-terminus of α-factor adopts a helical conformation in the presence of lipid vesicles. In contrast we find no evidence for a prevalent conformation other than the Type II β-turn spanning residues 7-10 of the [D-Ala^9]α-factor.

a-Factor:

The results and conclusions for a-factor and the a-factor analogues are presented in Table 32. The two non-sequential connectivities ($Val^6_{\alpha CH}$-Trp^8_{NH} and possibly Lys^4_{NH}-Val^6_{NH} or Val^6_{NH}-Trp^8_{NH}) observed in the NOESY spectrum of the a-factor are consistent with a β-turn or an α-helical conformation (3,83). However there is little additional support for either of these conformations. Although, the presence of many of the possible NH_i-NH_{i+1} connectivities would appear to support

TABLE 32

a-Factor and a-Factor analogues in DMSO:

Observations:

1) Non-sequential $Val^{6}_{\alpha CH}$-Trp^{8}_{NH}, and Lys^{4}_{NH}-Val^{6}_{NH} or Val^{6}_{NH}-Trp^{8}_{NH} NOESY connectivities present.

2) Many of the possible NH_i-NH_{i+1} connectivities present.

3) NH_i-NH_{i+1} connectivities are significantly weaker than the sequential αCH_i-NH_{i+1} connectivities.

4) $^{3}J_{\alpha NH}$ coupling constants are in the range expected for highly flexible peptides.

5) NH temperature coefficients are above the range associated with intramolecular hydrogen bonding.

6) Two minor resonances at 7.94 ppm and 8.32 ppm gave rise to exchange cross-peaks with the Asp^{9}_{NH} and Ala^{11}_{NH}, respectively. Similar resonances were observed for all a-factor analogues.

7) Saturation transfer effects between the minor resonance at 7.94 ppm and the Asp^{9}_{NH} and the minor resonance at 8.32 ppm and the Ala^{11}_{NH} were only observable at elevated temperatures.

8) Corresponding residues in all of the a-factor analogues exhibit similar chemical shifts, NH temperature coefficients, and $^{3}J_{\alpha NH}$ coupling constants.

9) All of the a-factor analogues exhibited NOESY cross-peaks of the same type and with similar intensity to those observed for a-factor.

Conclusions:

1) a-Factor is predominantly unstructured in DMSO.

2) All a-factor peptides have similar conformations in DMSO.

an α-helical structure (3,83) the NH_i-NH_{i+1} connectivities are significantly weaker than the sequential αCH_i-NH_{i+1} connectivities. In an α-helical structure the NH_i-NH_{i+1} connectivities would be expected to be stronger than the sequential αCH_i-NH_{i+1} cross-peaks (3,83). In addition, the fact that all of the αCH_i-NH_{i+1} cross-peaks are strong relative to the NH_i-NH_{i+1} connectivities is inconsistent with the presence of a β-turn conformation. For a β-turn at least one very weak αCH_i-NH_{i+1} cross-peaks would be expected to be observed (3,83). No non-sequential NOE connectivities were observed other than those described above. Finally, neither the NH temperature coefficients nor the $^3J_{\alpha NH}$ coupling constants reflect the presence of a long lived secondary structure. Therefore, the sequential NH_i-NH_{i+1} connectivities appear to be associated with a predominantly disordered peptide as concluded for the α-factor analogues in DMSO (*vide supra*).

The chemical shifts, NH temperature coefficients, and $^3J_{\alpha NH}$ coupling constants of corresponding residues in all of the a-factor peptides were extremely similar to those of the a-factor. In addition all of the a-factor analogues exhibited NOESY cross-peaks of the same type (including the non-sequential $Val^6{}_{\alpha CH}$-$Trp^8{}_{NH}$ cross-peak) and with similar intensity to those observed for a-factor. Finally, all of the a-factor analogues exhibited

the additional minor resonances and exchange cross-peaks due to the *cis-trans* isomerism of the Pro^{10} amide bond. These results indicate that all of the a-factor peptides adopt similar conformations. Therefore, it appears that in DMSO the size and degree of saturation of the S-alkyl group and the presence of the methyl ester does not influence the conformation of the a-factor peptide. The function of the farnesyl group may be to direct the pheromone to the cell membrane. This conclusion is consistent with evidence coming from the biochemical and genetic studies of prenylated proteins (167,168,169). Future studies on the a-factor should focus on the interaction of these peptides with lipid. It would also be of interest to compare the interaction of a-factor and several analogues, in particular the S-hexadecanyl a-factor, with model membranes.

CONCLUSIONS:

Based on NOE connectivities and temperature coefficients residues 7-10 of the [D-Ala^9]a-factor analogue exhibit a significant preference for a Type II b-turn in solution and in the lipid-bound state, while the [L-Ala^9]a-factor analogue appears to be predominantly unstructured. The findings of this study support the conclusions of Jelicks *et al.* (77,78) that a Type II b-

turn conformation spanning residues 7-10 is correlated with the activity of the mating factor. However, the similar activities of the cyclo^{7,10}[Cys^{7},D-Ala^{9},Cys^{10},Nle^{12}] and cyclo^{7,10}[Cys^{7},L-Ala^{9},Cys^{10},Nle^{12}] analogues suggests that the presence of a β-turn may contribute more to the activity of the pheromone than the specific type of β-turn conformation. A corollary of this thesis would be that the lower activity of the [L-Ala^{9}]α-factor relative to the native pheromone may be due to the lower preference of the [L-Ala^{9}]α-factor for a β-turn. However, a β-turn conformation is apparently not the only feature important for α-factor activity. Specifically, although the des-Trp^{1}[Cha^{3},L-Ala^{9}] dodecapeptide was more than 200 fold less active than the corresponding D-homologue (74), the [L-Ala^{9}]α-factor is only 10-fold less active than the [D-Ala^{9}]α-factor. The central residues of both the des-Trp^{1} dodecapeptides and corresponding tridecapeptide analogues are expected to have similar conformational preferences. Therefore, it would appear that the N-terminal residues play a significant role in binding to and then triggering the receptor. This hypothesis is supported by the finding that the des-Trp^{1}[L-Ala^{3}]- and des-Trp^{1}[Phe^{3}]α-factor analogues act as antagonists to α-factor (73).

The biological significance of the *cis-trans* isomerism of the Pro^{10} amide bond of α-factor or of a

possible transient β-turn centered on residue Val^6 and Phe^8 is not at present understood. The results of this study indicate that in DMSO prenylation does not affect the conformation of a-factor and suggest that prenylation functions primarily to ensure the proper membrane association of a-factor.

Finally, we have presented preliminary evidence that VCD spectroscopy may be able to differentiate between Type I and Type II β-turns. Although a great deal of work remains to be done our results suggest that VCD spectroscopy may be able to detect elements of secondary structure which may not be observed by NMR spectroscopy.

REFERENCES

1. Noggle, J. H. and Schirmer, R. E. (1971) in "The Nuclear Overhauser Effect: Chemical Applications", Academic Press, New York.

2. Sanders, J. K. M. and Hunter, B. K. (1987) in "Modern NMR Spectroscopy. A Guide for Chemists", Oxford University Press, New York.

3. Neuhaus, D., and Williamson, M. (1989) in "The Nuclear Overhauser Effect in Structural and Conformational Analysis", VCH Publishers, Inc., New York.

4. Deshpande, M. S., Boylan, J., Hamilton, J. A., and Burton, J. (1991) Int. J. Peptide Protein Res. 37, 536.

5. Nieto, J. L., Rico, M., Santoro, M., Herranz, J., and Bermejo, F. J. (1986) Int. J. Peptide Protein Res. 28, 315.

6. O'Hare, P., and Williams, G. (1992) Biochemistry. 31, 4150.

7. Laussac, J. P., and Sarkar, B. (1985) Int. J. Peptide Protein Res. 26, 425.

8. London, R. E., Stewart, J. M. Cann, J. R., and Matwiyoff, N. A. (1978) Biochemistry 17, 2270.

9. Carver, J. A (1987) Eur. J. Biochem. 168, 193.

10. Mammi, S., Goodman, M., Peggion, E., Foffani, M. T., Moroder, L., and Wuensch, E. (1986) Int. J. Peptide Protein Res. 27, 145.

11. Bax, A., and Davis, D. G. (1985) J. Magn. Reson. 63, 207.

12. Brown, L. R., and Farmer II, B. T. (1989) Methods Enzym. 176, 199.

13. Amodeo, P., Motta., A., Picone, D., Saviano, G., Tancredi, T., and Temussi, P. A. (1991) J. Magn. Reson. 95, 201.

14. Kessler, H., Griesinger, C., Lautz, J., Müller, A., van Gunsteren, W., and Berendsen, H. (1988) J. Am. Chem. Soc. 110, 3393.

15. Landis, C., and Allured, V. (1991) J. Am. Chem. Soc. 113, 9493.

16. Wyssbrod, H.R., and Diem, M. (1992) Biopolymers 32, 1237.

17. Gupta, V. P., and Keiderling, T. A. (1992) Biopolymers 32,239.

18. Lee, O., Roberts, G. M., and Diem, M. (1989) Biopolymers 28, 1759.

19. Dukor, R. K., and Keiderling, T. A., (1991) Biopolymers 31, 1747.

20. DuKor, R., Pancoska, P., Kiederling, T., Prestrelski, S. J., and Arakawa, T. (1992) Arch. Biochem. Biophys. 298, 678.

21. Yasui, S. C., and Keiderling, T. A. (1986) J. Am. Chem. Soc. 108, 5576.

22. Sen, A. C., and Keiderling, T. A. (1984) Biopolymers 23, 1519.

23. Birke, S. S., Agbaje, I., and Diem, M. (1992) Biochemistry 31, 450.

24. Paterlini, M. G., Freedman, T. B., and Nafie, L. A. (1986) Biopolymers 25, 1751.

25. Baumruk, V., and Keiderling, T. A. (1993) J. Am. Chem. Soc. 115, 6939.

26. Milon, A., Miyazawa, T., and Higashijima, T. (1990) Biochemistry 29, 65.

27. Wakamatsu, K. Okada, A., Higashijima, T., and Miyazawa, T. (1986) Biopolymers 25, s193.

28. Robinson, R. M., Blakeney Jr., E. W., and Mattice, W. L. (1982) Biopolymers 21, 1217.

29. Higashijima, T., Fujimura, K., Masui, Y., Sakakibara, S., and Miyazawa, T. (1983) FEBS Lett. 159, 229.

30. Wu, C. -S. C., Hachimori, A., and Yang, J. T. (1982) Biochemistry 21 4556.

31. Cavatorta, P., Spisni, A., Szabo, A. G., Farruggia, G., Franzoni, L., and Masotti, L. (1989) Biopolymers 28, 441.

32. Honda, S., Ohashi, S., Morii, H., and Uedaira, H. (1991) Biopolymers 31, 869.

33. Higashijima, T., Wakamatsu, K., Takemitsu, M., Fujino, M., Nakajima, T., and Miyazawa, T. (1983) FEBS Lett. 152, 227.

34. Cascio, M., and Wallace, B. A. (1988) Proteins Struc. Func. Gen. 4, 89.

35. Benham, B. A., and Deber, C. M. (1984) J. Biol. Chem. 259, 14935.

36. Deber, C. M., and Benham, B. A. (1984) Proc. Natl. Acad. Sci. USA 81, 61.

37. Sargent, D. F., and Schwyzer, R. (1986) Proc. Natl. Acad. Sci. USA 83, 5774.

38. Thorner, J. (1980) in " Molecular Genetics of Development: An Introduction to Resent Research on Experimental systems" Leighton, T.J. and Lommis, W. A., Jr., Eds.; Academic Pres, New york, 119.

39. Masui, Y., Chino, N., Sakakibara, S., Tanaka, T., Murakami, T., and Kita, H. (1977) Biochem. Biophys. Res. Commun. 78, 534.

40. Anderegg, R. J., Betz, R., Carr, S. A., Crabb, J. W., and Duntze, W. (1988) J. Biol. Chem. 263, 18236.

41. Cross, F., Hartwell, L. H. Jackson, C., and Konopka, J. B. (1988) Ann. Rev. Cell Biol. 4, 429.

42. Herskowitz, I. (1988) Microbiol. Rev. 52, 536.

43. Sprague, G. F., Jr., Blair, L. C., and Thorner, J. (1983) Ann. Rev. Microbiol. 37, 623.

44. Burkholder, A. C., and Hartwell, L. H. (1985) Nucleic Acids Res. 13, 8463.

45. Hagen, D., McCaffrey, G., and Sprague, G. F., Jr. (1986) Proc. Natl. Acad. Sci. USA 83, 1418.

46. Blumer, K. J., and Thorner, J. (1991) Ann Rev. Physiol. 53, 37.

47. Kurjan, J. (1992) Annu. Rev. Biochem. 61, 1097.

48. Bucking-Throm, E., Duntze, W., Hartwell, L. H. and Manny, T. R. (1973) Exp. Cell Res. 76, 99.

49. Hartwell, L. H. (1973) Exp. Cell Res. 76, 111.

50. Samokhin, G. P., Lizlova, L. V., Bespalova, J. D., Titov, M. I., and Smirnov, V. N. (1980) Exp. Cell Res. 181, 267.

51. Lipke, P. N., Taylor, A., and C. E. Ballou (1976) J. Bacteriol. 127, 610.

52. Rose, M. D., Price, B. R., and Fink, G. R. (1986) Mol. Cell. Biol. 6, 3490.

53. Trueheart, J., Boeke, J. D., and Fink, G. R. (1987) Mol. Cell. Biol. 7, 2316.

54. Terrance, K., and Lipke, P. N. (1987) J. Bacteriol. 169, 4811.

55. Nakayama, N. Miyajima, A., and Arai, K. (1985) EMBO J. 4, 2648.

56. Sibley, D. R., Benovic, J. L., Caron, M. G., and Lefkowitz, R. J. (1987) Cell 48, 913.

57. Dixon, R. A. F., Kobilka, B. K., Strader, D. J., Benovic, J. L., Dohlman, H. G., Frielle, T., Bolanowski, M. A., Bennett, C. D., Rands, E., Diehl, R. E., Mumford, R. A., Slater, E. E., Sigal, I. S., Caron, M. G., Lefkowitz, R. J., and Strader, C. D. (1986) Nature 321, 75.

58. Marsh, L., Neiman, A. M., and Herskowitz, I. (1991) Annu. Rev. Cell Biol 7, 699.

59. Fujimura, H. A. (1989) Mol. Cell. Biol. 9, 152.

60. Dietzel, C., and Kurjan, J. (1987) Cell 50, 1001.

61. Whiteway, M., Hougan, L., and Thomas, D. Y. (1990) Mol. Cell. Biol. 10, 217.

62. Jahng, K. Y., Ferguson, J., and Reed, S. I. (1988) Mol. Cell. Biol. 8, 2484.

63. Nakafuku, M., Itoh, H., Nakamura, S., and Kaziro, Y. (1987) Proc. Natl. Acad. Sci. USA 84, 2140.

64. Stryer, L., and Bourne, H. R. (1986) Ann. Rev. Cell Biol. 2, 391.

65. King, K., Dohlman, H. G., Thorner, J., Caron, M. G., and Leftowitz, R. J. (1990) Science 250, 121.

66. Masui, Y., Tanaka, T., Chino, N., Kita, H., and Sakakibara, S. (1979) Biochem. Biophys. Res. Commun. 86, 982.

67. Baffi, R. A., Becker, J. M., Lipke, P., and Naider, F. (1985) Biochemistry 24, 3332.

68. Tallon, M. A., Shenbagamurthi, P., Marcus, S., Becker, J. M., and Naider, F. (1987) Biochemistry 26, 7767.

69. Naider, F, Kundu, B., Shenbagamurthi, P., Baffi, R., Becker, J. M., and Pousman, C. (1983) in "Peptides: Structure and Function" Hruby, V. J., and Rich, D. H., Eds., Pierce Chemical Company, USA, 677.

70. Xue, C.-B., Eriotou-Bargiota, E., Miller, D., Becker, J. M., and Naider, F. (1989) J. Biol. Chem. 264, 19161.

71. Eriotou-Bargiota, E., Xue, C.-B., Naider, F. and Becker, J. (1992) Biochemistry 31, 551.

72. Shenbagamurthi, P., Baffi, R., Khan, S. A., Lipke, P., Pousman, C., Becker, J. M., and Naider, F. (1983) Biochemistry 22, 1298.

73. Raths, S. K., Naider, F., & Becker, J. M. (1988) J. Biol. Chem. 263, 17333.

74. Shenbagamurthi, P.,Kandu, B., Raths, S., Becker, J. M., and Naider, F. (1985) Biochemistry 24, 7070.

75. Ventkatchalam, C. M. (1968) Biopolymers 6, 1425.

76. Rose, G. D., Gierasch, L. M., and Smith, J. A. (1985) Adv. Protein Chem. 37, 1.

77. Jelicks, L. A., Broido, M. S., Becker, J. M. and Naider, F. R. (1989) Biochemistry 28, 4233.

78. Jelicks, L. A., Naider, F. R., Shenbagamurthi, P., Becker, J. M. and Broido, M. S. (1988) Biopolymers 27, 431.

79. Higashijima, T., Masui, Y., Chino, N., Sakakibara, S., Kita, H. and Miyazawa, T. (1984) Eur. J. Biochem. 140 163.

80. Wakamatsu, K., Okada, A., Suzuki, M., Higashijima, T., Masui, Y., Sakakibara, S., and Miyazawa, T. (1986) Eur. J. Biochem. 154 607.

81. Wakamatsu, K., Okada, A., Miyazawa, T., Masui, Y., Sakakibara, S., and Higashijima, T. (1987) Eur. J. Biochem. 163 331.

82. Higashijima, T., Miyazawa, T., Masui, Y., Chino, N., Sakakibara, S., and Kito, H. (1979) in "Peptide Chemistry,"Yonahara, H., Ed., Protein Res. Found., Osaka, 155.

83. Wüthrich, K. (1986) in "*NMR of Proteins and Nucleic acids*", John Wiley & Sons, New York.

84. Garcia-Echeverria, C., Albericio, F., Pons, M., Barany, G. and Giralt, E. (1989) Tetrahed. Lett. 30, 2441.

85. Garcia-Echeverria, C., Siligardi, G., Mascagani, P., Gibbons, W., Giralt, E. and Pons, M. (1991) Biopolymers 31, 835.

86. Rao, B. N. N., Kumar, A., Balaram, H., Ravi, A., and Balaram, P. (1983) J. Am. Chem. Soc. 105, 1723.

87. Brake, A. J., Brenner, C., Najarian, R., Laybourn, P., and Merryweather, J. (1985) in "Current Communications in Molecular Biology" Gething, M.-J., Ed., Cold Spring Harbor Laboratory, Cold Spring Harbor, New York, pp. 103.

88. Capon, D. J., Seeburg, P. H., McGrath, J. P., Hayflick, J. S., Edman, U., Levinson, A. D., and Goeddel, D. V. (1983) Nature 304, 507.

89. McGrath, J. P., Capon, D. J., Smith, D. H., Chen, E. Y., Seeburg, P. H., Goeddel, D. V., and Levinson, A. D. (1983) Nature 304, 501.

90. Capon, D. J., Chen, E. Y., Levinson, A. D., Seeburg, P. H., and Goeddel, D. V. (1983) Nature 302, 33.

91. Powers, S., Kataoka, T., Fassano, O., Goldfarb, M., Strathern, J., Broach, J., and Wigler, M. (1984) Cell 36, 607.

92. Fisher, D. Z., Chaudhary, N., and Blobel, G. (1986) Proc. Natl. Acad. Sci. USA 83, 6450.

93. Wolin, S. L., Krohne, G., and Kirschner, M. W. (1987) EMBO J. 6, 3809.

94. Westaway, D., Papkoff, J., Moscovici, C., and Varmus, H. E. (1986) EMBO J. 5, 301.

95. Reymond, C. D., Gomer, R. H., Mehdy, M. C., and Firtel, R. A. (1984) Cell 39, 141.

96. Tsuchida, N., Ryder, T., and Ohtsubo, E. (1982) Science 217, 937.

97. Dhar, R., Ellis, R. W., Shih, T. Y., Oroszlan, S., Shapiro, B., Maizel, J., Lowy, D., and Scolnick (1982) Science 217, 934.

98. Peter, M., Kitten, G. T., Lehner, C. F., Vorburger, K., Bailer, S. M., Maridor, G., and Nigg, E. A. (1989) J. Mol. Biol. 208, 393.

99. Holtz, D., Tanaka, R. A., Hartwig, J., & McKeon, F. (1989) Cell 59, 969.

100. Stimmel, J. B., Deschenes, R. J., Volker, C., Stock, J., and Clarke, S. (1990) Biochemistry 29, 9651.

101. Farrell, F. X., Yamamoto, K., and Lapetina, E. G., (1993) Biochem. J. 289, 349.

102. Gutierrez, L., Magee, A. I., Marshall C. J., & Hancock, J. F. (1989) EMBO J. 8, 1093.

103. Hancock, J. F., Magee, A. I., Childs, J. E., and Marshall, C. J. (1989) Cell 57, 1167.

104. Casey, P. J., Solski, P. A., Der, C. J., & Buss, J. E. (1989) Proc. Natl. Acad. Sci. USA 86, 8323.

105. Schafer, W. R., Trueblood, C. E., Yang, C., Mayer, M. P., Rosenberg, S., Poulter C. D., Kim, S., & Rine, J. (1990) Science 249, 1133.

106. Schafer, W. R., Kim, R., Sterne, R., Thorner, J., Kim, S., & Rine, J. (1989) Science 245, 379.

107. Davey, J. (1992) EMBO J. 11, 951.

108. Marcus, S., Caldwell, G. A., Miller, D., Xue, C. B.,

Naider, F., and Becker, J. M. (1991) Mol Cell. Biol. 11, 3603.

109. Xue, C., Ewenson, A., Becker, J., & Naider, F. (1990) Int. J. Peptide Protein Res. 36, 362.

110. Wemmer, D. E., (1989) Concepts Magn. Reson. 1, 59.

111. Müller, N., Ernst, R. R., and Wüthrich, K. (1986) J. Am. Chem. Soc. 108, 6483.

112. Marion, D., and Wüthrich, K. (1983) Biochem. Biophys. Res. Commun. 113, 967.

113. Rance, M., Sørensen, O. W., Bodenhausen, G., Wagner, G., Ernst, R. R., and Wüthrich, K. (1983) Biochem. Biophys. Res. Commun. 117, 479.

114. Kessler, H., Gehrke, M., and Griesinger, C.(1987) Angew. Chem. Int. Ed. Engl. 27, 490.

115. Macura, S., and Ernst, R. R. (1980) Mol. Phys. 41, 95.

116. Saultis, J. and Liepins, E. (1990) J. Magn. Reson. 87, 80.

117. Macura, S., Huang, Y., Suter, D., and Ernst, R. R. (1981) J. Magn. Reson. 43, 259.

118. Macura, S., Wüthrich, K., and Ernst, R. R. (1982) J. Magn. Reson. 47, 351.

119. Lippens, G., Cerf, C. and Hallenga, K. (1992) J. Magn. Reson. 99, 268.

120. Campbell, A. P., and Sykes, B. D. (1991) J. Magn. Reson. 93, 77.

121. Bevilaqua, V. L., Thomson, D. S., and Prestegard, J. H. (1990) Biochemistry 29, 5529.

122. London, R. E., Perlman, M. E., and Davis, D. G., (1992) J. Magn. Reson. 97, 79.

123. Ni, F. (1992) J. Magn. Reson. 96, 651.

124. Clore, G. M., and Gronenborn, A. M. (1982) J. Magn. Reson. 48, 402.

125. Clore, G. M., and Gronenborn, A. M. (1983) J. Magn.

Reson. 53, 423.

126. Nirmala, N. R., Lippens, G. M., and Hallenga, K. (1992) J. Magn. Reson. 100, 25.

127. Bothner- By, A. A., Stephens, R. L., and Lee, J. (1984) J. Am. Chem. Soc. 106, 811.

128. Bauer, C. J., Frenkiel, T. A., and Lane, A. N. (1990) J. Magn. Reson. 87, 144.

129. Griesinger, C., and Ernst, R. R. (1987) J. Magn. Reson. 75, 261.

130. Farmer II, B. T., Macura, S., and Brown, L. (1988) J. Magn Reson. 80, 1.

131. Davis, D. G. (1987) J. Am. Chem. Soc. 109, 3471.

132. Müller, L., and Ernst, R. R. (1979) Mol. Phys. 38, 963.

133. Bax, A. (1988) J. Magn. Reson. 77, 134.

134. Bax, A. (1989) Methods Enzym. 176, 151.

135. Kessler, H., Griesinger, C., Kerresbaum, R., Wagner, K., and Ernest, R. R. (1987) J. Am. Chem. Soc. 109 607.

136. Tinoco, I., Jr. (1963) Radiation Research 20, 133.

137. Zhong, W., Gulotta, M., Goss, D. J., and Diem, M. (1990) 29, 7485.

138. Kaiser, E., Colescott, R. L., Bossinger, C. D. and Cook, P. I. (1970) Anal. Biochem. 34, 595.

139. Xue, C.-B., Caldwell, G. A., Becker, J. M., and Naider, F. (1989) Biochem. Biophys. Res. Commmun. 162, 253.

140. Xue, C., Becker, J., & Naider, F. (1991) Int. J. Peptide Protein Res. 37, 476.

141. Barrow, D. A. and Lentz, B. R. (1980) Biochim. Biophys. Acta 597 92.

142. States, D. J., Haberkorn, R. A., and Ruben, D. J. (1982) J. Magn. Reson. 48 286.

143. Otting, G.,Widmer, H., Wagner, G., and Wüthrich (1985) J. Magn. Reson. 66, 187.

144. Allerhand, A., and Oldfield, E. (1973) Biochemistry 12, 3428.

145. Dyson, J. H., Rance, M., Houghten R. A., Lerner, R. A., & Wright, P. E. (1988) J. Mol. Biol. 201, 161.

146. Torchia, D. A., Lyerla Jr., J. R., and Quattrone, A. J. (1975) Biochemistry 14, 887.

147. Wright, P. E., Dyson, J. H., & Lerner, R. A. (1988) Biochemistry 27, 7169.

148. Balaram, P. (1985) Proc. Indian Acad. Sci. (Chem. Sci.) 95 21.

149. Kessler, H. (1982) Angnew. Chem. Int. Ed. Engl. 21, 512.

150. Naider, F., Jelicks, L. A., Becker, J. M., and Broido, M. S. (1989) Biopolymers 28, 487.

151. Parente, R., Nir, S. and Szoka, F. (1990) Biochemistry 29, 8720.

152. Stockton, G. W., Polnaszek, C. F., Tulloch, A. P., Hasan, F., and Smith, I. C. P. (1976) Biochemistry 15, 954.

153. Esposito, G. and Pastore, A. (1988) J. Magn Reson. 76, 331.

154. Macura, S., Farmer II, B. T., and Brown, L. (1986) J. Magn Reson. 70, 493.

155. Mirau, P. A. (1988) J. Magn. Reson. 80, 439.

156. Mirau, P. A., & Bovey, F. A. (1986) J. Am. Chem. Soc. 108, 5130.

157. Behling, R. W., Yamane, T., Navon, G., Sammon, M. J., & Jelinski, L. W. (1988) Proc. Natl. Acad. Sci. USA 85, 6721.

158. Valensin, G., Kushnir, T., & Navon, G. (1982) J. Magn. Reson. 46, 23.

159. Stradley, R. J., Rizo, J., Bruch, M. D., Stroup, A. N. and Gierasch, L. M. (1990) Biopolymers 29, 263.

160. Hruby, H. J., Kao, L. F., Pettitt, B. M., and Karplus, M. (1988) J. Am. Chem. Soc. 110, 3351.

161. Bystrov, V. F. (1976) Prog. NMR Spectroscopy 10, 41.

162. Scherf T., Hiller, R., Naider, F., Levitt, M., Anglister, J. (1992) 31, 6884.

163. Van Echteld, C. J. A., Van Stigt, R., De Kruijff, B., Leunissen-Bijvelt, J., Verkleij, A. J., and De Gier, J. (1981) Biochim. Biophys. Acta 648, 287.

164. Hanke, W., Methfessel, C., Wilmsen, H.-U., Katz, E., and Jung, G. (1983) Biochim. Biophys. Acta 727, 108.

165. Schwarz, G., Zong, R.-t, and Popescu, T. (1992) Biochim. Biophys. Acta 1110, 97.

166. Forti, S., and Menestrina, G. (1989) Eur. J. Biochem. 181, 767.

167. Wildman, D. E., Tamir, H., Leberer, E., Northup, J. K., and Dennis, M. (1993) Proc. Natl. Acad. Sci. USA 90, 794.

168. DeVos, A. M., Tong, L., Milburn, M. V., Matias, P. M., Jancarik, J., Noguchi, S., Nishimvra, S., Miura, K., Ohtsuka, E., and Kim S.-H. (1988) Science 239, 888.

169. Milburn, M. V., Tong, L., Matias, P.,DeVos, A. M., Brünger, A., Yamaizumi, Z., Nishimvra, S., and Kim S.-H. (1990) Science 247, 939.